Aus der Klinik und Poliklinik für Neurologie

der Universitätsmedizin der Johannes Gutenberg-Universität Mainz

Grey Matter Age Prediction as a Biomarker for Neurodegeneration / Die abnormalen Alterungsdynamiken der Großhirnrinde und Basalganglien als Biomarker bei neurodegenerativen Erkrankungen

Inauguraldissertation

zur Erlangung des Doktorgrades der

Medizin

der Universitätsmedizin

der Johannes Gutenberg-Universität Mainz

Vorgelegt von

Philopatir Farag

aus Alexandria

Mainz, 2022

Wissenschaftlicher Vorstand:

1. Gutachter:

2. Gutachter:

Tag der Promotion: 12. Juli 2022

Table of Contents

TABLE OF CONTENTS **2**

LIST OF ABBREVIATIONS **4**

LIST OF FIGURES **5**

LIST OF TABLES **5**

1. INTRODUCTION **6**

1.1 Effect of Age on Brain 6
1.2 Brain Age Analysis 7
1.3 Cortical Atrophy in Neurodegenerative Diseases 10
1.3.1 Parkinson's disease 10
1.3.2 Multiple sclerosis 12
1.3.3 Frontotemporal lobar degeneration 13
1.3.4 Mild cognitive impairment 14
1.3.5 Alzheimer's disease 15

2. METHODS **18**

2.1 Participants: 18
2.1.1 Healthy individuals 18
2.1.2 Patient groups 19
2.2 MRI Preprocessing: 20
2.2.1 Structural MRI 20
2.2.2 Freesurfer pipeline 21
2.2.3 Cortical and subcortical parcellation 22
2.3 Morphometric Measures 22
2.3.1 Cortical thickness 22
2.3.2 Cortical thickness standard deviation 22
2.3.3 Surface area 22
2.3.4 Grey matter cortical volume 23
2.3.5 Subcortical volume 24
2.4 Statistical Analyses 24
2.4.1 Comparison of brain morphometrics between groups 24
2.4.2 Regression analysis for brain age prediction 25
2.4.3 Statistical learning algorithms used for brain age prediction 27
2.4.4 Brief introduction to statistical learning 27
2.4.5 Assessing the performance of statistical learning models 30
2.4.6 First model: multiple linear regression 31
2.4.7 Second model: ridge regression 32
2.4.8 Third model: least absolute shrinkage and selection operator (LASSO) 33
2.4.9 Fourth model: elastic net regression 33
2.4.10 Fifth model: support vector machine 34
2.4.11 Sixth model: PRISM toolbox 35
2.5 Clinical Tests Used for the Regression Analysis 35
2.5.1 Mini-Mental State Examination (MMSE) 35
2.5.2 Delayed memory recall test (LDELTOT) & immediate memory recall test (LIMMTOT) 36
2.5.3 Unified Parkinson's disease rating scale (UPDRS) 36
2.5.4 Clinical Dementia Rating (CDR) 36
2.5.5 Expanded Disability Status Scale (EDSS) 37

3. RESULTS **38**

3.1 Differences in Morphometric Measures Across Neurodegenerative Diseases 38
3.1.1 Mean morphometrical measures differentiate across neurodegenerative groups 38
3.1.2 Sex differentiates mean morphometric measures across neurodegenerative groups 39
3.1.3 FTLD patients and the DG differ in regional CT and SubVol 42
3.1.4 PD patients and the RG differ in regional CVol, SubVol, SA and CTSD 43
3.1.5 CVol and SA regions differ most across all groups when taking sex as a factor 44
3.2 Differences in Actual Age Across Groups 45

3.2.1 PD and FTLD patients have similar actual ages to individuals in the DG ... 45
3.3 Age Predictions Vary Across Groups and Sex ... 45
3.3.1 Best overall age predictions achieved by healthy individuals ... 45
3.3.2 Best age predictions among patient groups achieved by MCI and PD ... 46
3.3.3 Better age predictions in males than in females ... 46
3.4 Predicted Age Strongly Associates with Clinical Parameters, but Delta Age Does not ... 49
3.4.1 Worse MMSE scores are associated with higher predicted ages in MCI ... 49
3.4.2 Worse UPDRS scores are associated with higher predicted ages in PD ... 51
3.4.3 Worse MMSE scores are associated with higher predicted ages in FTLD ... 51
3.4.4 MMSE scores do not show a significant association to any age variable in AD ... 52
3.4.5 Worse EDSS scores are strongly associated with higher predicted ages in MS ... 53

4. DISCUSSION ... 54

4.1 Widespread Morphometric Heterogeneity Across Neurodegenerative Disorders ... 54
4.2 Age Prediction as Biomarker Across Neurodegenerative Conditions ... 55
4.3 Predicted Age as a Predictor for Clinical Presentation of the Disease ... 56
4.4 Limitations ... 59

5. SUMMARY ... 60

6. ABSTRACT ... 61

7. ZUSAMMENFASSUNG ... 63

REFERENCES ... 65

APPENDIX ... 80

ACKNOWLEDGMENTS ... 98

TABELLARISCHER LEBENSLAUF ... 99

List of Abbreviations

AD ..... *Alzheimer's disease*
ANCOVA ..... *analysis of covariance*
ANOVA ..... *analysis of variance*
bvFTD ..... *behavioural variant frontotemporal dementia*
CDR ..... *Clinical Dementia Rating*
CSF ..... *cerebrospinal fluid*
CT ..... *cortical thickness*
CTSD ..... *cortical thickness standard deviation*
CV ..... *cross validation*
CVol ..... *cortical volume*
DC ..... *discovery cohort*
DG ..... *discovery group*
DK ..... *Desikan-Killiany*
EDSS ..... *Expanded Disability Status Scale*
EN ..... *elastic net regression*
FTLD ..... *frontotemporal lobar degeneration*
GM ..... *grey matter*
HI ..... *healthy individuals*
LASSO ..... *least absolute shrinkage and selection operator*
LDELTOT ..... *delayed memory recall test*
LIMMTOT ..... *immediate memory recall test*
MAE ..... *mean absolute error*
MANCOVA ..... *multivariate analysis of covariance*
MANOVA ..... *multivariate analysis of variance*
MCI ..... *mild cognitive impairment*
MdAE ..... *median absolute error*
MLR ..... *multiple linear regression*
MMSE ..... *Mini-Mental State Examination*
MR ..... *magnetic resonance*
MRI ..... *magnetic resonance imaging*
MS ..... *multiple sclerosis*
MSE ..... *mean squared error*
PD ..... *Parkinson's disease*
R^2 ..... *coefficient of determination*
RC ..... *replication cohort*
RR ..... *ridge regression*
RSE ..... *residual standard error*
RVR ..... *relevance vector regression*
SA ..... *surface area*
SSR ..... *sum of squared residuals*
SubVol ..... *subcortical volume*
SVM ..... *support vector machine*
SVR ..... *support vector regression*
UPDRS ..... *Unified Parkinson's disease rating scale*
WM ..... *white matter*

List of Figures

Figure 2.1. Composition of the discovery cohort (DC). 18
Figure 2.2 Illustration of a gyrus and a sulcus 1. 23
Figure 2.3 Illustration of a gyrus and a sulcus 2. 24
Figure 2.4 From MR scans to age predictions. 26
Figure 2.5 Linear and non-linear, non-parametric regression. 30
Figure 2.6 Illustration of a function estimated using a SVR. 35
Figure 3.1 Plots of brain morphometrics across groups. 39
Figure 3.2 Plots of brain morphometrics grouped by sex. 42
Figure 3.3 R^2-coefficient plots from predicted vs. actual age regressions. 47
Figure 3.4 Mean absolute error (MAE) plots from predicted vs. actual age regressions. 48
Figure 3.5 Median absolute error (MdAE) plots from predicted vs. actual age regressions. 49
Figure 3.6 Regression plots with clinical variables in mild cognitive impairment. 50
Figure 3.7 Regression plots with clinical variables in Parkinson's disease 51
Figure 3.8 Regression plots with clinical variables in frontotemporal lobar degeneration. 52
Figure 3.9 Regression plots with clinical variables in Alzheimer's disease. 53
Figure 3.10 Regression plots with clinical variables in multiple sclerosis. 53

List of Tables

Table 1.1 Summary of previously used age prediction models. 8
Table 2.1 Overview of the different databases of healthy individuals 18
Table 2.2 Overview of the different patient cohorts 19
Table 2.3 Overview of the MRI acquisition parameters for all groups 20
Table 2.4 Overview of clinical tests and scores. 37
Table 3.1 Summary of MANOVAs: discovery group (DG). 43
Table 3.2 Summary of MANOVAs: replication group (RG). 43
Table 3.3 Summary of MANCOVAs: discovery group (DG). 44
Table 3.4 Summary of MANCOVAs: replication group (RG). 45
Table 3.5 Summary of ANOVA for actual age. 45

1. Introduction

1.1 Effect of Age on Brain

The brain permanently suffers modifications that respond to intrinsic and extrinsic factors, which are closely linked to brain maturation, development and aging. One of the ways the brain changes in response to those factors is through atrophy. Brain atrophy is expected in brains of patients with neurodegenerative disorders, and yet, even ostensibly healthy individuals (HI) lose structural integrity in the brain over time. Such age-related morphological brain variations have been well documented, from observations in post-mortem studies (Flood and Coleman, 1988, Miller et al., 1980) to *in vivo* studies using magnetic resonance imaging (MRI) brain scans. One way to detect such age-effects on a macroscopic level from *in vivo* MRI data, is to compute and analyze morphometric measures, such as cortical thickness (CT), surface area (SA) or cortical volume (CVol). A CT atrophy might signify a decrease in the number, size and density of neuronal cells as well as a change in the arrangement of cells, dendritic spines and myelination (Hutton et al., 2008, Jung et al., 2011). SA was found to be another indicator of cerebral morphology, and unlike CT, has shown to differ greatly across species (Fish et al., 2008, Winkler et al., 2018). Atrophy in CVol, which measures tissue density, would mean a reduction in the amount of grey matter (GM) tissue (Li et al., 2014). For instance, a longitudinal study conducted in subjects between 23 and 87 years with a follow-up of about 3.6 years, revealed that aging had a specific effect on brain morphology (Storsve et al., 2014). This study, among others, has found a general reduction of CT, SA and CVol over time (Lemaitre et al., 2012, Storsve et al., 2014, Madan and Kensinger, 2018, Hogstrom et al., 2013). The reported morphological alterations, however, were not uniform across age or brain regions. This means that some age intervals and some cortical regions had higher rates of atrophy than others. Notably, cortical thinning tended to accelerate after the age of 60. In addition, cortical thinning as well as a reduction in SA were found to be main contributors to CVol loss over time (Choi et al., 2019).

Interesting for our study are the prevalent linear (McKay et al., 2014) and non-linear relationships found between CT and age, (Pfefferbaum and Sullivan, 2015) as well as between volume and age (Pfefferbaum and Sullivan, 2015). Another study had as well observed a negative quadratic effect of age on CT, meaning that as age increased, CT decreased quadratically (Hogstrom et al., 2013). Parallel to that, a study using volumetric analyses (i.e.

voxel based morphometry) found that the rate of GM atrophy was higher in women than in men (Crivello et al., 2014).

Furthermore, biological age was associated with a decline in mean CT and memory performance. Yet, mean CT was negatively correlated with memory performance in younger participants and positively correlated in older ones, suggesting a reversing relationship between mean CT and memory performance with advancing age (de Chastelaine et al., 2019).

1.2 Brain Age Analysis

Over the years, many studies have attempted to predict the so-called "brain age" of human beings based on brain morphometrics, using some kind of MRI image preprocessing technique. This "brain age" is equivalent to any given subject's predicted age. Most of the times, a machine learning algorithm is trained on a subsample of the healthy subjects cohort, and tested on another set of the same healthy subjects, yielding the age predictions. If the test sample contains subjects from a different cohort than the subjects in the training sample, factors such as genetics, education, diet and scan-related differences might have a stronger impact on the age predictions (Madan and Kensinger, 2018). Subsampling the training set randomly to yield a test set can thereby improve a model's performance (Le et al., 2018). Derived from the age predictions, the differences between a subject's actual and predicted age is known as the "delta age", which can be either positive (which may reflect accelerated ageing) or negative (may reflect resilience) (Smith et al., 2019).

When performing age predictions, the result of the algorithms' performance, in other words, the success of the age predictions, is expressed in the form of a coefficient of determination (R^2), mean absolute error (MAE) or median absolute error (MdAE). Several morphometric variables, either alone or in combination with other variables, have proven to be better suited at predicting a brain's age than others. Some of those variables, which directly result from the Freesurfer preprocessing pipeline include CT (Khundrakpam et al., 2015, Liem et al., 2017, Madan and Kensinger, 2018, Wang et al., 2014, Valizadeh et al., 2017, Aycheh et al., 2018), CVol (Valizadeh et al., 2017), SA (Valizadeh et al., 2017, Liem et al., 2017) and subcortical volume (SubVol) (Liem et al., 2017, Valizadeh et al., 2017). Alternatively, GM and white matter (WM) volumetrics using statistical parametric mapping software with the voxel based morphometry technique have successfully been used by some authors for the age predictions (Cole et al., 2015, Cole et al., 2017, Franke et al., 2010). The results of the age

predictions thereby depend on many factors, which are summarized (Table 1.1) below for some studies in the last few years.

Not only has "brain age" been computed for HI, but also in individuals with neurological disorders. For instance, Alzheimer's disease patients were predicted in average 10 years older than their actual age (Franke et al., 2010), and longitudinally, the "brain age" of AD and mild cognitive impairment (MCI) patients over the period of 36 months, increased, suggesting an accelerated brain aging process (Franke et al., 2012). Furthermore, APOE ε4-carriers with MCI or AD were found to have an accelerated increase in "brain age" in comparison with MCI and AD patients that are APOE ε4-non-carriers (Lowe et al., 2016).

Likewise, several other factors such as psychiatric disorders (Nenadic et al., 2017), individual health, type 2 diabetes mellitus (Franke et al., 2013), long term meditation (Luders et al., 2016), and music making (Rogenmoser et al., 2018) have been found to influence "brain age" (Franke and Gaser, 2019).

Table 1.1 Summary of previously used age prediction models. *The following parameters result from predictions in healthy individuals in several studies over the past years.*

Paper citation	MRI Morphometrics	Algorithm	Age range (years)	Number of healthy subjects (training & test sets)	R^2	MAE (years)
(Franke et al., 2010)	GM voxel intensity values	RVR	18 – 86	650	0.85	5
(Sabuncu and Van Leemput, 2011)	GM voxel intensity values	RVM	18 – 93	336	0.85	__
(Wang and Pham, 2011)	GM, WM and CSF voxel intensity values with DWT	HMM	50 – 86	20	__	*2.5
(Groves et al., 2012)	CT, VBM, FA, MD, MO	ICA	8 – 85	484	0.94	__
(Kandel et al., 2013)	CT	Sparse linear regression	__	216	0.27	5 – 6.5
(Konukoglu et al., 2013)	Whole-brain voxel-wise tissue density	NAF	__	414	0.89	__

(Mwangi et al., 2013)	FA, MD, axial diffusivity and radial diffusivity	RVR	4 – 85	188	0.81	**9.08
(Wang et al., 2014)	CT, SA, curvatures	RVR	20 – 82	547	0.88	4.6
(Cole et al., 2015)	GM and WM voxel-wise tissue density	GPR	18 – 90	1650	0.85	4.66
(Steffener et al., 2016)	GM volumes and SubVol	Scaled subprofile modeling	19 – 79	331	0.47	-
(Lin et al., 2016)	Network metrices: FA, fiber number, fiber length	ANN	50 – 79	112	0.64	4.29
(Schnack et al., 2016)	GM voxel-wise tissue density	SVR	16 – 67	386	0.79	4.31
(Luders et al., 2016)	GM voxel-wise tissue density using SPM and VBM	RVR	24 – 77	50	0.78	-
(Cole et al., 2017)	SPM GM and WM voxel intensity values	CNN	18 – 90	2001	0.92	4.16
(Liem et al., 2017)	CT, SA, SubVol, connectivity matrices	SVR and RF	19 – 82	2354	-	4.29
(Madan and Kensinger, 2018)	CT, gyrification and FD	RVR	18 - 97	1232	0.80	***6 – 7
(Aycheh et al., 2018)	CT	Sparse Group LASSO & GPR	45 – 91	2705	0.50	4.05

ANN: artificial neural network, CNN: convolutional neural network, CSF: cerebrospinal fluid, CT: cortical thickness, DWT: discrete wavelet transform, FA: fractional anisotropy, FD: fractal dimensionality, GM: grey matter, GPR: Gaussian process regression, HMM: hidden Markov model, ICA: independent component analysis, MAE: mean absolute error, MD: mean diffusivity, MO: mode of the diffusion tensor, NAF: neighborhood approximation forests, RVM: relevance vector machine, RVR: relevance vector regression, SA: surface area, SPM: statistical parametric mapping, SubVol: subcortical volume, SVR: support vector regression, VBM: voxel-based morphometry, WM: white matter

** ANGE: Average Normalized Age-gap Error*

*** for subjects over the age of 30*

**** MdAE: median absolute error*

1.3 Cortical Atrophy in Neurodegenerative Diseases

The fact that several studies have discovered that patients with particular neurodegenerative disorders were predicted older than their actual age, means that the "brain age" could potentially help differentiate between healthy and atrophied brains. Going further, "brain age" could help differentiate between those neurodegenerative diseases, which have commonalities such as brain atrophy. Depending on the disease, the atrophy would be more or less pronounced and affect different brain regions, hopefully creating a profile of atrophy pattern that is specific to each disease. With this in mind, a computed "brain age" based on those atrophy patterns, could potentially serve as a non-invasive biomarker for various neurodegenerative diseases. The following sections are meant to outline those morphometric alterations and possible associations to clinical variables in the following 5 neurodegenerative diseases: Parkinson's disease, multiple sclerosis, frontotemporal lobar degeneration, mild cognitive impairment and Alzheimer's disease.

1.3.1 Parkinson's disease

Parkinson's disease (PD) is a neurological disorder characterized by cardinal motor symptoms including bradykinesia, rigidity, tremor at rest, and impaired posture. PD has been associated with factors such as family history, cigarette smoking, alcohol, vitamin D exposure and urate levels (Tysnes and Storstein, 2017). PD has a higher prevalence in men, and affects about 1% of the population over 60 years old (Khan et al., 2019). The neuropathological PD manifestations, include a loss of neurons and an α-synuclein-containing Lewy body accumulation in the substantia nigra, which disrupt motor circuits (Tysnes and Storstein, 2017). There is a growing evidence, however, that alpha synuclein may not be playing the main role in neurodegeneration, but rather immune-induced inflammation and excitotoxicity (Blaylock, 2017). The latter is thought to be triggered by the signaling cascade caused by the inflammation (Blaylock, 2017). PD pathology, in fact, has an impact on the whole-brain, commonly seen as disrupted brain networks when compared to healthy age-matched individuals (Koirala et al., 2019). CT in specific regions was found to be correlated to connectivity to a so-called "disease reservoir", which is nothing other than subcortical areas showing atrophy in PD patients in comparison to HI (Yau et al., 2018). Therefore, despite microstructural patterns, neurodegeneration in PD patients may show increased vulnerability

in several specific brain regions (Koirala et al., 2019); neurodegeneration in PD is not necessarily restrained to specific brain areas.

GM atrophy may take many forms in PD patients: from thinning of the cortical mantle, to decreased GM tissue in cortical and subcortical structures. Usually such changes manifest themselves in specific brain regions rather than throughout the entire cortex. Out of all morphometric variables, CT seems to be the variable with the most associations to clinical variables. As such, CT in patients with PD, has shown hemisphere (Claassen et al., 2016) and gender specific variations. More specifically, male PD patients had a significantly reduced CT in multiple brain regions compared to female PD patients (Yadav et al., 2016). Not only has CT shown to correlate with PD characteristic motor symptoms (Gao et al., 2018, Vastik et al., 2017, Wilson et al., 2019) but also with non-motor symptoms in PD patients including mild cognitive impairment (Mak et al., 2014, Segura et al., 2014, Uribe et al., 2016), depressive symptoms (Hanganu et al., 2017), visuospatial and visuoperceptual changes, (Segura et al., 2014) and neuropsychiatric symptoms (Ye et al., 2018). Furthermore, disease severity, which in some cases was determined using the Hoehn and Yahr scale, was associated to CT (Gao et al., 2018, Guimaraes et al., 2016). Interesting for our study, is the association found between the motor evaluation section of the Unified Parkinson's disease rating scale (UPDRS) (part III) and CT, (Gao et al., 2018) as well as the thalamic subnuclei volumes (Chen et al., 2020). In fact, CT seems to be so relevant that it has even been reported to be associated with outcomes from deep brain stimulation therapy. Notably, PD and dystonia patients with a higher degree of cortical thinning needed a higher stimulation voltage to achieve an optimal clinical response (Gonzalez-Escamilla et al., 2019, Muthuraman et al., 2017).

Regarding cortical thinning in PD patients, a study found three different atrophy patterns in a cohort of 88 non-demented PD patients. Roughly a third of patients had the worse cognitive performance out of all groups, which was coupled with a parieto-temporal cortical thinning. Another third had a younger disease onset with an occipital and frontal cortical thinning. The last third of patients showed no atrophy at all (Uribe et al., 2016). These findings demonstrate once again the diversity in cortical atrophy patterns in PD patients and the numerous associations to clinical variables. Nevertheless, an attempt to separate PD patients from healthy controls using a combination of morphometric variables with a support vector machine (SVM) was successful with an accuracy of 85.78% (Peng et al., 2017). This implies that PD patients could be distinguished from HI by a combination of morphometric variables.

Another such useful variable includes the SubVol of different regions. Most studies cited above, have found, in addition to the CT correlations, an association between subcortical volumes and clinical variables. Interestingly, one study noticed that striatal atrophy was more prominent in early disease stages, whereas extra-striatal cortical atrophy occurred in later disease stages (Lewis et al., 2016). Only a few studies relied solely on GM and WM volumes, which either included an association to diabetes mellitus (Ong et al., 2017, Petrou et al., 2016) or to cortical Lewy Body deposition (Gee et al., 2017).

1.3.2 Multiple sclerosis

Multiple sclerosis (MS) is an autoimmune disease resulting in a multifocal demyelination, mainly in young people between the age of 20 and 40 (Vidal-Jordana and Montalban, 2017). Genetic predisposition and environmental factors might be involved in the development of the disease, yet the real etiology is still unknown. Not only is it an inflammatory disease but also a neurodegenerative one (Correale et al., 2017). Symptoms of MS depend on the site of lesions and can affect motor, sensory, visual and autonomic systems (Doshi and Chataway, 2016). Especially age has been one of the strongest predictors for the buildup of severe disability. Thus, factors linked with age such as hypoxia, mitochondrial dysfunction and iron accumulation have been associated with age and contribute to neural damage. Also, cerebral small vessel disease may influence the age-related neurodegenerative pathology seen in MS (Geraldes et al., 2017). One study has found that the percent brain volume change decreased significantly in an MS cohort compared to a HI cohort, when looking at two different age groups (20-59 and 60-79), suggesting that aging with MS has an influence on brain volume (Ghione et al., 2019). An onset of MS at the age of 40 to 50 doubled and tripled, respectively, the risk of developing progressive MS forms, compared with patients within common onset age ranges (Sanai et al., 2016).

Additionally, neurodegeneration and cortical atrophy have shown to correlate with the degree of disability in progressive MS (Correale et al., 2017). GM atrophy has even shown to be more strongly associated to disease progression than T2-hyperintensive lesions (Fisniku et al., 2008). Regarding subcortical structures, GM nuclei were affected by neuronal loss in absence of demyelinated lesions (Correale et al., 2017), for instance, thalamic atrophy resulted from microstructural alterations rather than from WM lesions (Deppe et al., 2016). Besides those lesions, network connectivity patterns derived from functional and structural

imaging have as well shown to provide additional insights into pathological processes in GM and WM (Fleischer et al., 2019).

MS patients have shown to have GM atrophy, similar to other diseases, mainly in the form of cortical thinning. Not to say that other forms of GM atrophies do not occur, but to accentuate the more frequent correlations between CT and various clinical variables. A confirmed disability progression in MS patients was related to GM atrophy in areas associated with motor functions and cognition (Bergsland et al., 2018).

Previous studies have mainly found a correlation between cortical thinning and some sort of cognitive impairment or dysfunction (Daams et al., 2016, Liu et al., 2014, Pitteri et al., 2017, Pravata et al., 2017). CT was found to be independently associated with miscellaneous variables such as disease duration (Orbach et al., 2018), depression (Pravata et al., 2017), visual & verbal memory (Tillema et al., 2016), and verbal & figural fluency (Geisseler et al., 2016). Some studies have even found correlations to MS-related brain lesions, which suggests an interdependence of brain lesions and brain atrophy (Pareto et al., 2015, Steenwijk et al., 2014). Furthermore, cortical thinning has been associated to age and to higher scores in the Expanded Disability Status Scale (EDSS) (Orbach et al., 2018, Righart et al., 2017, Steenwijk et al., 2016). Thus, cortical atrophy in the form of cortical thinning seems to be intricately connected to disease progression in MS patients, since it is independently associated to two of the most responsible factors for morbididty: brain lesions and advancing age. Whether CT can be regarded as a reliable predictor for morbididty in MS patients, however, will be explored in this study.

1.3.3 Frontotemporal lobar degeneration

Frontotemporal lobar degeneration (FTLD) describes a loss of neurons, gliosis, and degeneration of the frontal and anterior temporal lobes, as well as of the anterior cingulate and insular cortices (Bang et al., 2015, Rabinovici and Miller, 2010). In terms of clinical presentation three distinct syndromes can be identified: behavioural variant frontotemporal dementia (bvFTD), semantic dementia and progressive non-fluent aphasia, which are usually associated with mutations in three main genes, MAPT, GRN or C9orf72 (Mann and Snowden, 2017). In nearly all variants of FTLD one of either tau, TDP-43, or FUS proteins are involved in the pathomechanism and contribute to the different atrophy patterns found in FTLD (Bang et al., 2015). Depending on the age of onset of FTLD, different types of clinical presentations and pathological correlates were more frequent. For instance,

FTLD-tau was the most common pathological diagnosis found in patients with late age at symptom onset, whereas FTLD-TDP was the most common in patients with early age (before the age of 65) at symptom onset (Seo et al., 2018). Additionally, the frequencies of comorbid neurological pathologies were higher in late-onset FTLD (Seo et al., 2018). This supports the possibility of heterogeneity in atrophy patterns within a group of FTLD patients with different ages of onset. Furthermore, the caudate nucleus and its network are believed to be important in determining the pathogenesis, which leads to neurodegeneration (Sobue et al., 2018).

Several studies of FTLD patients have suggested that brain volume is reduced, even when the disease is still asymptomatic, making brain morphometric measures attractive as potential biomarkers (Papma et al., 2017, Rohrer et al., 2015). Each of the clinical symptoms of FTLD, ranging from motor neuron disease and parkinsonism to socioemotional, language, and speech disorders that can initially occur alone or in various combinations, are associated with a specific pattern of brain atrophy (Rohrer and Rosen, 2013). Accordingly, the earliest brain morphometric alterations vary across individuals.

Due to the fact that no known indicators that predict which neural systems will be affected first are currently available, previous work in FTLD and its subtypes has focused on tracking global brain measures or regional variations that might be specific to FTLD subtypes (Whitwell et al., 2015). However, this type of approach is limiting and does not permit optimal tracking of the disease progression since these measures can present high inter-individual variability (Staffaroni et al., 2019).

Moreover, recent studies seem to have found widespread cortical thinning in patients with bvFTD (Canu et al., 2017). Specifically the atrophy patterns seem to manifest as thinning in the temporal and frontal lobes bilaterally, as well as in the insula bilaterally (Rohrer et al., 2015). Decrease of CT over time showed similar atrophy patterns and a steeper rate of cognitive decline for bvFTD patients compared to HI (Moller et al., 2016). Furthermore, some studies have attempted to differentiate between the different FTLD clinical subtypes using machine learning (Kim et al., 2019). Associations between cortical thinning patterns and different FTLD genetic variants have as well been found, suggesting a heterogeneity of cortical atrophy configurations, even within this single dementia type (Paternico et al., 2016).

1.3.4 Mild cognitive impairment

Mild cognitive impairment (MCI) is sometimes described as a transition between normal cognition and dementia (AD, as well as other types of dementias (Matthews et al.,

2008)). Some studies have even detected cognitive deficits characteristic of MCI in prodromal PD patients and in patients at risk for PD (Weil et al., 2018). MCI results in the deterioration of memory, attention and cognitive function without impairing daily activities (Eshkoor et al., 2015). MCI has a prevalence of 10% - 20% over the age of 65 (Langa and Levine, 2014). The male gender and advancing age increase the risk of developing MCI (Langa and Levine, 2014). In 10% – 15% of cases, MCI proceeds AD (Eshkoor et al., 2015). The diagnosis of MCI relies mostly on the use of cognitive assessment tests such as the Montreal Cognitive Assessment or the Mini-Mental Sate Examination (MMSE). Rather uncommon, is the use of imaging techniques such as MRI, where volumetric measures of the hippocampus show atrophy (Langa and Levine, 2014), especially in the CA1 subfield (Chetelat et al., 2008). Concerning MCI pathology, a number of different, quite heterogenous phenomena have been observed: brain amyloid beta (Aβ) plaques accumulation in allocortical regions, tau induced neurofibrillary tangles in the subiculum and inferior parietal cortex, neural cell loss in the limbic medial temporal lobe, and synaptodegeneration in the hippocampus and in the cortex (Mufson et al., 2012). Also, many studies have found a decreased connectivity in the default mode network in MCI patients compared to HI (Joo et al., 2016).

Compared to HI, patients with MCI have shown to have a lower GM volume in the right temporal lobes as well as in several subcortical structures (Csukly et al., 2016, Groeneveld et al., 2018, Yi et al., 2016). Additionally, MCI patients were described as having multiple regions of cortical thinning including in the left caudal anterior cingulate, lateral occipital, right superior temporal and in the entorhinal cortices (Cheng et al., 2018). Therefore, an attempt to classify MCI patients based on morphometric data has proven to be quite difficult since MCI is based on a clinical diagnosis and not so much on typical brain alterations. The idea of MCI being a stage on a continuum from cognitively normal to AD variants further supports the notion of heterogeneity in a given MCI cohort, which would present itself as a wide range of varying clinical symptoms and morphometrics (Bron et al., 2015).

1.3.5 Alzheimer's disease

Alzheimer's disease (AD) is the main neurodegenerative disease, and the most common cause of dementia in old persons (Scheltens et al., 2016, Jack et al., 2018). AD histopathological hallmarks are an accumulation of misfolded amyloid protein and formation of neurofibrillary tangles (Jeong, 2017), both with differentiable patterns of accumulation across the brain (Grothe et al., 2016, Iaccarino et al., 2018), which leads to abnormal neuronal

functioning and progressive loss of the brain tissue (Lane et al., 2018). The characteristics of protein deposits differentiate AD from other neurodegenerative processes (Jack et al., 2018), making AD a collective of neuropathologic alterations, rather than a syndrome encompassing multiple symptoms. Therefore, a given syndrome is neither sensitive nor specific for the neuropathological alterations seen in AD, and patients with apparent disease-specific neuropathological alterations but without symptoms cannot be thereby identified (Jack et al., 2018). AD is related with a decline in two or more cognitive domains including working and long-term declarative memory (Jahn, 2013), language, executive and visuospatial functions, often accompanied by personality, and behavior changes, which lead to a significant impairment of daily activities and a reduction in the overall quality of life (Weller and Budson, 2018).

The prevalence of AD is about 10-30% in the human population over 65 years old (Masters et al., 2015). Among AD patients different forms, determined by their age at onset, are known: the sporadic form characterized by a late onset (after the age of 65)(Rabinovici, 2019); and the genetic form, with rather an early onset (~45 years of age) (Masters et al., 2015). The latter AD form is mainly caused by mutations in three genes: the amyloid precursor protein, presenilin 1 and presenilin 2 (Lane et al., 2018). Furthermore, the age of onset of AD seems to play a role in disease manifestation: in comparison to late onset or sporadic AD (Moon et al., 2018) (after the age of 65), early onset AD patients have delays in diagnosis, a more aggressive course, distress and confusion over symptoms, and age-related psychological needs (Mendez, 2017). Regarding brain morphology, early onset AD patients tend to have a more pronounced atrophy of the parietal lobe, and a smaller reduction in hippocampal volume compared to those with late onset AD (Mendez, 2017). Even before regional atrophy, reorganization and disconnection of the brain networks have been found in asymptomatic patients (Mendez, 2017).

Patients with AD have been shown to have a decreased CT in the right hippocampus (Ma et al., 2016), medial temporal lobes and parietal lobes (Hwang et al., 2016). As well, a decrease in GM volume (Ma et al., 2016) and SA (Yang et al., 2019) have been observed. A decrease in CT over time has also been spotted in a longitudinal study with AD patients (Moller et al., 2016). Interestingly, another study has even found a more rapid cortical thinning in women than in men (Lee et al., 2018). Especially cortical thinning has often been associated with different cognitive domains. For instance, CT and CVol have been found to decline linearly with MMSE scores (Choi et al., 2019). A major temporal lobe atrophy has been correlated to

deficits in all cognitive domains (Kunst et al., 2019). Furthermore, CT has been a suitable morphometric variable for assessing brain changes during cognitive decline in AD patients (Choi et al., 2019). Attempts to separate AD patients from HI using classification algorithms such as SVM, have been successful when CT was combined with other variables (Gupta et al., 2019, Shaikh and Ali, 2019, Zhang and Liu, 2018).

2. Methods

2.1 Participants:

2.1.1 Healthy individuals

There were two different groups of healthy individuals (HI): a discovery cohort (DC) and a replication cohort (RC). The DC has a total of 816 subjects aged between 40 and 89 years coming from 7 different databases: ADNI, ABIDE, FCON, IXI, NKI, PPMI and TAOWU (Figure 2.1)(Table 2.1). The RC contained 687 HI between the age of 42 and 95 from the OASIS-3 database.

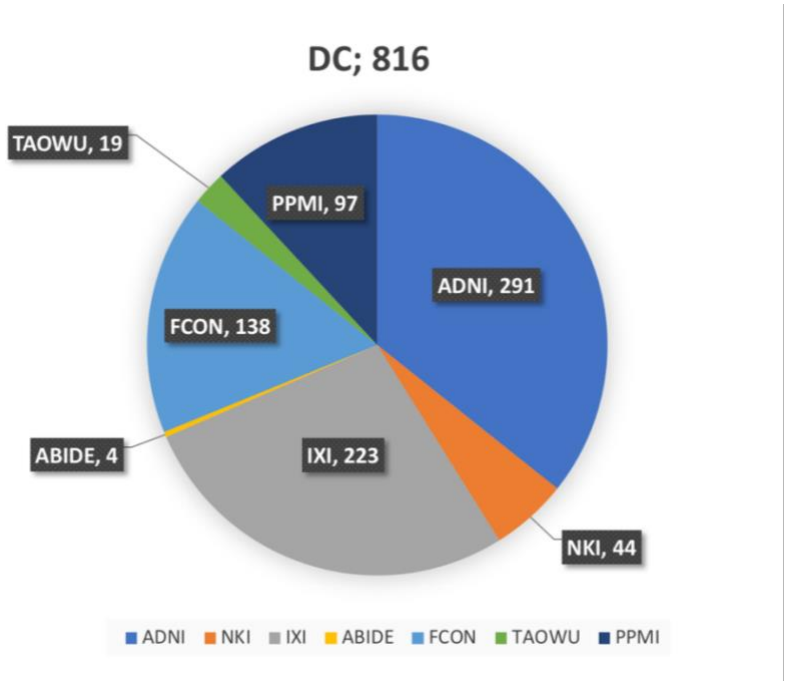

Figure 2.1. Composition of the discovery cohort. *Pie chart illustrating the database composition of the discovery cohort (DC) with the number of subjects.*

Table 2.1 Overview of the different databases of healthy individuals

Healthy Individuals group	Cohort	n (male/female)	Age range (years)
DC	Alzheimer's Disease Neuroimaging Initiative (ADNI) database From the International Neuroimaging Data-Sharing Initiative (INDI), Nathan Kline Institute (NKI) sample Publicly available Information eXtraction from Images (IXI) dataset From the Autism Brain Imaging Data Exchange (ABIDE) dataset.	816 (384 /432)	40 - 89

	Parkinson's Disease Datasets from the International Neuroimaging Data-Sharing Initiative (INDI), Tao Wu dataset From the Parkinson's Progression Markers Initiative (PPMI) From the 1000 Functional Connectomes Project		
RC	Open Access Series of Imaging Studies (OASIS), OASIS-3 Subset: Longitudinal Neuroimaging, Clinical, and Cognitive Dataset for Normal Aging and Alzheimer's Disease	687 (279/408)	42 - 95

DC: discovery cohort, RC: replication cohort

2.1.2 Patient groups

In total 1202 patients between the age of 40 and 92 years were included in the study. Included patients had one of the following disorders: PD, MS, FTLD, MCI or AD. The PD group is composed of three different databases, whereas the other groups originate each from a single database (Table 2.2).

Table 2.2 Overview of the different patient cohorts

Patient Group	Cohort	n (male/female)	Age range (years)
PD	From the Parkinson's Progression Markers Initiative (PPMI) Parkinson's Disease Datasets from the International Neuroimaging Data-Sharing Initiative (INDI), Tao Wu dataset Department of Neurology, University Medical Center of the Johannes Gutenberg University Mainz, Mainz, Germany	289 (182/107)	41 – 82
MS	Department of Neurology, University Medical Center of the Johannes Gutenberg University Mainz, Mainz, Germany	209 (59/150)	40 – 72
FTLD	The Frontotemporal Lobar Degeneration Neuroimaging Initiative from the Laboratory of Neuro Imaging (LONI)	218 (125/93)	44 – 85
MCI	Alzheimer's Disease Neuroimaging Initiative (ADNI) database	401 (218/183)	48 – 92
AD	Alzheimer's Disease Neuroimaging Initiative (ADNI) database	85 (49/36)	56 – 90

AD: Alzheimer's disease, FTLD: frontotemporal lobar degeneration, MCI: mild cognitive impairment, MS: multiple sclerosis, PD: Parkinson's disease

2.2 MRI Preprocessing:

2.2.1 Structural MRI

Magnetic resonance (MR) yields images of different contrasts depending on the relaxation times used (Huk and Gademann, 1984). Short relaxation time or T1-weighted imaging allow to differentiate between brain tissue types according to the signal intensity: the WM is brightest, followed by GM, and cerebrospinal fluid (CSF) (darkest). For comparability of the results, criteria to include participants was based on brain images originated from a 3T scanner with varying acquisition parameters (Table 2.3). MR preprocessing tools such as Freesurfer use image contrast intensities at each voxel to define brain tissues, and then, delineate GM and WM, as well as CSF and GM boundaries to quantify meso- and macro-structural properties of brain.

Table 2.3 Overview of the MRI acquisition parameters for all groups

Cohort/ Group	TR (ms)	TI (ms)	TE (ms)	Flip angle	Slice thickness (mm)	Voxel sizes (mm)	Matrix size (cm^2)
TAOWU	1100	_	3.39	90°	_	1×1×1	_
IXI	9800	_	4.6	8°	1.2	0.94×0.94 ×1.2	240×240
FCON	750 - 3000	_	_	_	1.2	1×1 ×1.2	256×256
ADNI	2300 - 3000	400 - 900	2.9 - 3.5	9 - 11°	1.2	1×1×1.2	256×256
PPMI	2300 - 11000	900	2 – 6	9°	1 – 1.5	1×1×1.2	240×256
MS	1900	900	2.52	9°	1	1×1×1	256×256
NKI	1900	900	2.52	9°	1	1×1×1	256×256
OASIS 3	2400	1000	3.1	8°	1	1×1×1	256×256
ABIDE	1590 - 1800	_	2.7 - 3.1	9 - 10°	1	1×1×1	240×256
FTLD	2300	900	3	9°	1	1×1×1	240×256

TE: echo time, TI: inversion time, TR: repetition time

2.2.2 Freesurfer pipeline

Cortical surface reconstruction and brain segmentation was performed with the Freesurfer image analysis suite, which is freely available for download online (http://surfer.nmr.mgh.harvard.edu/). The technical details of these procedures are described in prior publications (Fischl, 2012). Briefly, this processing includes motion correction and averaging (Reuter et al., 2010) of multiple volumetric T1 weighted images (when more than one is available), removal of non-brain tissue using a hybrid watershed/surface deformation procedure (Segonne et al., 2004), automated Talairach transformation, segmentation of the subcortical WM and deep GM volumetric structures (including hippocampus, amygdala, caudate, putamen, ventricles) (Fischl et al., 2002, Fischl et al., 2004a) intensity normalization (Sled et al., 1998), tessellation of the GM - WM boundary, automated topology correction (Fischl et al., 2001, Segonne et al., 2007), and surface deformation following intensity gradients to optimally place the gray/white and gray/cerebrospinal fluid borders at the location where the greatest shift in intensity defines the transition to the other tissue class (Dale et al., 1999, Dale and Sereno, 1993, Fischl and Dale, 2000). Once the cortical models are complete, a number of deformable procedures can be performed for further data processing and analysis including surface inflation (Fischl et al., 1999a), registration to a spherical atlas which is based on individual cortical folding patterns to match cortical geometry across subjects (Fischl et al., 1999b), parcellation of the cerebral cortex into units with respect to gyral and sulcal structure (Desikan et al., 2006b, Fischl et al., 2004b), and creation of a variety of surface based data including maps of curvature and sulcal depth. This method uses both intensity and continuity information from the entire three dimensional MR volume in segmentation and deformation procedures to produce representations of different morphometric GM properties. These cortical surface maps are created using spatial intensity gradients across tissue classes and are therefore not simply reliant on absolute signal intensity. The maps produced are not restricted to the voxel resolution of the original data thus are capable of detecting submillimeter differences between groups. Freesurfer morphometric procedures have been demonstrated to show good test-retest reliability across scanner manufacturers and across field strengths (Han et al., 2006b, Reuter et al., 2012).

2.2.3 Cortical and subcortical parcellation

The Desikan-Killiany (DK) atlas is one of the standard parcellation schemes used by Freesurfer, which divides the brain into 68 distinct regions. We used this parcellation scheme as it is anatomically valid and reliable, and can be used for morphometric studies (Desikan et al., 2006a).

2.3 Morphometric Measures

2.3.1 Cortical thickness

Cortical thickness (CT), calculated as the closest distance from the grey/white boundary to the gray/CSF boundary at each vertex on the tessellated surface (Fischl and Dale, 2000). Procedures for the measurement of CT have been validated against histological analysis (Rosas et al., 2002) and manual measurements (Kuperberg et al., 2003, Salat et al., 2004). The way CT is computed is by finding the shortest distance from a point on the WM surface, then, taking a point on the pial surface and calculating the shortest distance to the WM surface. The average of both distances is then taken as the CT at that location (Han et al., 2006a).

2.3.2 Cortical thickness standard deviation

A cortical thickness standard deviation (CTSD) computed by Freesurfer is used to represent the variability of CT across different cortical regions.

2.3.3 Surface area

The surface area (SA) of the brain is computed using vertex-wise cortical maps. The SA analyses rely on the registration of the cortical surface and interpolation to a common resolution, which in the case of Freesurfer, is done through the nearest neighbour method (Winkler et al., 2018). The calculation of cortical SA is an essential step early in the Freesurfer pipeline and results from multiple transformations of the MR image. First, the skull is stripped, then voxels corresponding to the WM are identified. A mass of connected WM voxels is then created for each hemisphere, followed by a mesh of triangular faces built around it. The mesh is built using 2 triangles for each exposed voxel face. The mesh of triangles is smoothed and the pial surface (cortical surface) is produced by nudging outward the white surface and inflating it to a sphere. There is a one to one mapping between faces and vertices of the native

brain surfaces and the newly computed sphere. The final surfaces are made of triangular faces from which the cortical SA can easily be computed (Winkler et al., 2012).

2.3.4 Grey matter cortical volume

Grey matter cortical volume (CVol) is a morphometric variable, which essentially represents the product of SA and CT for any given brain region (Cox et al., 2018). On a didactic level, this methods seems like the best way to calculate the CVol at any given point on the cortical surface. Yet, such a method leads to an underestimation of the CVol when the volume of tissue is external to the convexity of the surface (in the case of gyri) and to an overestimation when the volume of tissue is internal to the convexity of the surface (in the case of sulci) (Winkler et al., 2018) (Figure 2.2).

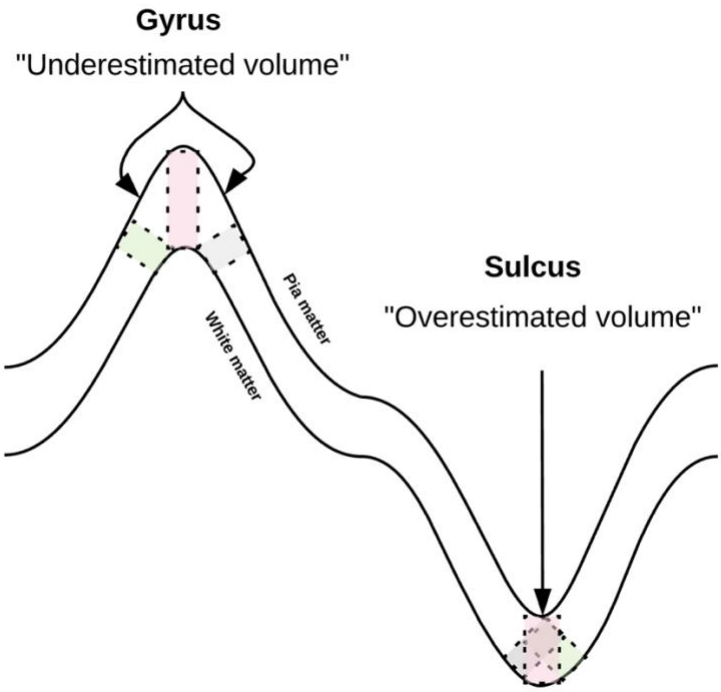

Figure 2.2 Illustration of a gyrus and a sulcus 1. *The product of surface area (SA) and cortical thickness (CT) is depicted as rectangles with the shorter side on the grey matter – white matter border and the long side equivalent to the CT. This method has shown to underestimate the volume in gyri and overestimate it in sulci.*

In the surface-based volume calculation used by Freesurfer, the pial and WM have matching vertices, which delineate an oblique truncated triangular pyramid. The latter structure thereby minimizes any volume calculation inaccuracies (Winkler et al., 2018) (Figure 2.3).

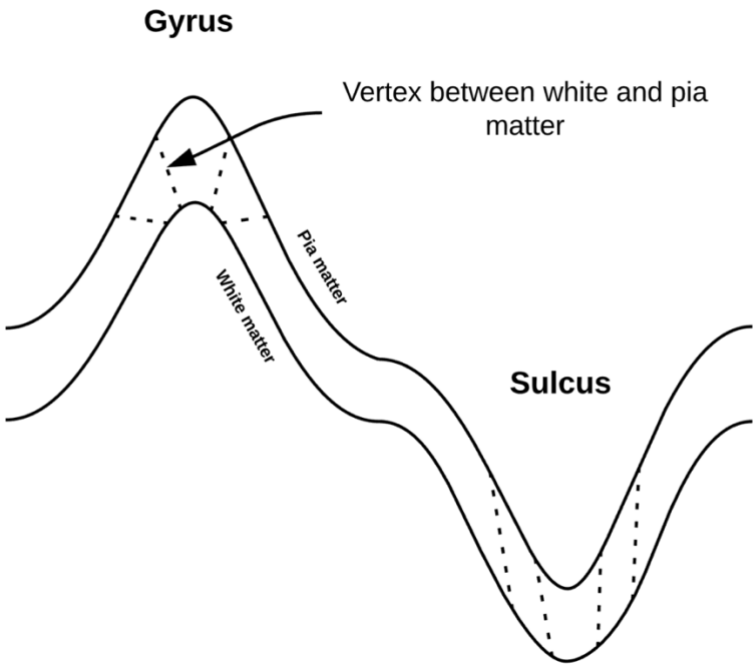

Figure 2.3 Illustration of a gyrus and a sulcus 2. *Here the surface-based volume calculation is used. In this case a matching vertex is computed between pia and white matter, creating an oblique truncated pyramid, which is used for a more precise calculation of the cortical volume (CVol).*

2.3.5 Subcortical volume

An automated subcortical segmentation method has shown to be comparable to manually labeling methods (Fischl et al., 2002). This method relies on the use of global and local spatial information. The global information is generated through statistical classifiers, and the local information is said to be incorporated into the classification by modeling the segmentation as a nonstationary anisotropic Markov random field (Fischl et al., 2002). A six-stage process of the described method in the Freesurfer pipeline results in subcortical structure labelling and computes volumes of the different structures.

2.4 Statistical Analyses

2.4.1 Comparison of brain morphometrics between groups

As previously mentioned in section **2.2**, five different morphometric measures were extracted (CT, CVol, SubVol, SA, CTSD). Here, for each of the morphometric measures a matrix (N x M) was made containing for each subject (N) the corresponding morphometric measures (M). For each variable obtained at the cortex level a total of 68 separate morphometric measures were obtained, corresponding to the 68 brain regions (34

for each brain hemisphere) delineated in the DK atlas (Desikan et al., 2006b). For morphometric variables of subcortical structures (volume), a total of 26 morphometric measures were obtained.

An analysis of variance (ANOVA) was used to compare the actual age of HI with that of the various patient groups. Like an ANOVA, the multivariate analysis of variance (MANOVA) belongs to the general linear model family. However, a MANOVA is commonly used instead of an ANOVA when there are multiple dependent variables (Warne, 2014), as in the current case. The MANOVAs were conducted using the 'ggpubr' package (Kassambara, 2019) in RStudio to evaluate the differences between groups across each cortical region.

Analysis of covariance (ANCOVA) were conducted using the mean across the cortex of each morphometric variable (sum across regions for CVol) as the dependent variable. The subjects' actual age was entered as a covariate in the models. Additionally, since we are dealing with multiple dependent variables, a multivariate analysis of covariance (MANCOVA) was used to explore the effects of groups and gender. Again, the actual age was used as a covariate, and both group and gender as factors.

In summary, ANCOVAs were performed to compare the variance in means across all groups for each morphometric variable and MANCOVAs were performed to compare the variance across all brain regions and groups for each morphometric variable. Both statistical tests were conducted using the 'jmv' package (Ravi Selker, 2019) in RStudio.

2.4.2 Regression analysis for brain age prediction

The preprocessed MRI data from the Freesurfer pipeline was fed for further analysis to different machine learning algorithms, aiming at predicting individual's age according to MRI-derived brain integrity measures. Besides the 5 variables computed from Freesurfer, 2 additional variables were put together to form combined variables. The 2 combined variables are CT + SubVol, and, CVol + SubVol. The combined variables thereby consisted of a total of 94 morphometric measures.

Training of the prediction algorithms was first conducted using the DC. In a first step, this group was divided into training set (80% of subjects) and a test set (the rest 20 % of the group participants, from now on discovery group – DG). To validate the algorithms, after the parameters for each algorithm were adjusted in the discovery 80% training set, each of the patient groups (MCI, PD, FTLD, AD, and MS) was further used as the validation set (Figure

2.4). From now on the latter set of predictions will be refered to as the main analysis. The main analysis set was repeated but dividing the groups into males and females and run for each separately. An additional replication analysis was conducted, which was identical to the main analysis with the difference of using a different cohort of HI, namely the replication group (RG) for training and testing. This replication analysis was again validated on all the patient groups and independently conducted for males and females. The main outcomes of the main analysis and replication analysis were individualized predicted ages. In order to provide objective scores of the algorithm performance R^2-coefficient, mean absolute error (MAE) and median absolute error (MdAE) for each set of age predictions were extracted.

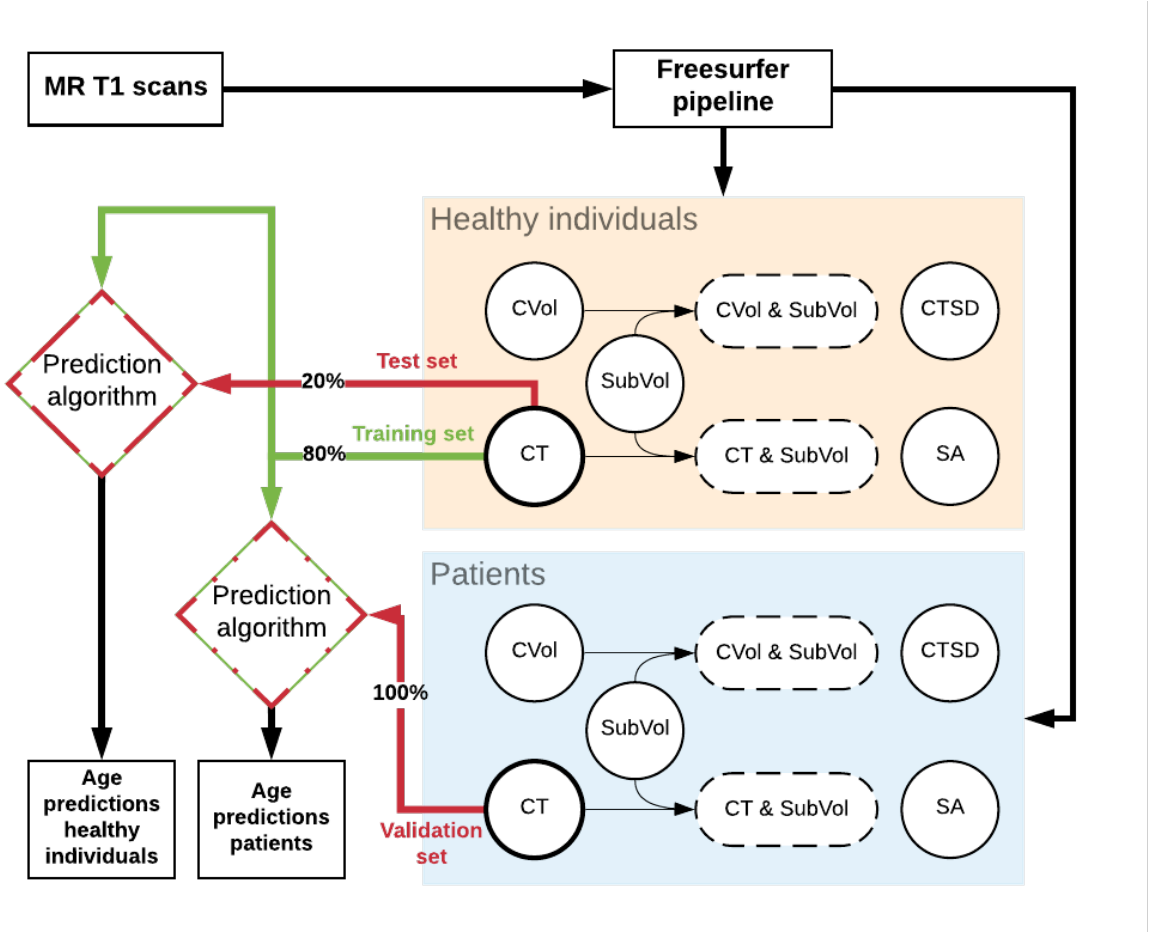

Figure 2.4 From MR scans to age predictions. *This figure illustrates the steps of analysing the acquired MR T1 brain scans. The 3T MR sagittal scans were processed by the Freesurfer software. Then, the following 5 morphometric measures were extracted: cortical thickness (CT), cortical volume (CVol), subcortical volume (SubVol), surface area (SA) and cortical thickness standard deviation (CTSD). CT and SubVol were combined in a table to create the new variable CT & SubVol. CVol and SubVol were combined in a table to create the new variable Cvol & SubVol. Starting from one variable (for example CT), healthy individuals were separated into a training (80% of individuals) and a test set (20% of individuals). The prediction algorithm was then trained and tested to yield the age predictions for the healthy individuals. For the age prediction in patients, 100% of subjects were taken as the validation set, and still the same cohort of healthy individuals (80%) was taken as the training set.*

2.4.3 Statistical learning algorithms used for brain age prediction

All statistical learning algorithms were run in **RStudio** version 1.1.456 (R Core Team, 2018), the open source professional software for data analysis. The morphometric measures data at each brain region were extracted from Freesurfer and summarized into an Excel table, then imported to **RStudio** using the "readxl" package (Bryan, 2019). Three different packages were used to implement the 5 different statistical learning algorithms to our data: the "caret" package (Max Kuhn et al., 2018) for the linear regression, "glmnet" package (Jerome Friedman, 2010) for the least absolute shrinkage and selection operator (LASSO), ridge regression (RR) and elastic net regression (EN), and finally, the "e1071" package (David Meyer, 2018) for the for the support vector regression (SVR). Additionally, a sperate spline based multiple regression toolbox (PRISM) for MATLAB, was used for comparison. The latter regression is described as using regularization, dimensionality reduction, and feature selection, through a combination of smoothing spline regression, PCA, relevance vector regression (RVR) and LASSO (Madan, 2016).

2.4.4 Brief introduction to statistical learning

The benefit of using statistical learning tools is that they can encompass and simultaneously process a large amount of information, which would have otherwise been uninterpretable. They usually require a series of input variables on which the model will be built and trained to "learn" one output variable. Then, the trained model can be used to predict the output variable in previously unseen data. In our case, the input variables are the large set of regional GM morphometric measures obtained from the T1-weighted MRI through FreeSurfer, whereas the output variable is the actual age of any given subject at the time of MRI acquisition.

Regardless of the statistical learning tool being used, all methods work by finding an estimate of the function $\boldsymbol{f}$, which describes as precisely as possible the relationship between the independent input variables $\boldsymbol{X}$ (GM morphometrics) and the dependent output variable $\boldsymbol{Y}$ (actual subject age).

$$\boldsymbol{Y} = \boldsymbol{f}(\boldsymbol{X}) + \boldsymbol{\epsilon} \qquad (1)$$

To find this estimate of the true function $\boldsymbol{f}$ (1), a statistical learning tool requires a so-called "*training set*", which, in this case, is a random subset of subjects each with their corresponding morphometric data and age. From these inputs and corresponding output, a statistical learning tool can estimate the function $\boldsymbol{f}$. The resulting function is $\hat{\boldsymbol{f}}$(2). Using the estimated function $\hat{\boldsymbol{f}}$ one can find the value of $\widehat{\boldsymbol{Y}}$, which is a prediction of any given subject's actual age $\boldsymbol{Y}$**.**

$$\widehat{\boldsymbol{Y}} = \hat{\boldsymbol{f}}(\boldsymbol{X}) + \boldsymbol{\epsilon}$$
$$\hat{\boldsymbol{f}}(\boldsymbol{X}) = \widehat{\boldsymbol{Y}} - \boldsymbol{\epsilon} \qquad \textit{(2)}$$

To make a such a prediction, a statistical learning tool will require a so-called ***"test set"****(James et al., 2017)*. In our case the test set is the remaining set of subjects, which were not contained in the training set. This time, however, only the morphometric data (**X**), without age values is entered to the model. The statistical tool will then calculate the so called "predicted age" ($\widehat{\boldsymbol{Y}}$) based on the function $\hat{\boldsymbol{f}}$ estimated earlier. The closer the predicted age is to the actual age of the subject, the higher was the accuracy of that prediction. The accuracy of this prediction depends on two factors: the reducible and the irreducible error.

The value of the irreducible error is $\boldsymbol{\epsilon}$. $\boldsymbol{Y}$ is a function of $\boldsymbol{\epsilon}$, which by definition cannot be predicted using $\boldsymbol{X}$, making this error "irreducible". The irreducible error is the collection of all immeasurable variables, which are also useful in predicting $\boldsymbol{Y}$ but are not available or are impossible to account for. In our case, such immeasurable variables could for example be the hydration level of the subject at the day the MRI was made. Such a variable could have potentially influenced the brain morphology, and thus is actually missing from the data used to estimate $\boldsymbol{f}$ and compute the subject's real age. The irreducible error is the reason why the predicted age can never be perfectly equal to the actual age in all subjects, and refers to all the unknown factors that cannot be controlled for.

On the other hand we have the reducible error, which results from the imperfect estimate of the function $\boldsymbol{f}$. This error, as its name suggests, can be reduced by using the most appropriate statistical learning method. The search for a reasonable statistical learning method was one of the main focus of this study, since thereby the accuracy of the age prediction could be increased.

There are two main methods, which work differently in estimating $\boldsymbol{f}$: parametric and non-parametric methods. Parametric methods make assumptions about the shape of the

function whereas non-parametric methods don't. For instance, an example of a parametric method would be to assume that $\boldsymbol{f}$ is linear. This means that in our case, the function would assign a regression coefficient $\boldsymbol{\beta}$ to each of our variables, which would either mean the morphometric variable has a positive or a negative correlation with the subject's actual age. Such a method would have a high interpretability, since it will give hints on which variable actually contributes in predicting the age. A low interpretability is expected from non-parametric methods, which have such complex estimates of $\boldsymbol{f}$ that it is hard to tell, which variables are associated with the response.

On the other hand, non-parametric methods do not assume that the function $\boldsymbol{f}$ has a specific shape. They take whatever shape the function of the training set has and applies it to the test set. Such methods are described as highly flexible. The downside of non-parametric methods is that they have a very low interpretability. One other major problem of highly flexible methods is overfitting. Overfitting means that a function adheres so much to data points in the training set that it picks up patterns that are just caused by random chance rather than by true properties of the unknown function. In that sense, overfitting becomes problematic for the prediction since a function that fits like a glove on the data points in the training set (Figure 2.5), is very unlikely to accurately predict the test data unless the test set has a similar variance to the training set. In other words, if the training set has a significantly different variance than the test set, the prediction using a highly flexible method is likely to reduce its accuracy.

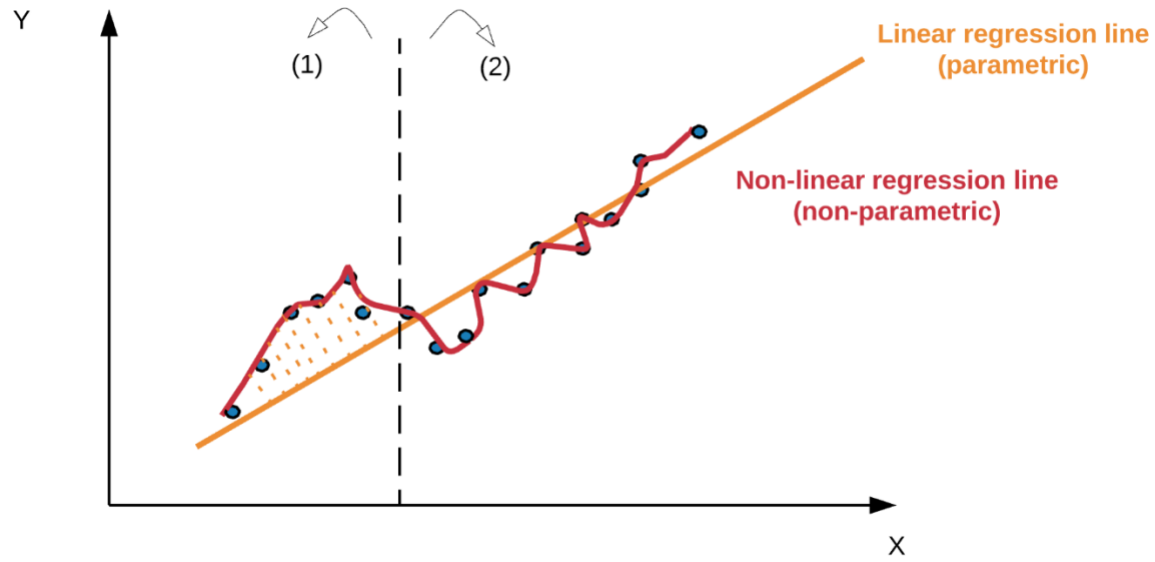

Figure 2.5 Linear and non-linear, non-parametric regression*. Example of a data simulation with the function f estimated with a linear regression method and a non-linear, non-parametric regression method. The latter is an example of an extremely flexible method, which goes through all points. On the first side of the graph (1), the linear regression line makes an error about the shape of the function (shown by the orange dashed lines), whereas the non-parametric method correctly adjusts to its shape. On the second side (2) however the points have a linear tendency, which could be well explained by the linear*

Generally one can say that methods with high interpretability, such as linear regression, have a low flexibility, and methods with high flexibility, such as SVMs, have a low interpretability. If one is more interested in the relationship between the input and output variable, one should choose a method with a high interpretability. If one wishes to predict a seemingly non-linearly explainable set of data, one should choose a more flexible method. In our case, we chose methods of both kinds. It is important to note that there is not one method which will dominate all others over all possible datasets.

2.4.5 Assessing the performance of statistical learning models

The performance of a model refers to how close the age predictions were to the actual ages. One way of assessing the performance of a model is by calculating the mean squared error (MSE) of its training set. The MSE tells us how close the predicted and actual age of the subjects were. A model will generally try to keep the training MSE as low as possible. Highly flexible models will usually have very low training MSE's. However, such methods tend to have high test MSE's. Such a combination of very low training MSE and high test MSE is a classic result of overfitting through a flexible method.

Since we are interested in precisely predicting a subject's actual age, we need to find a systematic way of reducing the test MSE as much as possible. One classical way of doing this is through cross validation (CV). A CV estimates what the MSE of the test set could potentially be, based only on the training data. Note that the real test MSE will be computed, not estimated, after the age predictions in the test set are performed. A CV usually selects from a series of model parameters, the best ones, which might lead to a low test MSE. Henceforth, selected model parameters are to be used on the test data, which hopefully will lead to a higher age prediction accuracy. In our case we chose a 10-fold CV method, which essentially splits the training data into 10 sets, then chooses 1 set to estimate the test MSE. As stated previously, we have tried several different regression methods with different morphometrics combinations so as to maximize the age prediction accuracy. In order to fully understand what makes a model have a better test set performance than another, we need to understand the concepts of model variance and bias.

Model variance is the amount by which our estimated function $\hat{f}$ would change if we estimated it using a different training data set. In other words, a model with a high variance will have a large change in its estimated function $\hat{f}$ when small changes are made to the training set. Consequently, models with a high flexibility would have an increased model variance. Model bias, on the other hand, is the error introduced by approximating a real-life problem, which may be extremely complicated. In our case, our real-life problem is indeed very complicated: brain ageing cannot possibly be explained by a single function, which takes into account every possible variable. As a result, our bias will never be zero. Yet, highly flexible methods tend to have low bias in comparison to less flexible ones since, as explained previously, they do not make assumptions about the true shape of f. Hence, a well-adjusted model needs to have both, a low variance and bias, in order to have a good test set performance.

2.4.6 First model: multiple linear regression

The first predictive model we are going to use is the multiple linear regression (MLR) (Lai et al., 1978). MLR is an extension of simple linear regression that explains the association between an observed value and a predicted value of the variable. It is a simple, yet widely used method to evaluate the effect of multiple variables on one output variable. In our case, such a model also tells us if at least one of the brain morphometrics will be useful in predicting age. Additionally, a MLR indicates whether all brain morphometrics are useful in predicting

age or whether just a subset of them are useful. Any MLR will take the form of a general linear model, where $\boldsymbol{Y}$ is the actual age of a subject, $\boldsymbol{X_p}$ the $\boldsymbol{p^{th}}$ morphometric variable, $\boldsymbol{\beta_p}$ the corresponding regression coefficient, and $\boldsymbol{\epsilon}$ the value of the irreducible error (3).

$$\boldsymbol{Y = \beta_0 + \beta_1 X_1 + \beta_2 X_2 + \cdots + \beta_p X_p + \epsilon} \qquad \textit{(3)}$$

In our case, the MLR will use the method of minimizing the sum of squared residuals (**SSR**) to create the function. To evaluate how well our model actually fitted the data we computed the residual standard error (RSE) and R^2 of every linear model using RStudio. RSE is the average amount that the response will deviate from the true regression line. It is associated with irreducible error $\boldsymbol{\epsilon}$ and is considered a measure for the *lack of fit* of the model to the data. RSE has shown to be lower when only the relevant variables are present in the model. For example, if RSE=9 for a given model, then the actual age of each subject will deviate from the true regression line an average of 9 years. The other way of evaluating how well the model fits the data is by computing R^2. R^2 is the proportion of variance in age that can be explained by the morphometrics. It has a value between 0 and 1, where 1 means that 100% of the variance in age can be explained by the morphometrics. R^2 tends to increase when more variables are added to the model, even if those are only weakly associated with the response. In our case we will be using R^2 rather than RSE to evaluate how well our models fit to the data.

2.4.7 Second model: ridge regression

The ridge regression (RR) (Tikhonov and Arsenin, 1977) is a type of MLR, which uses a different mechanism of finding the regression coefficients $\boldsymbol{\beta}$. As previously stated, MLR's generally try to minimize the **SSR** in order to find the regression coefficient for each morphometric variable. It is so called the least squares method. On the other hand, a RR tries to minimize **SSR** and $\boldsymbol{\lambda}$ multiplied by the sum of all regression coefficients squared (4).

$$\boldsymbol{SSR + \lambda(\beta_1{}^2 + \beta_2{}^2 + \cdots + \beta_p{}^2)} \qquad \textit{(4)}$$

$\boldsymbol{\lambda(\beta_1{}^2 + \beta_2{}^2 + \cdots + \beta_p{}^2)}$ adds a penalty to the traditional least squares method and $\boldsymbol{\lambda}$ determines how severe that penalty is. In order to keep the equation (4) to a minimum, the RR not only needs to keep the squared residuals, but also the regression coefficients $\boldsymbol{\beta}$, to a

minimum. Keeping the regression coefficients to a minimum means that the slopes of the lines are going to be less steep than the slopes of the conventional least squares method. Such a method leads to a regression line that is less adherent to the training data. By increasing the value of $\boldsymbol{\lambda}$, one will increase the penalty, which will result in regression lines that are even less adherent to the training set. Finding the right $\boldsymbol{\lambda}$ value so as to keep the equation (4) to a minimum is done through CV. In **RStudio**, the $\boldsymbol{\lambda}$ value associated with the lowest root mean square error is selected. The resulting regression line is one that has a lower variance but a higher bias than the common least squares fit line. By increasing the value of $\boldsymbol{\lambda}$, one can essentially decrease the flexibility of a RR.

2.4.8 Third model: least absolute shrinkage and selection operator (LASSO)

The least absolute shrinkage and selection operator (LASSO) (Tibshirani, 1996) and RR are in a way very similar to each other. While a RR tries to minimize the penalty in the form of: $\boldsymbol{\lambda(\beta_1{}^2 + \beta_2{}^2 + \cdots + \beta_p{}^2)}$, the LASSO tries to minimize the absolute values of the regression coefficients (5).

$$\boldsymbol{SSR + \lambda(|\beta_1| + |\beta_2| + \cdots + |\beta_p|)} \qquad \textit{(5)}$$

This method leads as well to a regression with a lower variance and a higher bias. The difference is, as the value of $\boldsymbol{\lambda}$ gets larger, regression coefficients with a low absolute value approach 0. Thereby, only regression coefficients, which have a relatively high value are kept in the equation. In other words, LASSO "selects" which morphometric variables are most relevant for predicting age and discards all the other ones.

2.4.9 Fourth model: elastic net regression

Our last MLR model, the elastic net regression (EN) (Zou and Hastie, 2005), is a combination of RR and LASSO. An EN tries to minimize the **SSR** as well as the sum of the RR and LASSO penalties (6).

$$\boldsymbol{SSR + \lambda_1(\beta_1{}^2 + \beta_2{}^2 + \cdots + \beta_p{}^2) + \lambda_2(|\beta_1| + |\beta_2| + \cdots + |\beta_p|)} \qquad \textit{(6)}$$

Note that each penalty has its own $\boldsymbol{\lambda}$ ($\boldsymbol{\lambda_1}$ **&** $\boldsymbol{\lambda_2}$), which are computed separately through ***cv***. In **RStudio**, CV chooses the combination of $\boldsymbol{\lambda}$'s, which yield the lowest RMSE. The benefit of EN is that it balances between keeping all regression coefficients (like in a RR) and removing those, which have a low value (like in the LASSO). This way EN produces a function, which contains a number of regression coefficients between the number of coefficients in a RR and in a LASSO. Since we are dealing with a complex model with many morphometric measures, which may or may not impact our age prediction, an EN seems like an appropriate tool for automatically choosing the variables for the predictions.

2.4.10 Fifth model: support vector machine

The support vector mashine (SVM) (Cortes and Vapnik, 1995) is often used for classification problems and generally works by creating a hyperplane, which separates two sets of data from another. This hyperplane is accompanied by support vectors, which are the points in a set that belong to one class, yet at the same time are very close to the opposing class.

In our case we have not used SVM for a classification, but for a regression problem. Henceforth, the term support vector regression (SVR) (Drucker et al., 1997) will be used. The benefit of using SVR is that one can use a "radial" kernel, which allows for a non-linear fit of the data. Such a kernel transforms the data into higher dimensional feature space in order to accommodate any form the function $\boldsymbol{f}$ may take. This is of course the reason why SVR's have such a high flexibility.

Generally, a SVR creates a tube around the estimated function $\boldsymbol{f}(\boldsymbol{x})$ with data points lying outside, and data points lying outside the tube. Data points that lie inside the tube do not influence the course of the regression line (Franke et al., 2010). Data points that lie on the edge or outside this tube are called support vectors. Support vectors are used by SVR's to fit the estimated function to the data points in the training set (Figure 2.6).

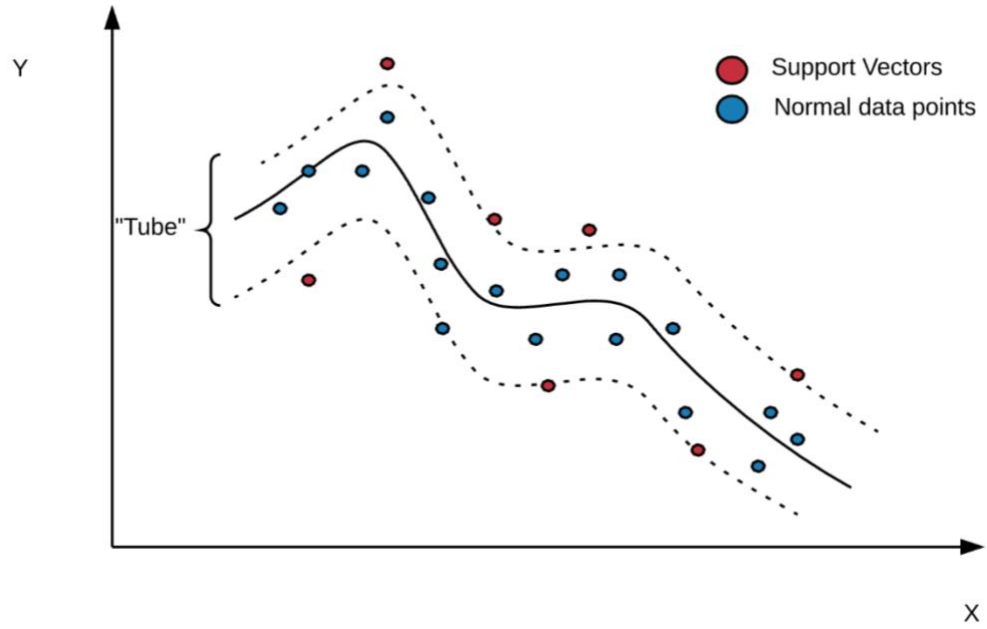

Figure 2.6 Illustration of a function estimated using a SVR. *Data points in red lying on the edge of the tube or outside the tube are called support vectors and are used to estimate the shape of the function.*

2.4.11 Sixth model: PRISM toolbox

The last model is a machine learning toolbox put together by Christopher R. Madan, utilizing a combination of RVR and LASSO, which is preceded by a PCA for dimensionality reduction (Madan, 2016). A RVR essentially functions the same way as a SVR except that it limits the number of support vectors used for creating the estimated function (Franke et al., 2010). It uses an automatic relevance determination to compute which features or variables contribute most in predicting the output variable. The benefit of using Madan's PRISM toolbox is to compare its age predictions to predictions from our other models using the same training and validation sets.

2.5 Clinical Tests Used for the Regression Analysis

All test scores were taken from the source from which the MRI scans were also acquired.

2.5.1 Mini-Mental State Examination (MMSE)

The Mini-Mental State Examination (MMSE) is a 15 minute test, which measures global cognitive impairment. It is composed of 6 areas: orientation in time and space, memory, attention and calculation, language and constructional praxis (Battista et al., 2017). The score

can range from 0 to 30 points, with 30 points indicating normal cognition. The MMSE scores of MCI, FTLD and AD patients were used for the clinical regression analysis (Table 2.4).

2.5.2 Delayed memory recall test (LDELTOT) & immediate memory recall test (LIMMTOT)

The delayed memory recall test (LDELTOT) & the immediate memory recall test (LIMMTOT) are part of the Logical Memory, a subtest in the Wechsler Memory Scale-Revised (Battista et al., 2017). For these two tests, a brief story is read to the patient out loud. For LIMMTOT, the patient is instructed to repeat the story immediately after the story is read, and the total number of story units recalled is recorded. Similarly, the LDELTOT assesses the ability to recall story units after 20 or 30 minutes (Chapman et al., 2016). Both tests were found appropriate measures for memory function in patients with MCI and were thus used for regression with clinical variables. ADNI implements cutoff scores for the LDELTOT, which are based on the person's education and range from 3 to 9 points for normal cognition (Table 2.4).

2.5.3 Unified Parkinson's disease rating scale (UPDRS)

The unified Parkinson's disease rating scale (UPDRS) is used to monitor the clinical manifestation of PD in patients over the course of time. It has four main sections for: assessing cognitive function, rating activities of daily living, examining motor manifestations of PD, and investigating therapy complications. Out of the four sections only part III was used, which is the motor evaluation done by the trained health professional. The UPDRS part III was used for the clinical regression and has a maximum of 108 points, which represents the worst possible disability (Perlmutter, 2009) (Table 2.4).

2.5.4 Clinical Dementia Rating (CDR)

The Clinical Dementia Rating (CDR) is used to evaluate the severity of dementia for patients in clinical and research settings. The CDR is used to assess function in the following areas: memory, orientation, judgement & problem solving, community affairs, home & hobbies, and personal care (O'Bryant et al., 2008). It has a five-point scale (0, 0.5, 1, 2 and 3 points). With increasing score the severity of the impairment increases. The CDR was used as the clinical regression variable for patients with FTLD (Table 2.4).

2.5.5 Expanded Disability Status Scale (EDSS)

The Expanded Disability Status Scale (EDSS) is commonly used to quantitively assess the level of disability in patients with MS. The EDSS encompasses the evaluation of the visual, brainstem, pyramidal, cerebellar, sensory, bowel and bladder, cerebral and ambulation functions, which can be more or less affected by the progressing disease (Sen, 2018). The scoring system goes from 0 to 10 points, where 0 represents a normal neurological status, and 10, death due to MS (Table 2.4).

Table 2.4 Overview of clinical tests and scores. *The following table gives an overview of the different clinical tests and scores that were utilized in the regression with the age variables.*

	MMSE	**LDELTOT & LIMMTOT**	**UPDRS part III**	**CDR**	**EDSS**
Score range	0 – 30	-*	0 – 108	0 – 3	0 – 10
Score interpretation	Higher score →**lower** morbidity	Higher score → **lower** morbidity	Higher score → **higher** morbidity	Higher score →**higher** morbidity	Higher score → **higher** morbidity
Patient groups for which clinical test was used	MCI, FTLD & AD	MCI	PD	FTLD	MS

AD: Alzheimer's disease, CDR: Clinical Dementia Rating, EDSS: Expanded Disability Status Scale, FTLD: frontotemporal lobar degeneration, LDELTOT: delayed memory recall test, LIMMTOT: immediate memory recall test, MCI: mild cognitive impairment, MMSE: Mini-Mental State Examination, MS: multiple sclerosis, PD: Parkinson's disease, UPDRS: Unified Parkinson's disease rating scale,.
**The normal score range for LDELTOT depends on the education level of the test taker and lies between 3-9 points.*

3. Results

3.1 Differences in Morphometric Measures Across Neurodegenerative Diseases

3.1.1 Mean morphometrical measures differentiate across neurodegenerative groups

The ANCOVA evaluating the difference between groups in CT, showed main effects of group ($F(6,2691) = 62.69$, $p = 2e\text{-}16$). In MCI and PD patients, mean CT values were comparable to both cohorts of HI ($p = 0.99$ in both cases) (Figure 3.1).

The ANCOVA evaluating the difference between groups in CVol, showed main effects of group ($F(6,2691) = 42.86$, $p = 2e\text{-}16$). In MCI and FTLD patients, CVol values were comparable to HI ($p = 0.11$ and $p = 0.15$ respectively) and to each other ($p = 0.99$). Similarly, CVol values were comparable in PD and MS patients ($p=0.11$) (Figure 3.1).

The ANCOVA evaluating the difference between groups in mean SubVol, showed main effects of group ($F(6,2691) = 70.34$, $p = 2e\text{-}16$). AD patients had comparable mean SubVol values to FTLD, MCI and HI ($p = 0.63$, $p = 0.27$ and $p = 0.21$ respectively). In MCI and FTLD patients, mean SubVol values were comparable to HI ($p = 1$ and $p = 0.99$ respectively) and to each other ($p = 0.99$), as it was the case with CVol (Figure 3.1).

The ANCOVA evaluating the difference between groups in mean SA, showed main effects of group ($F(6,2691) = 31.05$, $p = 2e\text{-}16$). AD patients had comparable mean SA values to FTLD, MCI and MS patients ($p = 0.21$, $p = 0.07$ and $p = 0.09$ respectively). FTLD patients had comparable mean SA values to MCI, MS and HI ($p = 0.99$ for all three). MS patients had comparable mean SA values to MCI patients ($p = 0.99$) (Figure 3.1).

The ANCOVA evaluating the difference between groups in mean CTSD, showed main effects of group ($F(5,2006) = 86.11$, $p = 2e\text{-}16$). MS patients had comparable mean CTSD values to AD patients ($p = 0.11$) and PD patients had comparable mean CTSD values to FTLD patients ($p = 0.24$) (Figure 3.1).

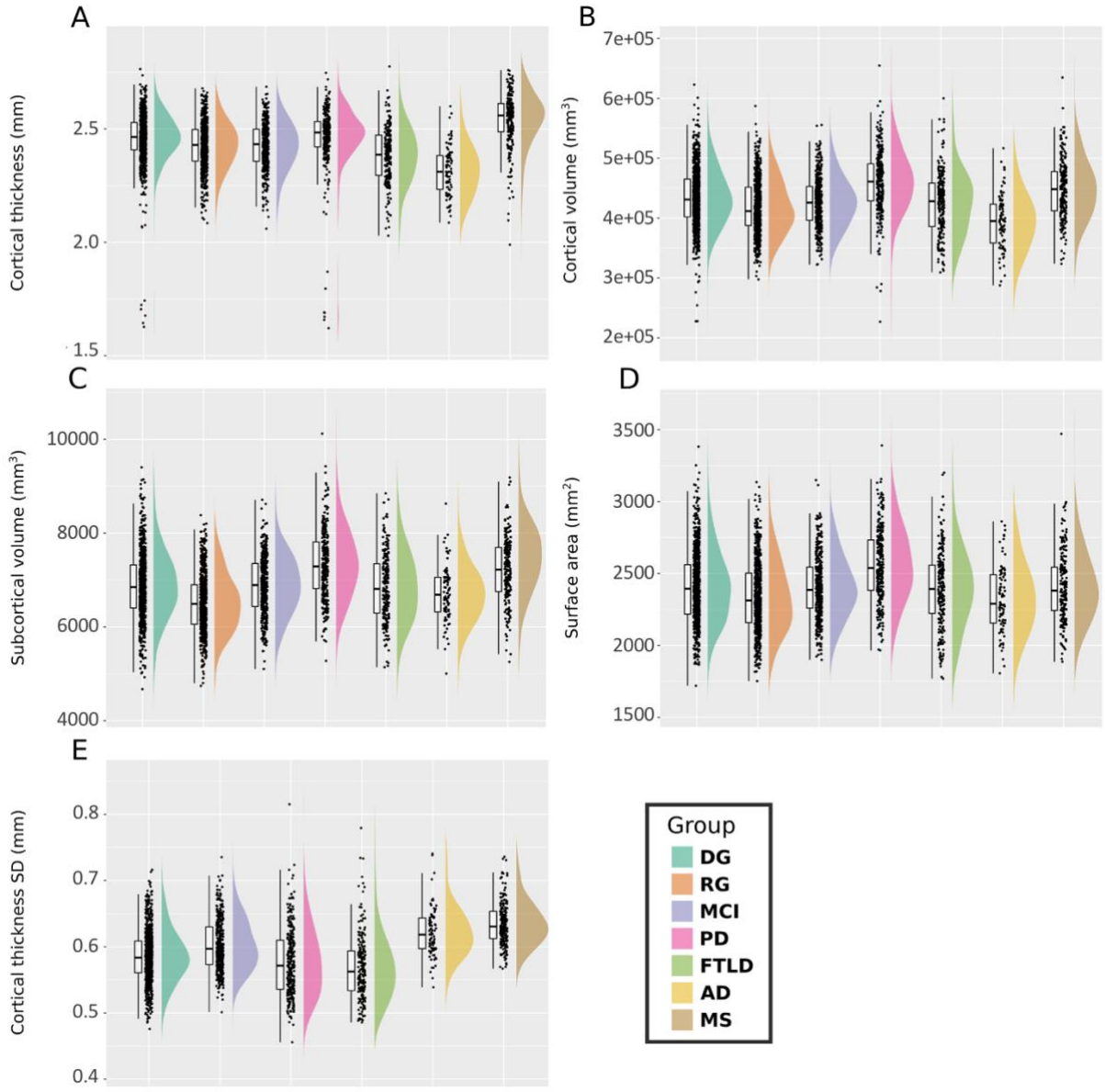

Figure 3.1 Plots of brain morphometrics across groups. *The morphometric plots are from the following groups: discovery group (DG), replication group (RG), mild cognitive impairment (MCI), Parkinson's disease (PD), frontotemporal lobar degeneration (FTLD), Alzheimer's disease (AD) and multiple sclerosis (MS). A) mean cortical thickness (CT) in mm, B) cortical volume (CVol) in mm³, C) mean subcortical volume (SubVol) in mm³, D) mean surface area (SA) in mm², E) mean cortical standard deviation (CTSD) in mm. The plots depict combined right and left hemispheres.*

3.1.2 Sex differentiates mean morphometric measures across neurodegenerative groups

The ANCOVA evaluating the difference between groups in CT, showed main effects of group in males (F(6,1282) = 24.43, p = 2e-16) and females (F(6,1395) = 37.48, p = 2e-16). Also, the factor sex showed main effects (F(1,2683) = 29.77, p = 5.3e-08). In male MCI and PD patients, mean CT values were comparable to male HI (p = 0.99 in both cases). Male FTLD patients had comparable mean CT values to AD, MCI and male HI (p = 0.11, p = 0.20 and p =

0.13 respectively). Similar to the males, female PD patients had comparable mean CT values to female HI (p = 0.90). On the other hand, female MCI patients had comparable mean CT values to PD patients and female HI (p = 0.14 and p = 0.13 respectively) (Figure 3.2).

The ANCOVA evaluating the difference between groups in CVol, showed main effects of group in males (F(6,1282) = 25.59, p = 2e-16) and females (F(6,1395) = 30.71, p = 2e-16). Also, the factor sex showed main effects (F(1,2683) = 728.19, p = 2e-16). In male MCI, CVol values were comparable to male HI (p = 1), and male PD patients had comparable values to male MS patients (p = 0.43). Male FTLD patients had comparable CVol values to MCI and male HI (p = 1 and p = 0.10 respectively). Similarly, female FTLD patients had comparable CVol values to female MCI patients and female HI (p = 0.45 and p = 1 respectively) Also, in female MCI patients, CVol values were comparable to female HI (p = 0.58), and female PD patients had comparable values to female MS patients (p = 1) (Figure 3.2).

The ANCOVA evaluating the difference between groups in mean SubVol, showed main effects of group in males (F(6,1282) = 30.98, p = 2e-16) and females (F(6,1395) = 56.16, p = 2e-16). Also, the factor sex showed main effects (F(1,2683) = 794.82, p = 2e-16). Male AD patients had comparable mean SubVol values to male FTLD, MCI and HI (p = 0.23, p = 0.29 and p = 0.08 respectively). In male MCI and FTLD patients, mean Subvol values were comparable to male HI (p = 0.98 and p = 1 respectively) and to each other (p = 1). Mean SubVol values were comparable in male PD and MS patients (p=0.27). Similar to male patients, female AD patients had comparable mean SubVol values to female FTLD, MCI and HI (p = 1, p = 0.56 and p = 0.19 respectively). In female MCI and FTLD patients, mean Subvol values were comparable to female HI (p = 0.94 and p = 1 respectively) and to each other (p = 1). Mean SubVol values were comparable in female PD and MS patients (p=1) (Figure 3.2).

The ANCOVA evaluating the difference between groups in mean SA, showed main effects of group in males (F(6,1282) = 14.64, p = 2e-16) and females (F(6,1395) = 17.74, p = 2e-16). Also, the factor sex showed main effects (F(1,2683) = 1110.56, p = 2e-16). Male AD patients had comparable mean SA values to male FTLD, MCI patients and HI (p = 0.13, p = 0.22 and p = 0.31 respectively). Male FTLD patients had comparable mean SA values to male MCI, MS and HI (p = 1, p = 0.05, and p = 0.96 respectively). Male MS patients had comparable mean SA values to male PD patients and HI (p = 0.96 and p = 0.12 respectively). Male MCI patients had comparable mean SA values to HI (p = 0.44). Similar to the males, female AD patients had comparable mean SA values to female FTLD, MCI patients and HI (p = 0.89, p = 0.06 and p = 0.92 respectively). Female FTLD patients had comparable mean SA values to MCI and HI (p =

0.24 and p = 0.08 respectively). Female MS patients had comparable mean SA values to female MCI patients and HI (p = 0.39 and p = 0.33 respectively). Female MCI patients had comparable mean SA values to female HI (p = 1) (Figure 3.2).

The ANCOVA evaluating the difference between groups in mean CTSD, showed main effects of group in males (F(5,1005) = 45.91, p = 2e-16) and females (F(5,989) = 45.07, p = 2e-16). Also, the factor sex showed main effects (F(1,1999) = 15.92, p = 6.85e-05). Male MS patients had comparable mean CTSD values to male AD patients (p = 0.66) and male PD patients had comparable mean CTSD values to male FTLD patients and HI (p = 0.34 and p = 0.14 respectively). Similarly, female PD patients had comparable mean CTSD values to female FTLD patients and HI (p = 0.93 and p = 0.17 respectively). Female AD patients had comparable mean CTSD values to female MCI and MS patients (p = 0.19 and p = 0.07 respectively) (Figure 3.2).

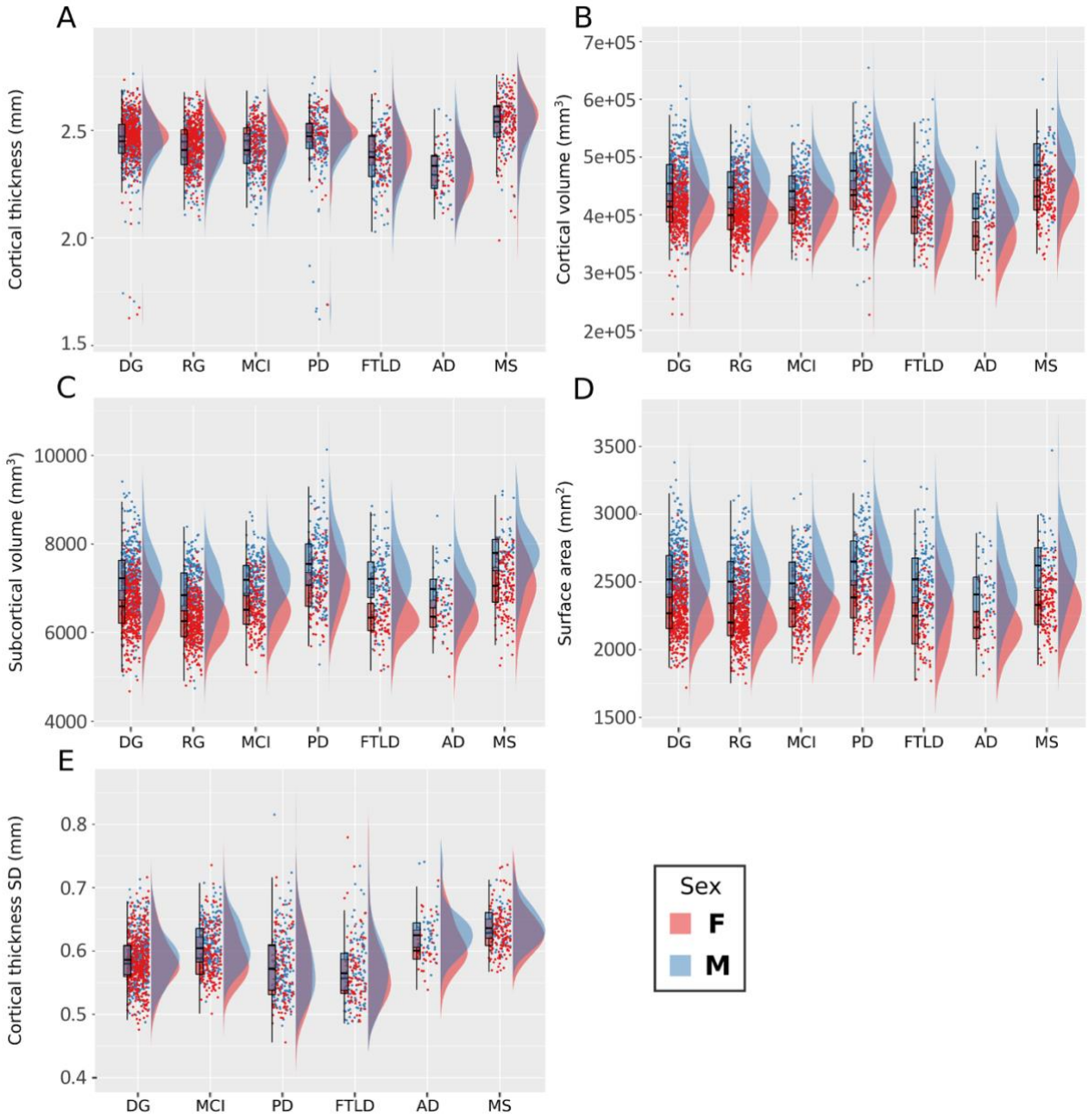

Figure 3.2 Plots of brain morphometrics grouped by sex. *The morphometric plots are from the following groups: discovery group (DG), replication group (RG), mild cognitive impairment (MCI), Parkinson's disease (PD), frontotemporal lobar degeneration (FTLD), Alzheimer's disease (AD) and multiple sclerosis (MS). A) mean cortical thickness (CT) in mm, B) cortical volume (CVol) in mm³, C) mean subcortical volume (SubVol) in mm³, D) mean surface area (SA) in mm², E) mean cortical standard deviation (CTSD) in mm. The plots depict combined right and left hemispheres.*

3.1.3 FTLD patients and the DG differ in regional CT and SubVol

FTLD patients had the highest number of significantly different CT regions when compared to DG (64 regions). Similarly, PD for CVol (63 regions), FTLD for SubVol (24 regions), PD for SA (67 regions), and MS for CTSD (60 regions) (Table 3.1).

Table 3.1 Summary of MANOVAs: discovery group (DG). *The following summary table depicts the number of significant regions when comparing each patient group to the discovery group (DG) across each variable.*

Group	No. of CT regions (p-value, F-value)	No. of CVol regions (p-value, F-value)	No. of SubVol regions (p-value, F-value)	No. of SA regions (p-value, F-value)	No. of CTSD regions (p-value, F-value)
PD	23 (**0.043,** 4.11)	63 (**0.027,** 4.93)	22 (**0.019,** 5.50)	67 (**0.044,** 4.07)	44 (**0.031,** 4.69)
MS	56 (**0.006,** 7.48)	50 (**0.038,** 4.29)	21 (**0.034,** 4.52)	18 (**0.038,** 4.32)	60 (**0.044,** 4.06)
AD	61 (**0.039,** 4.26)	55 (**0.041,** 4.16)	18 (**3.8e-05,** 17.16)	29 (**0.020,** 5.40)	56 (**0.044,** 4.05)
MCI	44 (**0.031,** 4.65)	35 (**0.047,** 3.96)	21 (**0.010,** 6.66)	10 (**0.035,** 4.47)	44 (**0.022,** 5.25)
FTLD	64 (**0.024,** 5.12)	52 (**0.035,** 4.48)	24 (**0.030,** 4.70)	38 (**0.033,** 4.70)	51 (**0.027,** 4.88)

AD: Alzheimer's disease, CT: cortical thickness, CTSD: cortical thickness standard deviation, CVol: cortical volume, FTLD: frontotemporal lobar degeneration, MCI: mild cognitive impairment, MS: multiple sclerosis, PD: Parkinson's disease, SA: surface area, SubVol: subcortical volume.
p-values and corresponding F-values inside brackets indicate the least (yet still significant) p-value among all other significant p-values.

3.1.4 PD patients and the RG differ in regional CVol, SubVol, SA and CTSD

MS patients had the highest number of significantly different CT regions when compared to RG (64 regions). Similarly, PD for CVol (60 regions), PD for SubVol (26 regions), PD for SA (67 regions), and PD for CTSD (62 regions) (Table 3.2).

Table 3.2 Summary of MANOVAs: replication group (RG). *The following summary table depicts the number of significant regions when comparing each patient group to the replication group (RG) across each variable.*

Group	No. of CT regions (p-value, F-value)	No. of CVol regions (p-value, F-value)	No. of SubVol regions (p-value, F-value)	No. of SA regions (p-value, F-value)
PD	53 (**0.035,** 4.47)	60 (**0.037,** 4.37)	26 (**0.018,** 5.66)	62 (**0.028,** 4.83)
MS	64 (**0.042,** 4.16)	55 (**0.049,** 3.88)	23 (**0.006,** 7.52)	51 (**0.047,** 3.97)
AD	58 (**0.046,** 3.99)	51 (**0.047,** 3.95)	22 (**0.008,** 7.16)	40 (**0.035,** 4.46)
MCI	54 (**0.046,** 3.98)	50 (**0.032,** 4.62)	23 (**0.001,** 10.86)	52 (**0.032,** 5.42)
FTLD	56 (**0.046,** 4.00)	51 (**0.035,** 4.45)	24 (**0.0001,** 14.62)	49 (**0.050,** 3.86)

AD: Alzheimer's disease, CT: cortical thickness, CVol: cortical volume, FTLD: frontotemporal lobar degeneration, MCI: mild cognitive impairment, MS: multiple sclerosis, PD: Parkinson's disease, SA: surface area, SubVol: subcortical volume.
p-values and corresponding F-values inside brackets indicate the least (yet still significant) p-value among all other significant p-values.

3.1.5 CVol and SA regions differ most across all groups when taking sex as a factor

When comparing all groups simultaneously to the DG, all except one region (CTSD region) are significantly different to DG. The highest number of significant regions when comparing all groups to DG with sex as a factor was achieved by CVol and SA (68 regions for both). Similarly, the interaction between group and sex yield the highest number of significantly different regions for CVol and SA regions (60 and 66 respectively) (Table 3.3).

Table 3.3 Summary of MANCOVAs: discovery group (DG). *The following summary table depicts the number of significant regions when comparing all patient groups simultaneously to the discovery group (DG) across each variable.*

Factor	No. of CT regions (p-value, F-value)	No. of CVol regions (p-value, F-value)	No. of SubVol regions (p-value, F-value)	No. of SA regions (p-value, F-value)	No. of CTSD regions (p-value, F-value)
Group	68 (**0.010,** 3.0)	68 (**<0.001,** 5.5)	26 (**<0.001,** 4.9)	68 (**0.002,** 3.7)	67 (**0.008,** 3.1)
Sex	36 (**0.050,** 3.8)	68 (**<0.001,** 33.4)	23 (**<0.001,** 34.3)	68 (**<0.001,** 56.6)	30 (**0.049,** 3.9)
***Group: Sex**	10 (**0.049,** 2.2)	60 (**0.049,** 2.2)	19 (**0.047,** 2.3)	66 (**0.026,** 2.5)	11 (**0.037,** 2.4)

CT: cortical thickness, CTSD: cortical thickness standard deviation, CVol: cortical volume, SA: surface area, SubVol: subcortical volume.
p-values and corresponding F-values inside brackets indicate the least (yet still significant) p-value among all other significant p-values.
**Group – Sex Interaction*

When comparing all groups simultaneously to RG, all regions are significantly different to RG. The highest number of significant regions when comparing all groups to RG with sex as a factor was achieved by CVol and SA (68 regions for both). Similarly, the interaction between group and sex yield the highest number of significantly different regions for CVol and SA regions (59 and 68 respectively) (Table 3.4).

Table 3.4 Summary of MANCOVAs: replication group (RG). *The following summary table depicts the number of significant regions when comparing all patient groups simultaneously to the replication group (DG) across each variable.*

Factor	No. of CT regions (p-value, F-value)	No. of CVol regions (p-value, F-value)	No. of SubVol regions (p-value, F-value)	No. of SA regions (p-value, F-value)
Group	68 *(**<0.001**, 8.2)	68 (**<0.001,** 5.5)	26 (**<0.001,** 21.2)	68 (**<0.001,** 6.7)
Sex	48 (**0.043,** 4.1)	68 (**<0.001,** 28.5)	24 (**0.045,** 4.0)	68 (**<0.001,** 65.0)
***Group: Sex**	12 (**0.044,** 2.3)	59 (**0.024,** 2.6)	20 (**0.012,** 2.9)	68 (**0.044,** 2.28)

CT: cortical thickness, CVol: cortical volume, SA: surface area, SubVol: subcortical volume.
p-values and corresponding F-values inside brackets indicate the least (yet still significant) p-value among all other significant p-values.
**Group – Sex Interaction*

3.2 Differences in Actual Age Across Groups

3.2.1 PD and FTLD patients have similar actual ages to individuals in the DG

The ANOVA between groups revealed that both PD and FTLD patients had comparable actual ages to individuals in the DG (p = 0.113 and p = 0.973 respectively) (Table 3.5).

Table 3.5 Summary of ANOVA for actual age. *The following ANOVA summary table depicts p-values for comparisons between the discovery/replication group and the patient groups for subjects' actual ages.*

Comparison Group	PD	MS	AD	MCI	FTLD
DG – p-value	0.113	**<0.001**	**<0.001**	**<0.001**	0.973
RG – p-Value	**<0.001**	**<0.001**	**<0.001**	**<0.001**	**<0.001**

AD: Alzheimer's disease, DG: discovery group, FTLD: frontotemporal lobar degeneration, MCI: mild cognitive impairment, MS: multiple sclerosis, PD: Parkinson's disease, RG: replication group
p-values in bold are statistically significant

3.3 Age Predictions Vary Across Groups and Sex

3.3.1 Best overall age predictions achieved by healthy individuals

The here conducted analyses evidenced that predicted and actual age had decreasing patterns across test groups in the form: DG/RG > MCI ≈ PD > FTLD > MS > AD. DG and RG had significantly higher R^2-coefficients than the patient groups regardless of the algorithm used for prediction. In the main analysis, the best age predictions were achieved in DG using SVR (R^2 = 0.72, MAE = 4.85, MdAE = 3.96), whereas the worst predictions resulted from RR and EN in AD (R^2 = 0.08, MAE = 7.34, MdAE = 6.11). In the replication analysis, the best age predictions

were achieved in RG using RR and EN (R^2 = 0.69, MAE = 4.25, MdAE = 3.68), whereas the worst predictions resulted from PRISM in AD (R^2 = 0.04, MAE = 7.26, MdAE = 6.31).

3.3.2 Best age predictions among patient groups achieved by MCI and PD

Main analysis predictions resulted in R^2 values between 0.5 and 0.7, whereas replication analysis predictions have values between 0.4 and 0.7 when predicting HI. For all subjects in the main analysis, regardless their gender, R^2 values for MCI and PD patients fall in the range between 0.2 and 0.4. With a few exceptions, R^2 values follow the same trend for the replication analysis. At the lower end of the spectrum are the R^2 values for FTLD, AD and MS patients, which lie, with some few exceptions, between 0 and 0.2. Out of FTLD, AD and MS patients, the R^2 for AD patients are lowest.

3.3.3 Better age predictions in males than in females

Overall, males had higher R^2-coefficients than females across test groups and algorithms. In the main analysis, in DG the best age predictions for males were achieved by RR, SVR and PRISM (R^2 = 0.74, MAE = 5.73, MdAE = 4.72), whereas the worst predictions were achieved by LASSO in FTLD (R^2 = 0.03, MAE = 10.14, MdAE = 8.78). In the replication analysis, the best age predictions for males were achieved by RR and EN in RG (R^2 = 0.66, MAE = 5.31, MdAE = 4.55), whereas the worst were made by PRISM in AD (R^2 = 0.02, MAE = 6.56, MdAE = 5.12). For females, in the main analysis, in DG the best age predictions were achieved by RR, EN and SVR (R^2 = 0.69, MAE = 5.15, MdAE = 4.02), whereas the worst were made by SVR in AD (R^2 = 0.01, MAE = 7.80, MdAE = 7.48). In the replication analysis, the best age predictions for females were achieved by RR and EN in RG (R^2 = 0.59, MAE = 4.70, MdAE = 3.85), whereas the worst were made by RR, EN, SVR and PRISM in AD (R^2 = 0.00, MAE = 7.81, MdAE = 6.90) (Figure 3.3, 3.4 & 3.5).

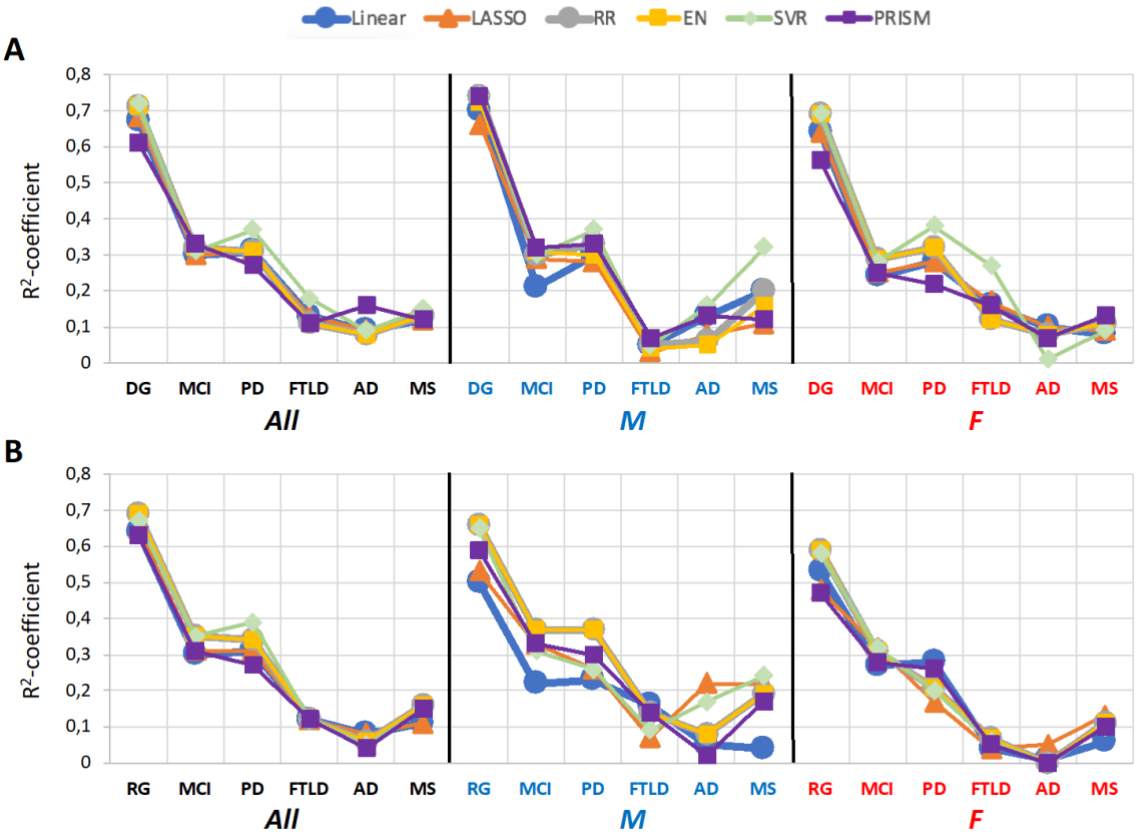

Figure 3.3 R^2-coefficient plots from predicted vs. actual age regressions. *R^2-coefficient plots for predicted age vs. actual age using the cortical thickness and subcortical volume (CT & SubVol) morphometric combination with the different statistical learning algorithms: linear, least absolute shrinkage and selection operator (LASSO), ridge regression (RR), elastic net regression (EN), support vector regression (SVR) and the multiple spline regression from the prism toolbox (Madan, 2016) (PRISM) across the different training and validation sets. A) Training set is 80% of the discovery group (DG) subjects. The left column illustrates the results from all subjects together, the middle column only the male subjects and the right column only the female subjects. Validation set groups are from left to right: remaining 20% of subjects in the DG, and the subjects in the groups mild cognitive impairment (MCI), Parkinson's disease (PD), frontotemporal lobar degeneration (FTLD), Alzheimer's disease (AD) and multiple sclerosis (MS) respectively. B) Same as A) but with the replication group (RG) instead of the DG.*

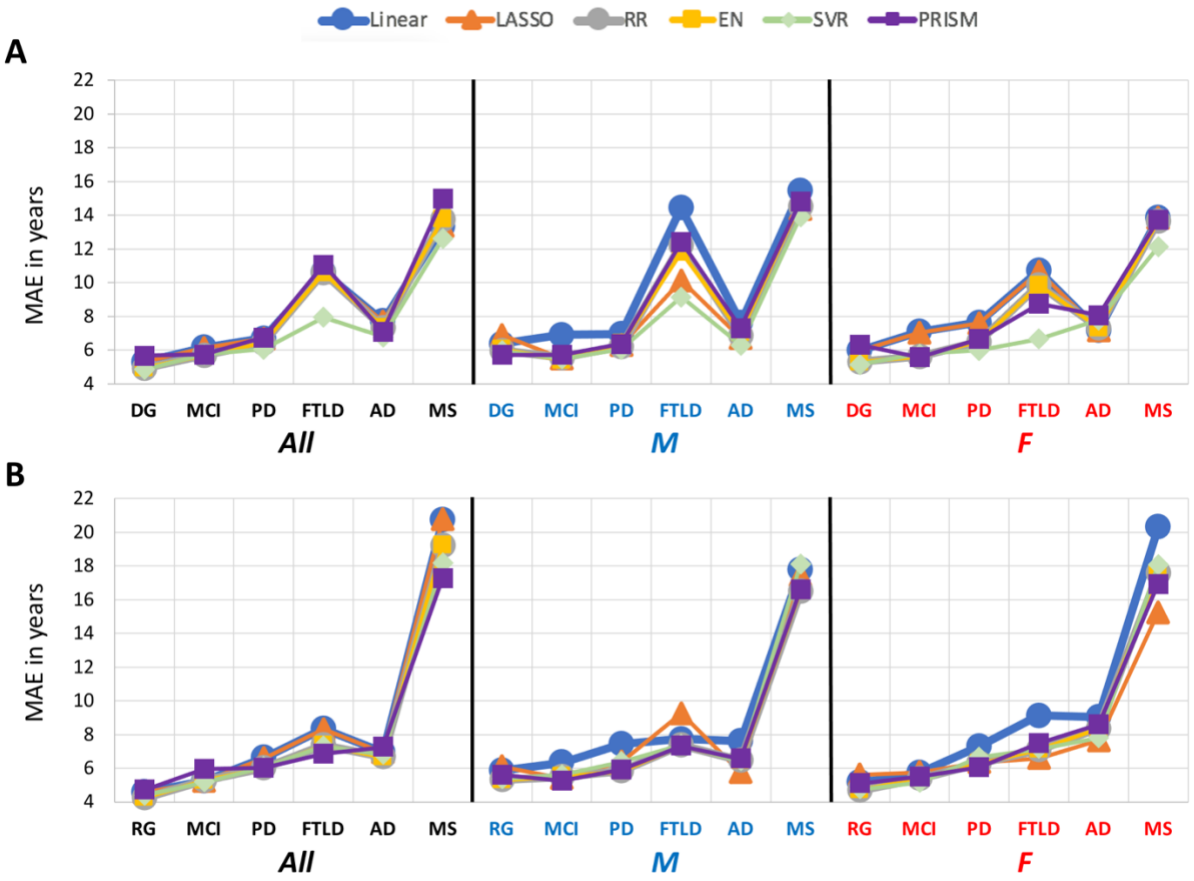

Figure 3.4 Mean absolute error (MAE) plots from predicted vs. actual age regressions. *Mean absolute error (MAE) plots in years from predicted age vs. actual age using the cortical thickness and subcortical volume (CT & SubVol) morphometric combination with the different statistical learning algorithms: linear, least absolute shrinkage and selection operator (LASSO), ridge regression (RR), elastic net regression (EN), support vector regression (SVR) and the multiple spline regression from the prism toolbox (Madan, 2016) (PRISM) across the different training and validation sets. A) Training set is 80% of the discovery group (DG) subjects. The left column illustrates the results from all subjects together, the middle column only the male subjects and the right column only the female subjects. Validation set groups are from left to right: remaining 20% of subjects in the DG, and the subjects in the groups mild cognitive impairment (MCI), Parkinson's disease (PD), frontotemporal lobar degeneration (FTLD), Alzheimer's disease (AD) and multiple sclerosis (MS) respectively. B) Same as A) but with the replication group (RG) instead of the DG.*

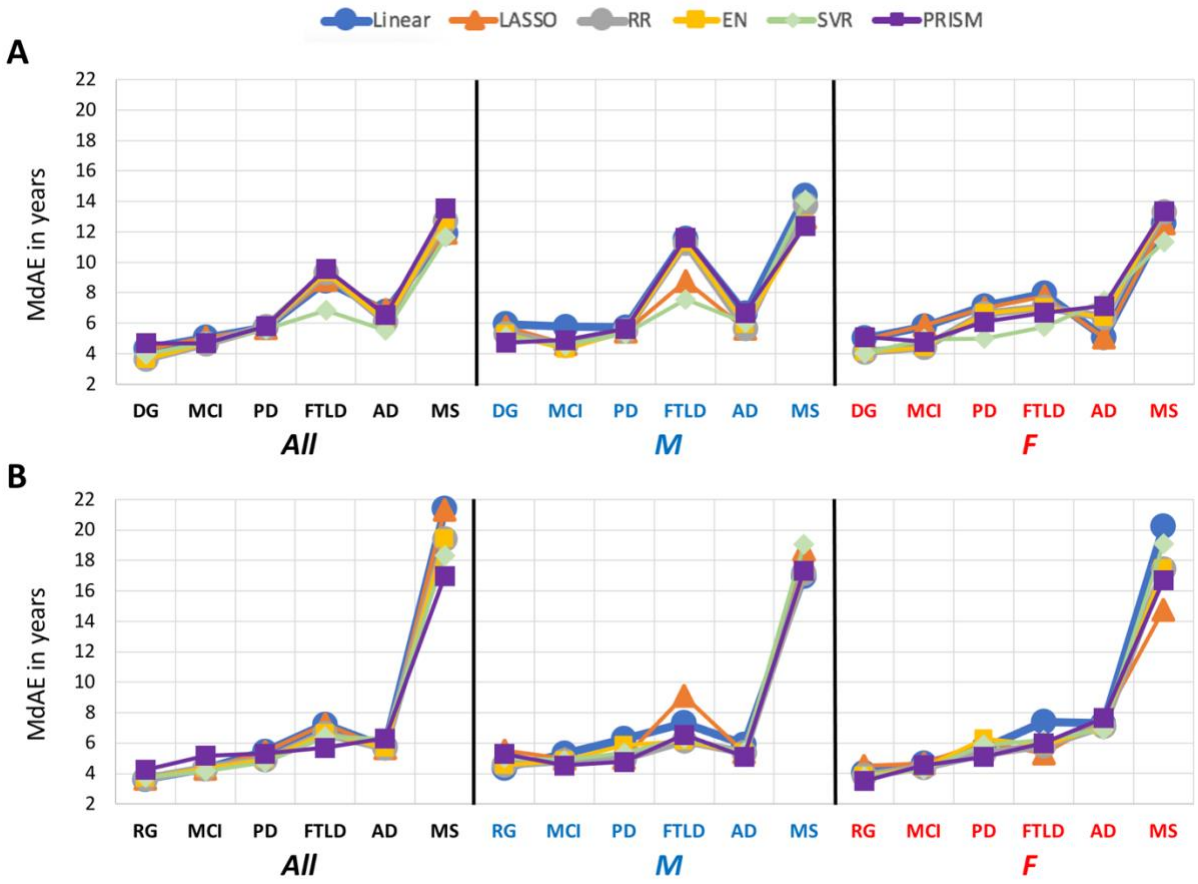

Figure 3.5 Median absolute error (MdAE) plots from predicted vs. actual age regressions. *Median absolute error (MdAE) plots in years from predicted age vs. actual age using the cortical thickness and subcortical volume (CT & SubVol) morphometric combination with the different statistical learning algorithms: linear, least absolute shrinkage and selection operator (LASSO), ridge regression (RR), elastic net regression (EN), support vector regression (SVR) and the multiple spline regression from the prism toolbox (Madan, 2016) (PRISM) across the different training and validation sets. A) Training set is 80% of the discovery group (DG) subjects. The left column illustrates the results from all subjects together, the middle column only the male subjects and the right column only the female subjects. Validation set groups are from left to right: remaining 20% of subjects in the DG, and the subjects in the groups mild cognitive impairment (MCI), Parkinson's disease (PD), frontotemporal lobar degeneration (FTLD), Alzheimer's disease (AD) and multiple sclerosis (MS) respectively. B) Same as A) but with the replication group (RG) instead of the DG.*

3.4 Predicted Age Strongly Associates with Clinical Parameters, but Delta Age Does not

3.4.1 Worse MMSE scores are associated with higher predicted ages in MCI

A statistically significant negative association was observed between MMSE scores of MCI patients and their actual (R = 0.21, p = 3.3E-05), as well as their predicted age (R = 0.19, p = 9.9E-05). The age difference, delta, however showed no significant association with MMSE scores (R = 0.014, p = 0.8). The regressions of both actual and predicted ages show very similar trajectories, which might explain the lack of association between delta age and MMSE scores. Regarding delayed memory assessed by the LDELTOT score, an association was found with the

predicted age (R = 0.16, p = 1.9E-03), whereas actual age merely showed a trend (R = 0.096, p = 0.05). The LIMMTOT is associated with both the actual (R = 0.11, p = 3.1E-02) and predicted age (R = 0.11, p = 2.8E-02) of MCI patients. Similar to MMSE, the LIMMTOT plots show very similar trajectories for actual and predicted ages, whereas delta age does not show any association (R = 0.0013, p = 1) (Figure 3.6).

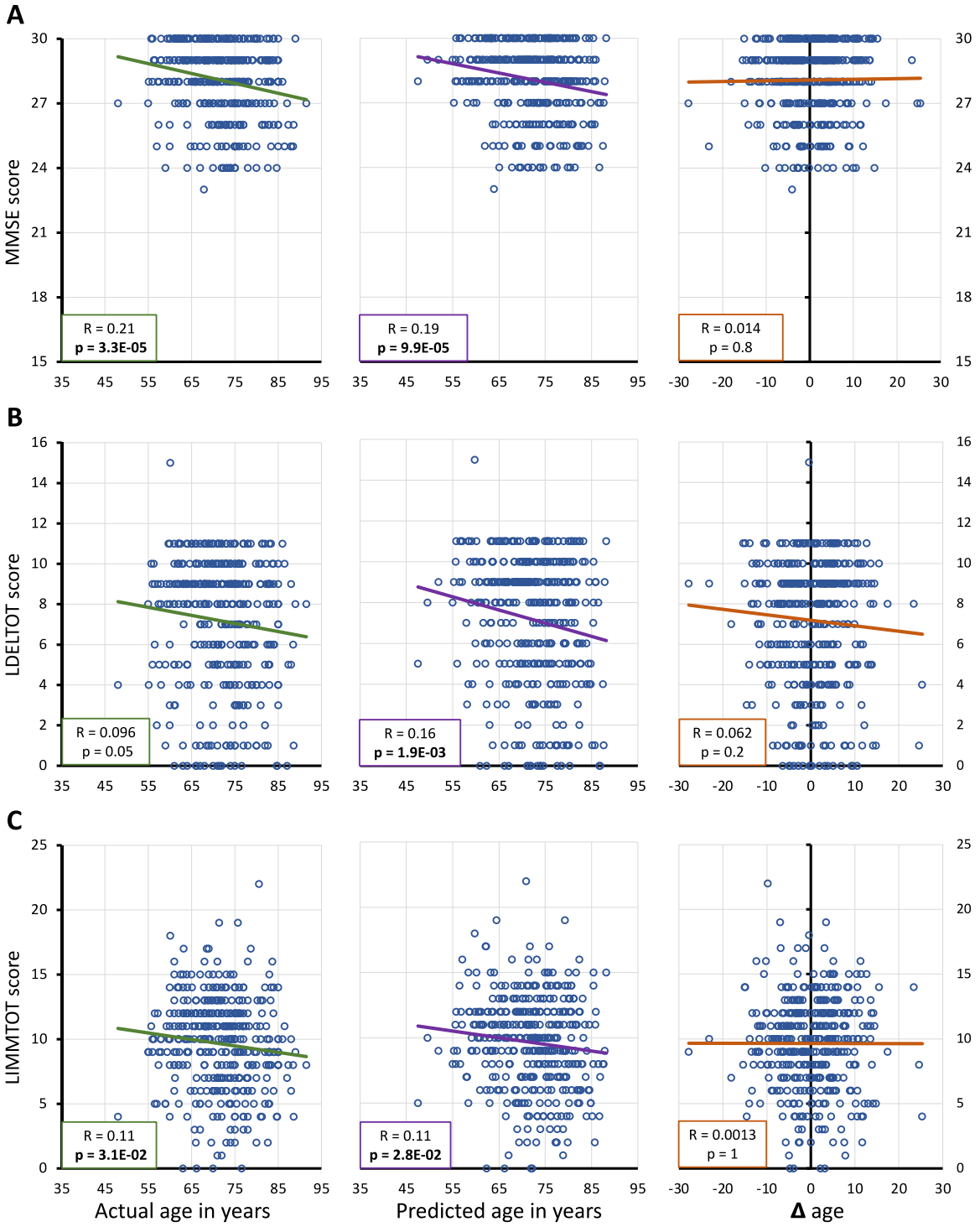

Figure 3.6 Regression plots with clinical variables in mild cognitive impairment. *Predicted age values were estimated using the support vector regression (SVR) algorithm. A) Regression plots of MMSE (Mini-Mental State Examination) scores with actual age (left plot), predicted age (middle plot) and delta age (right plot). B) Regression plots of LDELTOT (delayed memory recall test) scores with*

actual age (left plot), predicted age (middle plot) and delta age (right plot). C) Regression plots of LIMMTOT (immediate memory recall test) with actual age (left plot), predicted age (middle plot) and delta age (right plot). p-values in bold are significant.

3.4.2 Worse UPDRS scores are associated with higher predicted ages in PD

The motor section of the UPDRS, shows a positive association with the actual (R = 0.14, p = 3.3E-02) and predicted ages (R = 0.14, p = 3.4E-02) of PD patients. The actual and predicted age plots have very similar trajectories. In this case as well, delta age has no association with the score (R = 0.0065, p = 0.9). Most data points in the delta age plot aggregate around 0, ranging from -15 years to +15 years, suggesting a rather consistent age prediction (Figure 3.7).

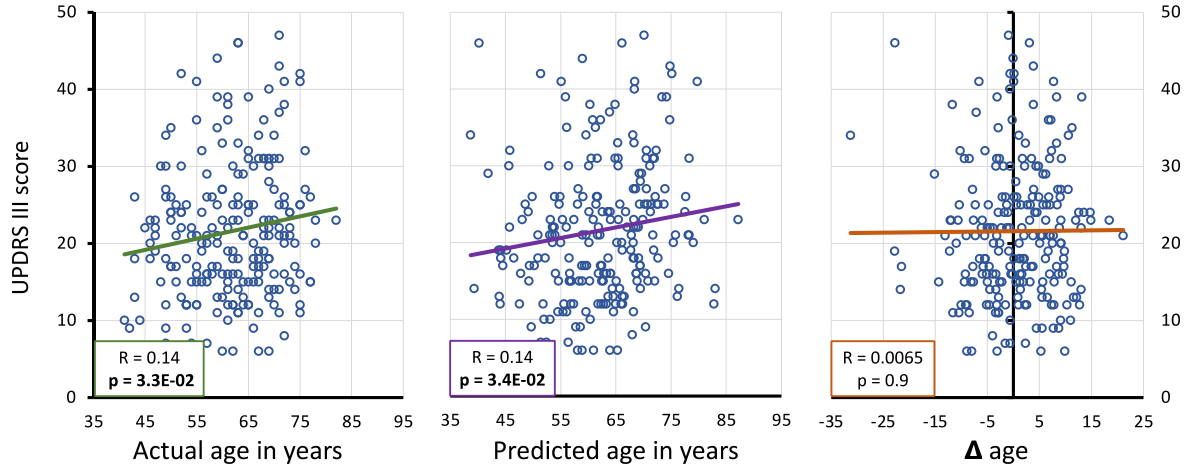

Figure 3.7 Regression plots with clinical variables in Parkinson's disease. *Predicted age values were estimated using the support vector regression (SVR) algorithm. Regression plots of UPDRS part III (unified Parkinson's disease rating scale) scores with actual age (left plot), predicted age (middle plot) and delta age (right plot). p-values in bold are significant.*

3.4.3 Worse MMSE scores are associated with higher predicted ages in FTLD

For FTLD patients, the predicted age has a rather strong negative association with the MMSE score (R = 0.25, p = 4.5E-04). More importantly, delta age is highly negatively associated with the MMSE score (R = 0.19, p = 7.0E-03), suggesting a worsening of cognitive function with an increasing age overprediction. The actual age, on the other hand, follows a similar trend, with a much weaker association and a statistically not significant p-value (R = 0.049, p = 0.5).

The CDR score is not associated with the actual age (R = 0.072, p = 0.3). The predicted and delta age, on the other hand, are highly positively associated with the CDR score (R = 0.31, p = 1.3E-05 and R = 0.36, p = 2.2E-07 respectively), indicating an age overprediction for patients with a higher dementia severity ratings (Figure 3.8).

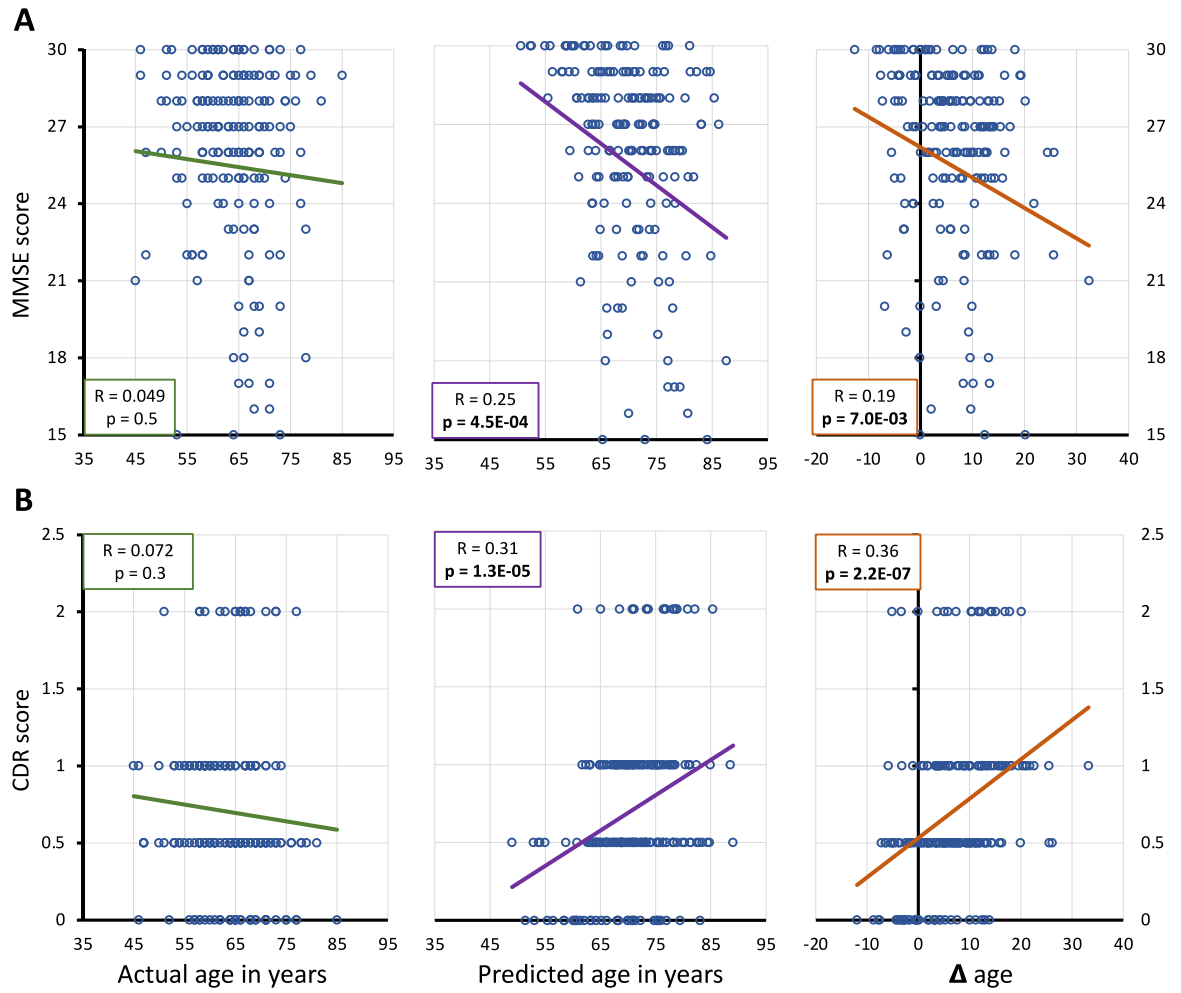

Figure 3.8 Regression plots with clinical variables in frontotemporal lobar degeneration. *Predicted age values were estimated using the support vector regression (SVR) algorithm. A) Regression plots of MMSE (Mini-Mental State Examination) scores with actual age (left plot), predicted age (middle plot) and delta age (right plot). B) Regression plots of CDR (Clinical Dementia Rating) scores with actual age (left plot), predicted age (middle plot) and delta age (right plot). p-values in bold are significant.*

3.4.4 MMSE scores do not show a significant association to any age variable in AD

Regarding AD, the MMSE scores are not significantly associated with any of the age variables (for actual age: R = 0.00027, p = 0.9). Yet, the predicted and delta age variables show a trend of a negative association with the MMSE scores (R = 0.21, p = 0.06 and R = 0.15, p = 0.2 respectively) (Figure 3.9).

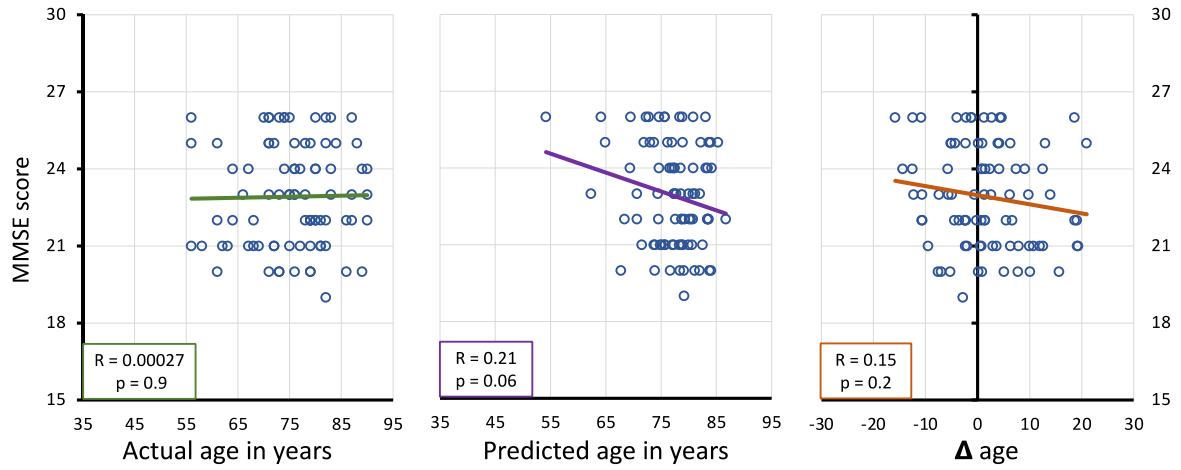

Figure 3.9 Regression plots with clinical variables in Alzheimer's disease. *Predicted age values were estimated using the support vector regression (SVR) algorithm. Regression plots of MMSE (Mini-Mental State Examination) scores with actual age (left plot), predicted age (middle plot) and delta age (right plot). p-values in bold are significant.*

3.4.5 Worse EDSS scores are strongly associated with higher predicted ages in MS

No clear association was found between the EDSS score and the actual age of MS patients (R = 0.019, p = 0.8). On the other hand, a clear and strong positive association was found between the EDSS score and the two computed variables, predicted age (R = 0.42, p = 1.1E-06) and delta age (R = 0.40, p = 2.4E-06). This suggests an age overprediction for patients with a higher degree of disability as quantified by the EDSS score (Figure 3.10).

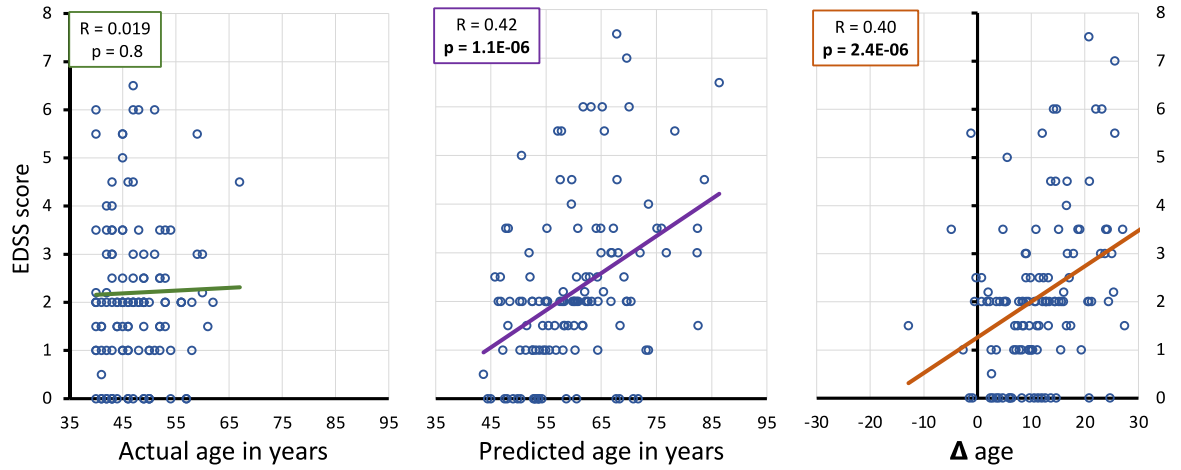

Figure 3.10 Regression plots with clinical variables in multiple sclerosis. *Predicted age values were estimated using the support vector regression (SVR) algorithm. Regression plots of EDSS (Expanded Disability Status Scale) scores with actual age (left plot), predicted age (middle plot) and delta age (right plot). p-values in bold are significant.*

4. Discussion

4.1 Widespread Morphometric Heterogeneity Across Neurodegenerative Disorders

From recent literature neurodegeneration has been described as a widespread reduction of morphometric integrity (Dugger and Dickson, 2017, Kovacs, 2019). Such reductions have been identified and labeled as cortical atrophy using MRI measurements in several disorders such as AD, FTLD, and MS. Moreover, such cortical atrophy was found restricted to brain regions vulnerable to brain aging, following distinct patterns that could serve as markers to differentiate among neurodegenerative diseases. In-line with prior results, our groups of patients presented some similarity in the regions where atrophy was evidenced, with some regions remaining altered in particular groups of patients.

Previously, several studies (Canu et al., 2017, Rohrer et al., 2015) have described an isolated cortical thinning in FTLD patients compared to HI. A study described localized rather than global cortical thinning in PD (Claassen et al., 2016), another, global GM atrophy, rather than SubVol atrophy in AD patients (Ma et al., 2016). Other studies have opposed our findings of no significant subcortical alterations in AD by reporting volume reductions in several subcortical structures (Stepan-Buksakowska et al., 2014, Cho et al., 2014).

Being a transition state between normal cognition and dementia (Matthews et al., 2008), MCI often showed similarly distributed morphometrics in comparison to same-aged HI. Our study exposed lower CT values in FTLD in comparison to HI. The similarly distributed CT values in PD and HI align with the aforementioned studies, as well as the similarly distributed SubVol values in AD and HI. Although results match some previous reports, mean values from MRI-derived morphometric measures are not suitable, considering the heterogeneous composition of the varying rates of atrophy of the different brain regions. In other words, the rate at which brain aging occurs varies not only between individuals, but also across brain regions (Cole et al., 2015, Cevenini et al., 2008, Cole et al., 2018). Intuitively it follows that a regional comparison of morphometrics would yield a more systematic analysis of differences. In AD patients, more than 80% of regions showed a reduced cortical integrity in comparison to HI for CT and CVol. AD patients had similar cortical thinning patterns to that of MCI patients, but with additional regions showing cortical thinning. Thus, our findings support the preliminary nature of the included MCI individuals as a prodromal stage to AD, with a lower extent of neurodegeneration. The AD patients were followed by FTLD and MCI patients respectively in terms of number of significantly atrophied regions. Three CT regions showed

significant atrophy across all patient groups except for MS patients: the right medial orbitofrontal, right pars orbitalis as well as the left middle temporal. These regions might be useful biomarkers in differentiating patients with neurodegeneration from HI, since they are found to be atrophic in several neurodegenerative disorders. The fact that MS patients do not show the latter atrophy pattern might be because of the high clinical variability found among the various MS types, which progress differently with time.

4.2 Age Prediction as Biomarker Across Neurodegenerative Conditions

The identification of biomarkers of healthy normal aging represents a crucial step in understanding neurodegenerative decline. Since many neurodegenerative diseases were found to be influenced by aging, age predictions based on morphometrics might offer useful biomarkers (Franke and Gaser, 2019). Establishing a good model for predicting age in HI is thereby key to detect accelerated aging in patients. Besides, discrepancies between brain and chronological age might point towards a vulnerability or resistance to age-related pathologies.

Since a decade, studies have strived to optimize the age predictions in HI by machine learning on the basis of brain features. Usually the prediction success depends on the algorithm used, the feature variables, the age range as well as the number of subjects used in prediction. Most studies have used MRI from individuals ranging from 18 to 90 years old, with 20 (Wang and Pham, 2011) to 2705 (Aycheh et al., 2018) healthy subjects. The R^2 values ranged from 0.27 (Kandel et al., 2013) to 0.92 (Cole et al., 2017). The only studies roughly matching our subjects' age range (40 to 95 years) had R^2 values of 0.64 (Lin et al., 2016) and 0.50 (Aycheh et al., 2018), comparing to 0.72 for our study. Future studies might want to explore how the age range of subjects affects the prediction accuracy. Regarding delta age, a study utilizing multiple imaging modalities including CT, SubVol and SA for age predictions, yield values ranging from -0.38 years for normal cognition to 1.72 years for major cognitive impairment in individuals between 19 and 82 years old. The results of this study suggest that brain aging is related to the severity of objective cognitive impairment (Liem et al., 2017). Other studies have exposed significant delta age differences between HI and patients with schizophrenia (Nenadic et al., 2017), as well as between HI and MCI/AD patients (Lowe et al., 2016). More specifically, AD and MS patients were found to be predicted 10 years older (delta age of 10) than they actually are (Cole Ph et al., 2020, Franke et al., 2010). These findings support delta age being a biomarker for various neurodegenerative diseases. Furthermore, a

recent study has even found that incorporating a patient's amyloid status improves the efficacy of brain age as biomarker in AD patients (Ly et al., 2020).

Predictions of the HI group were the best, as we strived to obtain the best possible, validated model for predicting patients' ages. The prediction performance then decreased for MCI and PD, finally reaching the lowest values for FTLD, MS and AD patients. For MCI patients, the predictions are better than those for AD patients, again, accentuating the comparatively little advancement in neurodegeneration and the heterogeneous composition of the cohort. Furthermore, MCI patients, which had around 50% of regions showing cortical thinning, had more accurate age predictions than MS patients, which surprisingly, had lower proportions of cortical thinning. PD patients, which had comparable CT&SubVol-based age predictions with MCI patients, also showed a relatively low proportion (12%) of atrophic CT regions with respect to the HI. This phenomenon has previously been described by a study in where a third of the included PD patients, had no detectable atrophy, whereas the rest had various patterns of cortical thinning (Uribe et al., 2016). The lowest age predictions, found in AD and FTLD patients, seem to correlate with the global atrophy found in both patient groups. This suggests that reduced cortical integrity is associated with poorer age predictions, but is not the only factor in determining the prediction performance. Regarding delta age, there was no significant difference observed for MCI and PD in comparison to the HI group. Nevertheless, delta age values aligned with previous results in MCI patients (Liem et al., 2017). FTLD, AD and MS patients, on the other hand, had, on average, significantly higher delta age values (+6.2 years, +1.7 years and +12.7 years respectively) than HI (-0.29 years).

4.3 Predicted Age as a Predictor for Clinical Presentation of the Disease

Clinical tests are either used to uncover an underlying neurological condition or to assess its severity once diagnosed. They are also essential in tracking the progression of a disease, or, remission after a certain therapy. Our study was interested in examining whether those clinical tests were somehow associated to biological changes in the brain. Since we used age predictions as a way to quantify such age-related changes in the brain, we wanted to assess whether those predictions were somehow related to a patient's clinical presentation assessed by such tests. The idea was to find a connection between accelerated aging in neurodegenerative diseases and their apparent manifestation in patients.

As a test for global cognitive impairment, the MMSE is considered best for ruling out dementia, rather than distinguishing MCI patients from HI (Mitchell, 2009). Out of eight cognitive tests, a study found that the MMSE had one of the lowest sensitivities for diagnosing MCI (Breton et al., 2019). This suggests that the MMSE cannot be regarded as a reliable test for differentiating MCI-related neurodegeneration from healthy brain aging. Further supporting that clause, are the distinct MCI subtypes found by several studies (amnestic, dysexecutive and mixed MCI) on the basis of neuropsychological tests (Delano-Wood et al., 2009, Libon et al., 2010). The amnestic subtype not only showed a higher rate of conversion to dementia in comparison to other MCI types (Fischer et al., 2007), but was also highly frequently associated to AD at autopsy (Busse et al., 2006). A such biologically and clinically heterogeneous disease, with patients ranging from nearly normal to demented, might pose a challenge in establishing a reliable morphometric-based biomarker. Regarding PD patients, few, if any studies have investigated the relationship between age predictions and clinical variables. Nevertheless, a positive association was found between PD patients' actual ages and UPDRS part III scores (Keezer et al., 2016). The later score was also associated with CT (Gao et al., 2018). Moving on to FTLD, the different clinical symptoms have been found to relate to distinct brain atrophy patterns (Rohrer and Rosen, 2013). Since we had different FTLD phenotypes in our cohort, potential differences within the FTLD spectrum might have been masked (Tan et al., 2013). Furthermore, the highly verbal nature of the MMSE makes it less sensitive in characterizing overall impairment in, for example, the bvFTLD phenotype (Osher et al., 2007). Conversely, the CDR-FTLD scale-modified, has been proven to reliably measure dementia severity and clinical change in FTLD patients (Mioshi et al., 2017, Borroni et al., 2010, Kim et al., 2012, Maiovis et al., 2017). In AD, a previous study has found that the MMSE score decreased with increasing age, which was not the case in our study. Also, women were found to have significantly lower MMSE scores than men of the same age and educational level (Pradier et al., 2014). Although the MMSE has been widely used to monitor disease progression (Henneges et al., 2016), and linearly decline with CT and CVol (Choi et al., 2019), it might not be an appropriate biomarker for disease-related aging processes. In MS, clinical symptoms as well as disability progression were found to be associated with age (Manouchehrinia et al., 2017, Tremlett et al., 2006). More importantly, the EDSS score was previously found to increase with age and with higher degrees of atrophy in the bilateral sensorimotor cortex and insula (Steenwijk et al., 2016). Such findings shed light upon morphometric age predictions as viable biomarkers for age-associated morbidity in MS. Going

beyond disease specific morbidities, a study has even found an association between higher delta ages and an increased mortality risk in HI (Cole et al., 2018). The latter and a consecutive study, uncovered an association between higher delta ages and weaker grip strength, poorer lung function, a slower walking speed, a lower fluid intelligence (Cole et al., 2018), higher blood pressure, a diagnosis of diabetes, a history of stroke, past or present smoking, and a greater frequency of alcohol intake (de Lange and Cole, 2020). The latter associations insinuate that premature brain aging extends beyond neurodegenerative diseases; a complex phenomenon influenced by environmental and genetic factors.

In MCI, the MMSE, LIMMTOT and LDELTOT scores were negatively associated with the actual and predicted ages, but not with delta age. This is expected from MCI patients, which have a close to normal cognition, and possibly, only little cortical atrophy. This was confirmed by the lack of significant difference between delta ages of HI and MCI patients. We would therefore not expect delta age to be associated with the tests in MCI, as one also would not expect the latter association in HI. In PD patients, a higher UPDRS-III score was associated with higher actual and predicted ages, but not with delta age. This follows the trend seen in MCI patients, as the delta ages of PD patients and HI were comparable. This does not mean that the UPDRS-III score is unrelated to potential cortical atrophy patterns in PD, but rather that delta age was not necessarily indicative of those patterns. In FTLD patients, higher MMSE scores were associated with higher predicted and delta ages. This points towards a disease-related neurodegeneration as a biomarker for clinical tests. On the other hand, the high clinical variability discussed earlier might have contributed to the later associations. Similar to MMSE, higher CDR-FTLD scores were associated with higher predicted and delta age of patients. The latter association to such a well-established score, advocates for the utilization of delta age as a measurable indicator of FTLD disease severity. In AD patients, the MMSE score showed no significant association with any age variable. Our deviating results might be due to the very detailed selection of the currently used AD sample, where patients had comparable clinical symptoms. They were selected for the good quality MR image and for amyloid deposition positivity, described in previous studies (Gonzalez-Escamilla et al., 2017, Grothe et al., 2018, Gonzalez-Escamilla et al., 2020). Regarding MS, the EDSS scores, which were found to be associated with increasing age (Steenwijk et al., 2016), did not show a significant association with the actual age of patients, despite that age had been considered the strongest predictor for buildup of severe disability (Geraldes et al., 2017). In contrast, higher EDSS scores were significantly associated with higher predicted and delta ages, pointing

towards a good potential biomarker for clinical use. Furthermore, our study is one of few, which has been conducted with relatively old MS patients (mean age of 48 years).

4.4 Limitations

Several studies have discussed the limitations of age prediction on the basis of MRI morphometrics. The first ones to emerge are those relating to the MR scan itself. Head motion has shown to influence the quality of the image, despite of the motion correction feature imbedded in the Freesurfer pipeline (Cole et al., 2015). Since we had MR images from several different cohorts and patient groups, the within and between scanner reliabilities might have influenced the variance of the morphometrics (Cole et al., 2017).

Regarding machine learning, the number of subjects in the training sample has been described as having one of the strongest effects on prediction accuracy (Franke et al., 2010). As the number of subjects increase, the prediction performance increases, as long as the variance in the set remains low. We had a number of subjects comparable to other studies, with similar prediction accuracies.

Some factors, which have known influence on the brain microstructure have not been accounted for such as the level of education (Luders et al., 2016), physical activity (Steffener et al., 2016), genetics (Cole Ph et al., 2020) and medication effects (Nenadic et al., 2017). It is yet important to understand that some prediction error will always persist due to the individual differences in brains of people (Liem et al., 2017), regardless of how many covariables were accounted for.

5. Summary

In conclusion, the best age predictions were made by SVR using a combination of the morphometric CT and SubVol. MCI and PD patients had similarly distributed morphometrics as HI, with predictions that come the closest to the actual age in comparison to any other patient group. For MCI and PD patients, worse MMSE and UPDRS part III scores respectively, were associated with higher actual and predicted ages. FTLD patients had a reduced cortical integrity with significant increase in delta age and an association between all age variables and worsening MMSE and CDR scores. The AD group had the highest number of regions with cortical thinning across all groups with a significant increase in delta age, yet no associations to MMSE. Finally, MS patients had no detectable cortical thinning, yet the highest increase in delta age (+ 12.7 years) with a clear association to worsening EDSS scores. The latter results highlight the clear morphological differences between the various neurodegenerative disorders. Diseases such as AD and FTLD, with an overall higher reduction in cortical integrity, revealed a predicted age that deviates significantly from the actual age. On the other hand, MCI patients with an expectedly lower progress of neurodegeneration showed morphological patterns comparable to HI, with little to no age overestimation. Despite the large bandwidth of atrophy configurations, understanding and recognizing those premature ageing patterns might enhance our ability to identify patients in preclinical stages of an underlying neurodegenerative disorder.

6. Abstract

Age predictions on the basis of brain MRIs through machine learning algorithms are becoming increasingly popular for assessing neurodegeneration in age-related disorders. The aim of this study was to find the combination of morphometric variables with machine learning algorithms, which maximizes the age prediction differentiation accuracy across various neurodegenerative disorders. Additionally, we evaluated the associations between predicted age, and patients' clinical presentation.

Brain T1w 3T MR images were collected from various databases. Among healthy individuals (HI) two cohorts were composed, i) a discovery cohort (n = 816, females: 432, males: 384, mean age = 64 ± 12 years) assembled from 7 different databases; and ii) a replication cohort (n = 687, females: 408, males: 279, mean age = 68 ± 9 years) derived from a single database. The patient collective comprised 5 neurological disorders, including Parkinson's disease (PD) (n = 289, females: 107, males: 182, mean age = 63 ± 9 years) frontotemporal lobar degeneration (FTLD) (n = 218, females: 93, males: 125, mean age = 64 ± 7 years), mild cognitive impairment (MCI) (n = 401, females: 183, males: 218, mean age = 72 ± 8 years), Alzheimer's disease (AD) (n = 85, females: 36, males: 49, mean age = 76 ± 8 years), and multiple sclerosis (MS) (n = 209, females: 150, males: 59, mean age = 48 ± 7 years). The patients were selected to closely match the age range of HI (aged from 40 to 92 years). All MR images were preprocessed using FreeSurfer to derive five morphometric measures: 1) cortical thickness (CT), 2) cortical volume (CVol), 3) subcortical volume (SubVol), 4) surface area (SA), and 5) cortical thickness standard deviation (CTSD); used to predict the participant's age. To build the 6 different statistical learning algorithms (multiple linear regression (MLR), ridge regression (RR), least absolute shrinkage and selection operator (LASSO), elastic net regression (EN), support vector regression (SVR) and PRISM toolbox), the cohorts of HI were split into a training group (80% of the sample size), used to train the models, and a test sample (the remaining 20% of individuals). The resulting predictions were compared to the individuals' actual ages and evaluated using R^2. Additionally, we looked for potential associations between patients predicted age and the respective clinical test scores (MMSE, CDR, UPDRS and EDSS).

When testing prediction accuracy in HI, the best overall age prediction resulted from the SVR and a combination of CT with SubVol (R^2 = 0.72). Validation on the patient cohorts, the MCI and PD showed the highest R^2 among patient groups ranging from 0.2 to 0.4. FTLD,

AD, and MS had the lowest R^2 ranging from 0.0 to 0.2. We further evaluated sex-effects on age prediction, where males had overall better predictions than females across all groups (R^2 range males: 0.74 – 0.03; R^2 range females: 0.69 – 0.01). Regarding the associations with clinical scores, higher predicted ages were associated with worse MMSE scores in MCI and FTLD. On the other hand, MMSE scores did not show any significant association to age prediction in AD. The motor section of the UPDRS and the EDSS showed worsening scores with higher predicted ages in PD and MS, respectively. Overall, diseases with an expectedly high proportion of neurodegeneration had lower age prediction accuracies, and, morbidity was generally associated to higher predicted ages regardless of the disorder. Understanding these microstructural patterns involved in premature brain ageing may enhance our ability to recognize early disease stages, where clinical and MRI findings are lacking.

7. Zusammenfassung

Neurodegeneration ist ein schrittweiser Abbau von Neuronen, der meist altersbedingt bei genetischer Prädisposition auftritt. Zu dessen Beurteilung wird häufig die Vorhersage des Patientenalters mittels künstlicher Intelligenz auf Basis von Magnetresonanztomographien des Schädels getroffen. Ziel dieser Studie war es, die Kombination aus MRT-morphometrischen Variablen zu ermitteln, die die Genauigkeit der Altersvorhersage mittels künstlicher Intelligenz bei verschiedenen neurodegenerativen Erkrankungen maximiert. Darüber hinaus wurden die Zusammenhänge zwischen dem vorhergesagten Alter und dem klinischen Erscheinungsbild der Patienten untersucht.

T1w 3T MR Bilder des Gehirns wurden aus verschiedenen Datenbanken entnommen. Aus dem Probandenkollektiv wurden zwei Kohorten gebildet: i) eine Entdeckungskohorte (DC) (n = 816, Frauen: 432, Männer: 384, Durchschnittsalter = 64 ± 12 Jahre), die aus 7 verschiedenen Datenbanken zusammengestellt wurde, und ii) eine Replikationskohorte (RC) (n = 687, Frauen: 408, Männer: 279, Durchschnittsalter = 68 ± 9 Jahre), die aus einer einzigen Datenbank stammte. Das Patientenkollektiv umfasste die folgenden 5 neurologischen Krankheitsbilder: Morbus Parkinson (PD) (n = 289, Frauen: 107, Männer: 182, Durchschnittsalter = 63 ± 9 Jahre), Frontotemporale Lobärdegeneration (FTLD) (n = 218, Frauen: 93, Männer: 125, Durchschnittsalter = 64 ± 7 Jahre), „mild cognitive impairment“ (MCI) (n = 401, Frauen: 183, Männer: 218, Durchschnittsalter = 72 ± 8 Jahre), Alzheimer-Krankheit (AD) (n = 85, Frauen: 36, Männer: 49, Durchschnittsalter = 76 ± 8 Jahre) und Multiple Sklerose (MS) (n = 209, Frauen: 150, Männer: 59, Durchschnittsalter = 48 ± 7 Jahre). Die Patienten wurden so ausgewählt, dass sie dem Altersspektrum gesunder Probanden (zwischen 40 und 92 Jahren) entsprachen. Alle MR-Bilder wurden mit FreeSurfer vorverarbeitet, um folgende fünf morphometrische Variablen, die zur Vorhersage des Alters der Teilnehmer verwendet wurden, abzuleiten: 1) kortikale Dicke (CT), 2) kortikales Volumen (CVol), 3) subkortikales Volumen (SubVol), 4) Hirnoberfläche (SA) und 5) Standardabweichung der kortikalen Dicke (CTSD). Zur Erstellung der sechs verschiedenen statistischen Lernalgorithmen (multiple lineare Regression (MLR), Ridge Regression (RR), Least Absolute Shrinkage and Selection Operator (LASSO), Elastic Net Regression (EN), Support Vector Regression (SVR) und Christopher Madan’s PRISM Toolbox) wurden die Kohorten gesunder Probanden in eine Trainingsgruppe (80 % des Stichprobenumfangs), mit der die Modelle trainiert wurden, und eine Testgruppe (die restlichen 20 % der Personen) aufgeteilt. Die

resultierenden Altersvorhersagen wurden mit dem tatsächlichen Alter der Personen verglichen und anhand des Determinationskoeffizients (R^2) bewertet. Außerdem wurde nach möglichen Zusammenhängen zwischen dem vorhergesagtem Alter und den jeweiligen klinischen Testergebnissen der Patienten (MMST, CDR, UPDRS und EDSS) gesucht.

Bei der Prüfung der Vorhersagegenauigkeit bei gesunden Probanden ergab sich die beste Altersvorhersage aus einer Kombination aus CT und SubVol unter Verwendung von SVR (R^2 = 0,72). MCI- und PD-Patienten wiesen die höchsten R^2-Werte unter den Patientengruppen auf, diese lagen zwischen 0,2 und 0,4. FTLD-, AD- und MS-Patienten wiederum wiesen die niedrigsten R^2-Werte auf, diese lagen zwischen 0,0 und 0,2. Außerdem wurde die Auswirkungen des Geschlechts auf die Altersvorhersage untersucht, wobei Männer in allen Gruppen insgesamt genauere Altersvorhersagen als Frauen aufwiesen (R^2-Bereich Männer: 0,74 - 0,03; R^2-Bereich Frauen: 0,69 - 0,01). Bezüglich der Assoziationen mit den klinischen Werten wiesen älter geschätzte MCI- und FTLD-Patienten niedrige MMST-Werte auf. Andererseits zeigten die MMST-Werte keinen signifikanten Zusammenhang mit der Altersvorhersage bei Patienten mit AD. Der motorische Teil des UPDRS und des EDSS zeigten bei PD-, beziehungsweise bei MS-Patienten eine Verschlechterung der Werte mit höherem vorhergesagtem Alter. Insgesamt wiesen Erkrankungen mit einem erwartungsgemäß hohen Anteil an Neurodegeneration eine geringere Genauigkeit bei der Altersvorhersage auf. Zusätzlich war die Morbidität, unabhängig von der Erkrankung, mit einem höheren vorhergesagten Alter verbunden. Das Verständnis dieser mikrostrukturellen Muster, die an der vorzeitigen Hirnalterung beteiligt sind, könnte unsere Fähigkeit verbessern, frühe Krankheitsstadien bei Abwesenheit klinischer Befunde zu erkennen.

References

AYCHEH, H. M., SEONG, J. K., SHIN, J. H., NA, D. L., KANG, B., SEO, S. W. & SOHN, K. A. 2018. Biological Brain Age Prediction Using Cortical Thickness Data: A Large Scale Cohort Study. *Front Aging Neurosci,* 10**,** 252.

BANG, J., SPINA, S. & MILLER, B. L. 2015. Frontotemporal dementia. *Lancet,* 386**,** 1672-82.

BATTISTA, P., SALVATORE, C. & CASTIGLIONI, I. 2017. Optimizing Neuropsychological Assessments for Cognitive, Behavioral, and Functional Impairment Classification: A Machine Learning Study. *Behav Neurol,* 2017**,** 1850909.

BERGSLAND, N., HORAKOVA, D., DWYER, M. G., UHER, T., VANECKOVA, M., TYBLOVA, M., SEIDL, Z., KRASENSKY, J., HAVRDOVA, E. & ZIVADINOV, R. 2018. Gray matter atrophy patterns in multiple sclerosis: A 10-year source-based morphometry study. *Neuroimage Clin,* 17**,** 444-451.

BLAYLOCK, R. L. 2017. Parkinson's disease: Microglial/macrophage-induced immunoexcitotoxicity as a central mechanism of neurodegeneration. *Surg Neurol Int,* 8**,** 65.

BORRONI, B., AGOSTI, C., PREMI, E., CERINI, C., COSSEDDU, M., PAGHERA, B., BELLELLI, G. & PADOVANI, A. 2010. The FTLD-modified Clinical Dementia Rating scale is a reliable tool for defining disease severity in frontotemporal lobar degeneration: evidence from a brain SPECT study. *Eur J Neurol,* 17**,** 703-7.

BRETON, A., CASEY, D. & ARNAOUTOGLOU, N. A. 2019. Cognitive tests for the detection of mild cognitive impairment (MCI), the prodromal stage of dementia: Meta-analysis of diagnostic accuracy studies. *Int J Geriatr Psychiatry,* 34**,** 233-242.

BRON, E. E., SMITS, M., VAN DER FLIER, W. M., VRENKEN, H., BARKHOF, F., SCHELTENS, P., PAPMA, J. M., STEKETEE, R. M., MENDEZ ORELLANA, C., MEIJBOOM, R., PINTO, M., MEIRELES, J. R., GARRETT, C., BASTOS-LEITE, A. J., ABDULKADIR, A., RONNEBERGER, O., AMOROSO, N., BELLOTTI, R., CARDENAS-PENA, D., ALVAREZ-MEZA, A. M., DOLPH, C. V., IFTEKHARUDDIN, K. M., ESKILDSEN, S. F., COUPE, P., FONOV, V. S., FRANKE, K., GASER, C., LEDIG, C., GUERRERO, R., TONG, T., GRAY, K. R., MORADI, E., TOHKA, J., ROUTIER, A., DURRLEMAN, S., SARICA, A., DI FATTA, G., SENSI, F., CHINCARINI, A., SMITH, G. M., STOYANOV, Z. V., SORENSEN, L., NIELSEN, M., TANGARO, S., INGLESE, P., WACHINGER, C., REUTER, M., VAN SWIETEN, J. C., NIESSEN, W. J., KLEIN, S. & ALZHEIMER'S DISEASE NEUROIMAGING, I. 2015. Standardized evaluation of algorithms for computer-aided diagnosis of dementia based on structural MRI: the CADDementia challenge. *Neuroimage,* 111**,** 562-79.

BRYAN, H. W. A. J. 2019. readxl: Read Excel Files. . R package version 1.3.1. ed.

BUSSE, A., HENSEL, A., GUHNE, U., ANGERMEYER, M. C. & RIEDEL-HELLER, S. G. 2006. Mild cognitive impairment: long-term course of four clinical subtypes. *Neurology,* 67**,** 2176-85.

CANU, E., AGOSTA, F., MANDIC-STOJMENOVIC, G., STOJKOVIC, T., STEFANOVA, E., INUGGI, A., IMPERIALE, F., COPETTI, M., KOSTIC, V. S. & FILIPPI, M. 2017. Multiparametric MRI to distinguish early onset Alzheimer's disease and behavioural variant of frontotemporal dementia. *Neuroimage Clin,* 15**,** 428-438.

CEVENINI, E., INVIDIA, L., LESCAI, F., SALVIOLI, S., TIERI, P., CASTELLANI, G. & FRANCESCHI, C. 2008. Human models of aging and longevity. *Expert Opin Biol Ther,* 8**,** 1393-405.

CHAPMAN, K. R., BING-CANAR, H., ALOSCO, M. L., STEINBERG, E. G., MARTIN, B., CHAISSON, C., KOWALL, N., TRIPODIS, Y. & STERN, R. A. 2016. Mini Mental State Examination and Logical Memory scores for entry into Alzheimer's disease trials. *Alzheimers Res Ther,* 8**,** 9.

CHEN, Y., ZHU, G., LIU, D., LIU, Y., YUAN, T., ZHANG, X., JIANG, Y., DU, T. & ZHANG, J. 2020. The morphology of thalamic subnuclei in Parkinson's disease and the effects of machine learning on disease diagnosis and clinical evaluation. *J Neurol Sci,* 411**,** 116721.

CHENG, C. P., CHENG, S. T., TAM, C. W., CHAN, W. C., CHU, W. C. & LAM, L. C. 2018. Relationship between Cortical Thickness and Neuropsychological Performance in Normal Older Adults and Those with Mild Cognitive Impairment. *Aging Dis,* 9**,** 1020-1030.

CHETELAT, G., FOUQUET, M., KALPOUZOS, G., DENGHIEN, I., DE LA SAYETTE, V., VIADER, F., MEZENGE, F., LANDEAU, B., BARON, J. C., EUSTACHE, F. & DESGRANGES, B. 2008. Three-dimensional surface mapping of hippocampal atrophy progression from MCI to AD and over normal aging as assessed using voxel-based morphometry. *Neuropsychologia,* 46**,** 1721-31.

CHO, H., KIM, J. H., KIM, C., YE, B. S., KIM, H. J., YOON, C. W., NOH, Y., KIM, G. H., KIM, Y. J., KIM, J. H., KIM, C. H., KANG, S. J., CHIN, J., KIM, S. T., LEE, K. H., NA, D. L., SEONG, J. K. & SEO, S. W. 2014. Shape changes of the basal ganglia and thalamus in Alzheimer's disease: a three-year longitudinal study. *J Alzheimers Dis,* 40**,** 285-95.

CHOI, M., YOUN, H., KIM, D., LEE, S., SUH, S., SEONG, J. K., JEONG, H. G. & HAN, C. E. 2019. Comparison of neurodegenerative types using different brain MRI analysis metrics in older adults with normal cognition, mild cognitive impairment, and Alzheimer's dementia. *PLoS One,* 14**,** e0220739.

CLAASSEN, D. O., MCDONELL, K. E., DONAHUE, M., RAWAL, S., WYLIE, S. A., NEIMAT, J. S., KANG, H., HEDERA, P., ZALD, D., LANDMAN, B., DAWANT, B. & RANE, S. 2016. Cortical asymmetry in Parkinson's disease: early susceptibility of the left hemisphere. *Brain Behav,* 6**,** e00573.

COLE, J. H., LEECH, R., SHARP, D. J. & ALZHEIMER'S DISEASE NEUROIMAGING, I. 2015. Prediction of brain age suggests accelerated atrophy after traumatic brain injury. *Ann Neurol,* 77**,** 571-81.

COLE, J. H., POUDEL, R. P. K., TSAGKRASOULIS, D., CAAN, M. W. A., STEVES, C., SPECTOR, T. D. & MONTANA, G. 2017. Predicting brain age with deep learning from raw imaging data results in a reliable and heritable biomarker. *Neuroimage,* 163**,** 115-124.

COLE, J. H., RITCHIE, S. J., BASTIN, M. E., VALDES HERNANDEZ, M. C., MUNOZ MANIEGA, S., ROYLE, N., CORLEY, J., PATTIE, A., HARRIS, S. E., ZHANG, Q., WRAY, N. R., REDMOND, P., MARIONI, R. E., STARR, J. M., COX, S. R., WARDLAW, J. M., SHARP, D. J. & DEARY, I. J. 2018. Brain age predicts mortality. *Mol Psychiatry,* 23**,** 1385-1392.

COLE PH, D. J., RAFFEL MD, J., FRIEDE PH, D. T., ESHAGHI MD PH, D. A., BROWNLEE PH, D. F. W. J., CHARD MD PH, D. D., DE STEFANO MD PH, D. N., ENZINGER MD, C., PIRPAMER, M. L., FILIPPI MD FEAN, M., GASPERINI MD, C., ROCCA MD, M. A., ROVIRA MD, A., RUGGIERI MD, S., SASTRE-GARRIGA MD PH, D. J., STROMILLO MD PH, D. M., UITDEHAAG MD PH, D. B., VRENKEN PH, D. H., BARKHOF MD PH, D. F., NICHOLAS MD PH, D. R., CICCARELLI PH, D. F. O. & GROUP, M. S. 2020. Longitudinal Assessment of Multiple Sclerosis with the Brain-Age Paradigm. *Ann Neurol*.

CORREALE, J., GAITAN, M. I., YSRRAELIT, M. C. & FIOL, M. P. 2017. Progressive multiple sclerosis: from pathogenic mechanisms to treatment. *Brain,* 140**,** 527-546.

CORTES, C. & VAPNIK, V. 1995. Support-vector networks. *Machine learning,* 20**,** 273-297.

COX, S. R., BASTIN, M. E., RITCHIE, S. J., DICKIE, D. A., LIEWALD, D. C., MUNOZ MANIEGA, S., REDMOND, P., ROYLE, N. A., PATTIE, A., VALDES HERNANDEZ, M., CORLEY, J., ARIBISALA, B. S., MCINTOSH, A. M., WARDLAW, J. M. & DEARY, I. J. 2018. Brain cortical characteristics of lifetime cognitive ageing. *Brain Struct Funct,* 223**,** 509-518.

CRIVELLO, F., TZOURIO-MAZOYER, N., TZOURIO, C. & MAZOYER, B. 2014. Longitudinal assessment of global and regional rate of grey matter atrophy in 1,172 healthy older adults: modulation by sex and age. *PLoS One,* 9**,** e114478.

CSUKLY, G., SIRALY, E., FODOR, Z., HORVATH, A., SALACZ, P., HIDASI, Z., CSIBRI, E., RUDAS, G. & SZABO, A. 2016. The Differentiation of Amnestic Type MCI from the Non-Amnestic Types by Structural MRI. *Front Aging Neurosci,* 8**,** 52.

DAAMS, M., STEENWIJK, M. D., SCHOONHEIM, M. M., WATTJES, M. P., BALK, L. J., TEWARIE, P. K., KILLESTEIN, J., UITDEHAAG, B. M., GEURTS, J. J. & BARKHOF, F. 2016. Multi-parametric structural magnetic resonance imaging in relation to cognitive dysfunction in long-standing multiple sclerosis. *Mult Scler,* 22**,** 608-19.

DALE, A., FISCHL, B. & SERENO, M. I. 1999. Cortical Surface-Based Analysis: I. Segmentation and Surface Reconstruction. *NeuroImage,* 9**,** 179-194.

DALE, A. M. & SERENO, M. I. 1993. Improved Localizadon of Cortical Activity by Combining EEG and MEG with MRI Cortical Surface Reconstruction: A Linear Approach. *J Cogn Neurosci,* 5**,** 162-76.

DAVID MEYER, E. D., KURT HORNIK, ANDREAS WEINGESSEL AND FRIEDRICH LEISCH 2018. e1071: Misc Functions of the Department of Statistics, Probability Theory Group (Formerly: E1071). TU Wien.

DE CHASTELAINE, M., DONLEY, B. E., KENNEDY, K. M. & RUGG, M. D. 2019. Age moderates the relationship between cortical thickness and cognitive performance. *Neuropsychologia,* 132**,** 107136.

DE LANGE, A. G. & COLE, J. H. 2020. Commentary: Correction procedures in brain-age prediction. *Neuroimage Clin,* 26**,** 102229.

DELANO-WOOD, L., BONDI, M. W., SACCO, J., ABELES, N., JAK, A. J., LIBON, D. J. & BOZOKI, A. 2009. Heterogeneity in mild cognitive impairment: differences in neuropsychological profile and associated white matter lesion pathology. *J Int Neuropsychol Soc,* 15**,** 906-14.

DEPPE, M., KRAMER, J., TENBERGE, J. G., MARINELL, J., SCHWINDT, W., DEPPE, K., GROPPA, S., WIENDL, H. & MEUTH, S. G. 2016. Early silent microstructural degeneration and atrophy of the thalamocortical network in multiple sclerosis. *Hum Brain Mapp,* 37**,** 1866-79.

DESIKAN, R. S., SEGONNE, F., FISCHL, B., QUINN, B. T., DICKERSON, B. C., BLACKER, D., BUCKNER, R. L., DALE, A. M., MAGUIRE, R. P., HYMAN, B. T., ALBERT, M. S. & KILLIANY, R. J. 2006a. An automated labeling system for subdividing the human cerebral cortex on MRI scans into gyral based regions of interest. *Neuroimage,* 31**,** 968-80.

DESIKAN, R. S., SÉGONNE, F., FISCHL, B., QUINN, B. T., DICKERSON, B. C., BLACKER, D., BUCKNER, R. L., DALE, A. M., MAGUIRE, R. P., HYMAN, B. T., ALBERT, M. S. & KILLIANY, R. J. 2006b. An automated labeling system for subdividing the human cerebral cortex on MRI scans into gyral based regions of interest. *NeuroImage,* 31**,** 968-980.

DOSHI, A. & CHATAWAY, J. 2016. Multiple sclerosis, a treatable disease. *Clin Med (Lond),* 16**,** s53-s59.

DRUCKER, H., BURGES, C. J., KAUFMAN, L., SMOLA, A. J. & VAPNIK, V. Support vector regression machines. Advances in neural information processing systems, 1997. 155-161.

DUGGER, B. N. & DICKSON, D. W. 2017. Pathology of Neurodegenerative Diseases. *Cold Spring Harb Perspect Biol,* 9.

ESHKOOR, S. A., HAMID, T. A., MUN, C. Y. & NG, C. K. 2015. Mild cognitive impairment and its management in older people. *Clin Interv Aging,* 10**,** 687-93.

FISCHER, P., JUNGWIRTH, S., ZEHETMAYER, S., WEISSGRAM, S., HOENIGSCHNABL, S., GELPI, E., KRAMPLA, W. & TRAGL, K. H. 2007. Conversion from subtypes of mild cognitive impairment to Alzheimer dementia. *Neurology,* 68**,** 288-91.

FISCHL, B. 2012. FreeSurfer. *Neuroimage,* 62**,** 774-81.

FISCHL, B. & DALE, A. M. 2000. Measuring the thickness of the human cerebral cortex from magnetic resonance images. *Proceedings of the National Academy of Sciences of the United States of America,* 97**,** 11050-11055.

FISCHL, B., LIU, A. & DALE, A. M. 2001. Automated manifold surgery: constructing geometrically accurate and topologically correct models of the human cerebral cortex. *IEEE Medical Imaging,* 20**,** 70-80.

FISCHL, B., SALAT, D. H., BUSA, E., ALBERT, M., DIETERICH, M., HASELGROVE, C., VAN DER KOUWE, A., KILLIANY, R., KENNEDY, D., KLAVENESS, S., MONTILLO, A., MAKRIS, N., ROSEN, B. & DALE, A. M. 2002. Whole brain segmentation: automated labeling of neuroanatomical structures in the human brain. *Neuron,* 33**,** 341-355.

FISCHL, B., SALAT, D. H., VAN DER KOUWE, A. J. W., MAKRIS, N., SÉGONNE, F., QUINN, B. T. & DALE, A. M. 2004a. Sequence-independent segmentation of magnetic resonance images. *NeuroImage,* 23**,** S69-S84.

FISCHL, B., SERENO, M. I. & DALE, A. 1999a. Cortical Surface-Based Analysis: II: Inflation, Flattening, and a Surface-Based Coordinate System. *NeuroImage,* 9**,** 195-207.

FISCHL, B., SERENO, M. I., TOOTELL, R. B. H. & DALE, A. M. 1999b. High-resolution intersubject averaging and a coordinate system for the cortical surface. *Human Brain Mapping,* 8**,** 272-284.

FISCHL, B., VAN DER KOUWE, A., DESTRIEUX, C., HALGREN, E., SÉGONNE, F., SALAT, D. H., BUSA, E., SEIDMAN, L. J., GOLDSTEIN, J., KENNEDY, D., CAVINESS, V., MAKRIS, N., ROSEN, B. & DALE, A. M. 2004b. Automatically Parcellating the Human Cerebral Cortex. *Cerebral Cortex,* 14**,** 11-22.

FISH, J. L., DEHAY, C., KENNEDY, H. & HUTTNER, W. B. 2008. Making bigger brains-the evolution of neural-progenitor-cell division. *J Cell Sci,* 121**,** 2783-93.

FISNIKU, L. K., CHARD, D. T., JACKSON, J. S., ANDERSON, V. M., ALTMANN, D. R., MISZKIEL, K. A., THOMPSON, A. J. & MILLER, D. H. 2008. Gray matter atrophy is related to long-term disability in multiple sclerosis. *Ann Neurol,* 64**,** 247-54.

FLEISCHER, V., RADETZ, A., CIOLAC, D., MUTHURAMAN, M., GONZALEZ-ESCAMILLA, G., ZIPP, F. & GROPPA, S. 2019. Graph Theoretical Framework of Brain Networks in Multiple Sclerosis: A Review of Concepts. *Neuroscience,* 403**,** 35-53.

FLOOD, D. G. & COLEMAN, P. D. 1988. Neuron numbers and sizes in aging brain: comparisons of human, monkey, and rodent data. *Neurobiol Aging,* 9**,** 453-63.

FRANKE, K. & GASER, C. 2019. Ten Years of BrainAGE as a Neuroimaging Biomarker of Brain Aging: What Insights Have We Gained? *Front Neurol,* 10**,** 789.

FRANKE, K., GASER, C. & INITIATIVE, F. 2012. Longitudinal Changes in Individual BrainAGE in Healthy Aging, Mild Cognitive Impairment, and Alzheimer's Disease. *GeroPsych - The Journal of Gerontopsychology and Geriatric Psychiatry,* 25**,** 235-245.

FRANKE, K., GASER, C., MANOR, B. & NOVAK, V. 2013. Advanced BrainAGE in older adults with type 2 diabetes mellitus. *Front Aging Neurosci,* 5**,** 90.

FRANKE, K., ZIEGLER, G., KLOPPEL, S., GASER, C. & ALZHEIMER'S DISEASE NEUROIMAGING, I. 2010. Estimating the age of healthy subjects from T1-weighted MRI scans using kernel methods: exploring the influence of various parameters. *Neuroimage,* 50**,** 883-92.

GAO, Y., NIE, K., MEI, M., GUO, M., HUANG, Z., WANG, L., ZHAO, J., HUANG, B., ZHANG, Y. & WANG, L. 2018. Changes in Cortical Thickness in Patients With Early Parkinson's Disease at Different Hoehn and Yahr Stages. *Front Hum Neurosci,* 12**,** 469.

GEE, M., DUKART, J., DRAGANSKI, B., WAYNE MARTIN, W. R., EMERY, D. & CAMICIOLI, R. 2017. Regional volumetric change in Parkinson's disease with cognitive decline. *J Neurol Sci,* 373**,** 88-94.

GEISSELER, O., PFLUGSHAUPT, T., BEZZOLA, L., REUTER, K., WELLER, D., SCHUKNECHT, B., BRUGGER, P. & LINNEBANK, M. 2016. Cortical thinning in the anterior cingulate cortex predicts multiple sclerosis patients' fluency performance in a lateralised manner. *Neuroimage Clin,* 10**,** 89-95.

GERALDES, R., ESIRI, M. M., DELUCA, G. C. & PALACE, J. 2017. Age-related small vessel disease: a potential contributor to neurodegeneration in multiple sclerosis. *Brain Pathol,* 27**,** 707-722.

GHIONE, E., BERGSLAND, N., DWYER, M. G., HAGEMEIER, J., JAKIMOVSKI, D., PAUNKOSKI, I., RAMASAMY, D. P., CARL, E., HOJNACKI, D., KOLB, C., WEINSTOCK-GUTTMAN, B. & ZIVADINOV, R. 2019. Aging and Brain Atrophy in Multiple Sclerosis. *J Neuroimaging,* 29**,** 527-535.

GONZALEZ-ESCAMILLA, G., LANGE, C., TEIPEL, S., BUCHERT, R., GROTHE, M. J. & ALZHEIMER'S DISEASE NEUROIMAGING, I. 2017. PETPVE12: an SPM toolbox for Partial Volume Effects correction in brain PET - Application to amyloid imaging with AV45-PET. *Neuroimage,* 147**,** 669-677.

GONZALEZ-ESCAMILLA, G., MIEDERER, I., GROTHE, M. J., SCHRECKENBERGER, M., MUTHURAMAN, M., GROPPA, S. & ALZHEIMER'S DISEASE NEUROIMAGING, I. 2020. Metabolic and amyloid PET network reorganization in Alzheimer's disease: differential patterns and partial volume effects. *Brain Imaging Behav*.

GONZALEZ-ESCAMILLA, G., MUTHURAMAN, M., REICH, M. M., KOIRALA, N., RIEDEL, C., GLASER, M., LANGE, F., DEUSCHL, G., VOLKMANN, J. & GROPPA, S. 2019. Cortical network fingerprints predict deep brain stimulation outcome in dystonia. *Mov Disord,* 34**,** 1537-1546.

GROENEVELD, O., REIJMER, Y., HEINEN, R., KUIJF, H., KOEKKOEK, P., JANSSEN, J., RUTTEN, G., KAPPELLE, L., BIESSELS, G. & GROUP, C.-I. S. 2018. Brain imaging correlates of mild cognitive impairment and early dementia in patients with type 2 diabetes mellitus. *Nutr Metab Cardiovasc Dis,* 28**,** 1253-1260.

GROTHE, M. J., SEPULCRE, J., GONZALEZ-ESCAMILLA, G., JELISTRATOVA, I., SCHOLL, M., HANSSON, O., TEIPEL, S. J. & ALZHEIMER'S DISEASE NEUROIMAGING, I. 2018. Molecular properties underlying regional vulnerability to Alzheimer's disease pathology. *Brain,* 141**,** 2755-2771.

GROTHE, M. J., TEIPEL, S. J. & ALZHEIMER'S DISEASE NEUROIMAGING, I. 2016. Spatial patterns of atrophy, hypometabolism, and amyloid deposition in Alzheimer's disease correspond to dissociable functional brain networks. *Hum Brain Mapp,* 37**,** 35-53.

GROVES, A. R., SMITH, S. M., FJELL, A. M., TAMNES, C. K., WALHOVD, K. B., DOUAUD, G., WOOLRICH, M. W. & WESTLYE, L. T. 2012. Benefits of multi-modal fusion analysis on a large-scale dataset: life-span patterns of inter-subject variability in cortical morphometry and white matter microstructure. *Neuroimage,* 63**,** 365-80.

GUIMARAES, R. P., ARCI SANTOS, M. C., DAGHER, A., CAMPOS, L. S., AZEVEDO, P., PIOVESANA, L. G., DE CAMPOS, B. M., LARCHER, K., ZEIGHAMI, Y., SCARPARO AMATO-FILHO, A. C., CENDES, F. & D'ABREU, A. C. 2016. Pattern of Reduced Functional Connectivity and Structural Abnormalities in Parkinson's Disease: An Exploratory Study. *Front Neurol,* 7**,** 243.

GUPTA, Y., LEE, K. H., CHOI, K. Y., LEE, J. J., KIM, B. C. & KWON, G. R. 2019. Alzheimer's Disease Diagnosis Based on Cortical and Subcortical Features. *J Healthc Eng,* 2019**,** 2492719.

HAN, X., JOVICICH, J., SALAT, D., VAN DER KOUWE, A., QUINN, B., CZANNER, S., BUSA, E., PACHECO, J., ALBERT, M., KILLIANY, R., MAGUIRE, P., ROSAS, D., MAKRIS, N., DALE, A., DICKERSON, B. & FISCHL, B. 2006a. Reliability of MRI-derived measurements of human cerebral cortical thickness: the effects of field strength, scanner upgrade and manufacturer. *Neuroimage,* 32**,** 180-94.

HAN, X., JOVICICH, J., SALAT, D., VAN DER KOUWE, A., QUINN, B., CZANNER, S., BUSA, E., PACHECO, J., ALBERT, M., KILLIANY, R., MAGUIRE, P., ROSAS, D., MAKRIS, N., DALE, A., DICKERSON, B. & FISCHL, B. 2006b. Reliability of MRI-derived measurements of human cerebral cortical thickness: The effects of field strength, scanner upgrade and manufacturer. *NeuroImage,* 32**,** 180-194.

HANGANU, A., BRUNEAU, M. A., DEGROOT, C., BEDETTI, C., MEJIA-CONSTAIN, B., LAFONTAINE, A. L., CHOUINARD, S. & MONCHI, O. 2017. Depressive symptoms in Parkinson's disease correlate with cortical atrophy over time. *Brain Cogn,* 111**,** 127-133.

HENNEGES, C., REED, C., CHEN, Y. F., DELL'AGNELLO, G. & LEBREC, J. 2016. Describing the Sequence of Cognitive Decline in Alzheimer's Disease Patients: Results from an Observational Study. *J Alzheimers Dis,* 52**,** 1065-80.

HOGSTROM, L. J., WESTLYE, L. T., WALHOVD, K. B. & FJELL, A. M. 2013. The structure of the cerebral cortex across adult life: age-related patterns of surface area, thickness, and gyrification. *Cereb Cortex,* 23**,** 2521-30.

HUK, W. J. & GADEMANN, G. 1984. Magnetic resonance imaging (MRI): method and early clinical experiences in diseases of the central nervous system. *Neurosurg Rev,* 7**,** 259-80.

HUTTON, C., DE VITA, E., ASHBURNER, J., DEICHMANN, R. & TURNER, R. 2008. Voxel-based cortical thickness measurements in MRI. *Neuroimage,* 40**,** 1701-10.

HWANG, J., KIM, C. M., JEON, S., LEE, J. M., HONG, Y. J., ROH, J. H., LEE, J. H., KOH, J. Y. & NA, D. L. 2016. Prediction of Alzheimer's disease pathophysiology based on cortical thickness patterns. *Alzheimers Dement (Amst),* 2**,** 58-67.

IACCARINO, L., TAMMEWAR, G., AYAKTA, N., BAKER, S. L., BEJANIN, A., BOXER, A. L., GORNO-TEMPINI, M. L., JANABI, M., KRAMER, J. H., LAZARIS, A., LOCKHART, S. N., MILLER, B. L., MILLER, Z. A., O'NEIL, J. P., OSSENKOPPELE, R., ROSEN, H. J., SCHONHAUT, D. R., JAGUST, W. J. & RABINOVICI, G. D. 2018. Local and distant relationships between amyloid, tau and neurodegeneration in Alzheimer's Disease. *Neuroimage Clin,* 17**,** 452-464.

JACK, C. R., JR., BENNETT, D. A., BLENNOW, K., CARRILLO, M. C., DUNN, B., HAEBERLEIN, S. B., HOLTZMAN, D. M., JAGUST, W., JESSEN, F., KARLAWISH, J., LIU, E., MOLINUEVO, J. L., MONTINE, T., PHELPS, C., RANKIN, K. P., ROWE, C. C., SCHELTENS, P., SIEMERS, E., SNYDER, H. M., SPERLING, R. & CONTRIBUTORS 2018. NIA-AA Research Framework: Toward a biological definition of Alzheimer's disease. *Alzheimers Dement,* 14**,** 535-562.

JAHN, H. 2013. Memory loss in Alzheimer's disease. *Dialogues Clin Neurosci,* 15**,** 445-54.

JAMES, G., WITTEN, D., HASTIE, T. & TIBSHIRANI, R. 2017. *An introduction to statistical learning : with applications in R [E-Book],* New York, Springer.

JEONG, S. 2017. Molecular and Cellular Basis of Neurodegeneration in Alzheimer's Disease. *Mol Cells,* 40**,** 613-620.

JEROME FRIEDMAN, T. H., ROBERT TIBSHIRANI 2010. Regularization Paths for Generalized Linear Models
via Coordinate Descent.: Journal of Statistical Software, 33(1), 1-22.
JOO, S. H., LIM, H. K. & LEE, C. U. 2016. Three Large-Scale Functional Brain Networks from Resting-State Functional MRI in Subjects with Different Levels of Cognitive Impairment. *Psychiatry Investig,* 13**,** 1-7.
JUNG, W. H., KIM, J. S., JANG, J. H., CHOI, J. S., JUNG, M. H., PARK, J. Y., HAN, J. Y., CHOI, C. H., KANG, D. H., CHUNG, C. K. & KWON, J. S. 2011. Cortical thickness reduction in individuals at ultra-high-risk for psychosis. *Schizophr Bull,* 37**,** 839-49.
KANDEL, B. M., WOLK, D. A., GEE, J. C. & AVANTS, B. 2013. Predicting cognitive data from medical images using sparse linear regression. *Inf Process Med Imaging,* 23**,** 86-97.
KASSAMBARA, A. 2019. 'ggplot2' Based Publication Ready Plots.
KEEZER, M. R., WOLFSON, C. & POSTUMA, R. B. 2016. Age, Gender, Comorbidity, and the MDS-UPDRS: Results from a Population-Based Study. *Neuroepidemiology,* 46**,** 222-7.
KHAN, A. U., AKRAM, M., DANIYAL, M. & ZAINAB, R. 2019. Awareness and current knowledge of Parkinson's disease: a neurodegenerative disorder. *Int J Neurosci,* 129**,** 55-93.
KHUNDRAKPAM, B. S., TOHKA, J., EVANS, A. C. & BRAIN DEVELOPMENT COOPERATIVE, G. 2015. Prediction of brain maturity based on cortical thickness at different spatial resolutions. *Neuroimage,* 111**,** 350-9.
KIM, E. J., KIM, B. C., KIM, S. J., JUNG, D. S., SIN, J. S., YOON, Y. J., CHIN, J., LEE, K. H. & NA, D. L. 2012. Clinical staging of semantic dementia in an FDG-PET study using FTLD-CDR. *Dement Geriatr Cogn Disord,* 34**,** 300-6.
KIM, J. P., KIM, J., PARK, Y. H., PARK, S. B., LEE, J. S., YOO, S., KIM, E. J., KIM, H. J., NA, D. L., BROWN, J. A., LOCKHART, S. N., SEO, S. W. & SEONG, J. K. 2019. Machine learning based hierarchical classification of frontotemporal dementia and Alzheimer's disease. *Neuroimage Clin,* 23**,** 101811.
KOIRALA, N., ANWAR, A. R., CIOLAC, D., GLASER, M., PINTEA, B., DEUSCHL, G., MUTHURAMAN, M. & GROPPA, S. 2019. Alterations in White Matter Network and Microstructural Integrity Differentiate Parkinson's Disease Patients and Healthy Subjects. *Front Aging Neurosci,* 11**,** 191.
KONUKOGLU, E., GLOCKER, B., ZIKIC, D. & CRIMINISI, A. 2013. Neighbourhood approximation using randomized forests. *Med Image Anal,* 17**,** 790-804.
KOVACS, G. G. 2019. Molecular pathology of neurodegenerative diseases: principles and practice. *J Clin Pathol,* 72**,** 725-735.
KUNST, J., MARECEK, R., KLOBUSIAKOVA, P., BALAZOVA, Z., ANDERKOVA, L., NEMCOVA-ELFMARKOVA, N. & REKTOROVA, I. 2019. Patterns of Grey Matter Atrophy at Different Stages of Parkinson's and Alzheimer's Diseases and Relation to Cognition. *Brain Topogr,* 32**,** 142-160.
KUPERBERG, G. R., BROOME, M., MCGUIRE, P. K., DAVID, A. S., EDDY, M., OZAWA, F., GOFF, D., WEST, W. C., WILLIAMS, S. C. R., VAN DER KOUWE, A., SALAT, D., DALE, A. & FISCHL, B. 2003. Regionally localized thinning of the cerebral cortex in Schizophrenia. *Archives of General Psychiatry,* 60**,** 878-888.
LAI, T. L., ROBBINS, H. & WEI, C. Z. 1978. Strong consistency of least squares estimates in multiple regression. *Proc Natl Acad Sci U S A,* 75**,** 3034-6.
LANE, C. A., HARDY, J. & SCHOTT, J. M. 2018. Alzheimer's disease. *Eur J Neurol,* 25**,** 59-70.
LANGA, K. M. & LEVINE, D. A. 2014. The diagnosis and management of mild cognitive impairment: a clinical review. *JAMA,* 312**,** 2551-61.

LE, T. T., KUPLICKI, R. T., MCKINNEY, B. A., YEH, H. W., THOMPSON, W. K., PAULUS, M. P. & TULSA, I. 2018. A Nonlinear Simulation Framework Supports Adjusting for Age When Analyzing BrainAGE. *Front Aging Neurosci,* 10**,** 317.

LEE, J., CHO, H., JEON, S., KIM, H. J., KIM, Y. J., LEE, J., KIM, S. T., LEE, J. M., CHIN, J., LOCKHART, S. N., LEE, A. Y., NA, D. L. & SEO, S. W. 2018. Sex-Related Reserve Hypothesis in Alzheimer's Disease: Changes in Cortical Thickness with a Five-Year Longitudinal Follow-Up. *J Alzheimers Dis,* 65**,** 641-649.

LEMAITRE, H., GOLDMAN, A. L., SAMBATARO, F., VERCHINSKI, B. A., MEYER-LINDENBERG, A., WEINBERGER, D. R. & MATTAY, V. S. 2012. Normal age-related brain morphometric changes: nonuniformity across cortical thickness, surface area and gray matter volume? *Neurobiol Aging,* 33**,** 617 e1-9.

LEWIS, M. M., DU, G., LEE, E. Y., NASRALAH, Z., STERLING, N. W., ZHANG, L., WAGNER, D., KONG, L., TROSTER, A. I., STYNER, M., ESLINGER, P. J., MAILMAN, R. B. & HUANG, X. 2016. The pattern of gray matter atrophy in Parkinson's disease differs in cortical and subcortical regions. *J Neurol,* 263**,** 68-75.

LI, S., YUAN, X., PU, F., LI, D., FAN, Y., WU, L., CHAO, W., CHEN, N., HE, Y. & HAN, Y. 2014. Abnormal changes of multidimensional surface features using multivariate pattern classification in amnestic mild cognitive impairment patients. *J Neurosci,* 34**,** 10541-53.

LIBON, D. J., XIE, S. X., EPPIG, J., WICAS, G., LAMAR, M., LIPPA, C., BETTCHER, B. M., PRICE, C. C., GIOVANNETTI, T., SWENSON, R. & WAMBACH, D. M. 2010. The heterogeneity of mild cognitive impairment: a neuropsychological analysis. *J Int Neuropsychol Soc,* 16**,** 84-93.

LIEM, F., VAROQUAUX, G., KYNAST, J., BEYER, F., KHARABIAN MASOULEH, S., HUNTENBURG, J. M., LAMPE, L., RAHIM, M., ABRAHAM, A., CRADDOCK, R. C., RIEDEL-HELLER, S., LUCK, T., LOEFFLER, M., SCHROETER, M. L., WITTE, A. V., VILLRINGER, A. & MARGULIES, D. S. 2017. Predicting brain-age from multimodal imaging data captures cognitive impairment. *Neuroimage,* 148**,** 179-188.

LIN, L., JIN, C., FU, Z., ZHANG, B., BIN, G. & WU, S. 2016. Predicting healthy older adult's brain age based on structural connectivity networks using artificial neural networks. *Comput Methods Programs Biomed,* 125**,** 8-17.

LIU, Y., XIE, T., HE, Y., DUAN, Y., HUANG, J., REN, Z., GONG, G., WANG, J., YE, J., DONG, H., BUTZKUEVEN, H., SHI, F. D., SHU, N. & LI, K. 2014. Cortical thinning correlates with cognitive change in multiple sclerosis but not in neuromyelitis optica. *Eur Radiol,* 24**,** 2334-43.

LOWE, L. C., GASER, C., FRANKE, K. & ALZHEIMER'S DISEASE NEUROIMAGING, I. 2016. The Effect of the APOE Genotype on Individual BrainAGE in Normal Aging, Mild Cognitive Impairment, and Alzheimer's Disease. *PLoS One,* 11**,** e0157514.

LUDERS, E., CHERBUIN, N. & GASER, C. 2016. Estimating brain age using high-resolution pattern recognition: Younger brains in long-term meditation practitioners. *Neuroimage,* 134**,** 508-513.

LY, M., YU, G. Z., KARIM, H. T., MUPPIDI, N. R., MIZUNO, A., KLUNK, W. E., AIZENSTEIN, H. J. & ALZHEIMER'S DISEASE NEUROIMAGING, I. 2020. Improving brain age prediction models: incorporation of amyloid status in Alzheimer's disease. *Neurobiol Aging,* 87**,** 44-48.

MA, X., LI, Z., JING, B., LIU, H., LI, D. & LI, H. 2016. Identify the Atrophy of Alzheimer's Disease, Mild Cognitive Impairment and Normal Aging Using Morphometric MRI Analysis. *Front Aging Neurosci,* 8**,** 243.

MADAN, C. 2016. Prism: Multiple spline regression with regularization, dimensionality reduction, and feature selection. *Journal of Open Source Software,* 1**,** 31.

MADAN, C. R. & KENSINGER, E. A. 2018. Predicting age from cortical structure across the lifespan. *Eur J Neurosci,* 47**,** 399-416.

MAIOVIS, P., IOANNIDIS, P., GERASIMOU, G., GOTZAMANI-PSARRAKOU, A. & KARACOSTAS, D. 2017. Frontotemporal Lobar Degeneration-Modified Clinical Dementia Rating (FTLD-CDR) Scale and Frontotemporal Dementia Rating Scale (FRS) Correlation With Regional Brain Perfusion in a Series of FTLD Patients. *J Neuropsychiatry Clin Neurosci,* 29**,** 26-30.

MAK, E., BERGSLAND, N., DWYER, M. G., ZIVADINOV, R. & KANDIAH, N. 2014. Subcortical atrophy is associated with cognitive impairment in mild Parkinson disease: a combined investigation of volumetric changes, cortical thickness, and vertex-based shape analysis. *AJNR Am J Neuroradiol,* 35**,** 2257-64.

MANN, D. M. A. & SNOWDEN, J. S. 2017. Frontotemporal lobar degeneration: Pathogenesis, pathology and pathways to phenotype. *Brain Pathol,* 27**,** 723-736.

MANOUCHEHRINIA, A., WESTERLIND, H., KINGWELL, E., ZHU, F., CARRUTHERS, R., RAMANUJAM, R., BAN, M., GLASER, A., SAWCER, S., TREMLETT, H. & HILLERT, J. 2017. Age Related Multiple Sclerosis Severity Score: Disability ranked by age. *Mult Scler,* 23**,** 1938-1946.

MASTERS, C. L., BATEMAN, R., BLENNOW, K., ROWE, C. C., SPERLING, R. A. & CUMMINGS, J. L. 2015. Alzheimer's disease. *Nat Rev Dis Primers,* 1**,** 15056.

MATTHEWS, F. E., STEPHAN, B. C., MCKEITH, I. G., BOND, J., BRAYNE, C., MEDICAL RESEARCH COUNCIL COGNITIVE, F. & AGEING, S. 2008. Two-year progression from mild cognitive impairment to dementia: to what extent do different definitions agree? *J Am Geriatr Soc,* 56**,** 1424-33.

MAX KUHN, J. W., STEVE WESTON, ANDRE WILLIAMS, CHRIS KEEFER, ALLAN ENGELHARDT, TONY, COOPER, Z. M., BRENTON KENKEL, THE R CORE TEAM, MICHAEL BENESTY, REYNALD LESCARBEAU, ANDREW ZIEM, & LUCA SCRUCCA, Y. T., CAN CANDAN AND TYLER HUNT. 2018. caret: Classification and Regression Training. R package version 6.0-81. ed.

MCKAY, D. R., KNOWLES, E. E., WINKLER, A. A., SPROOTEN, E., KOCHUNOV, P., OLVERA, R. L., CURRAN, J. E., KENT, J. W., JR., CARLESS, M. A., GORING, H. H., DYER, T. D., DUGGIRALA, R., ALMASY, L., FOX, P. T., BLANGERO, J. & GLAHN, D. C. 2014. Influence of age, sex and genetic factors on the human brain. *Brain Imaging Behav,* 8**,** 143-52.

MENDEZ, M. F. 2017. Early-Onset Alzheimer Disease. *Neurol Clin,* 35**,** 263-281.

MILLER, A. K., ALSTON, R. L. & CORSELLIS, J. A. 1980. Variation with age in the volumes of grey and white matter in the cerebral hemispheres of man: measurements with an image analyser. *Neuropathol Appl Neurobiol,* 6**,** 119-32.

MIOSHI, E., FLANAGAN, E. & KNOPMAN, D. 2017. Detecting clinical change with the CDR-FTLD: differences between FTLD and AD dementia. *Int J Geriatr Psychiatry,* 32**,** 977-982.

MITCHELL, A. J. 2009. A meta-analysis of the accuracy of the mini-mental state examination in the detection of dementia and mild cognitive impairment. *J Psychiatr Res,* 43**,** 411-31.

MOLLER, C., HAFKEMEIJER, A., PIJNENBURG, Y. A. L., ROMBOUTS, S., VAN DER GROND, J., DOPPER, E., VAN SWIETEN, J., VERSTEEG, A., STEENWIJK, M. D., BARKHOF, F., SCHELTENS, P., VRENKEN, H. & VAN DER FLIER, W. M. 2016. Different patterns of cortical gray matter loss over time in behavioral variant frontotemporal dementia and Alzheimer's disease. *Neurobiol Aging,* 38**,** 21-31.

MOON, S. W., LEE, B. & CHOI, Y. C. 2018. Changes in the Hippocampal Volume and Shape in Early-Onset Mild Cognitive Impairment. *Psychiatry Investig,* 15**,** 531-537.
MUFSON, E. J., BINDER, L., COUNTS, S. E., DEKOSKY, S. T., DE TOLEDO-MORRELL, L., GINSBERG, S. D., IKONOMOVIC, M. D., PEREZ, S. E. & SCHEFF, S. W. 2012. Mild cognitive impairment: pathology and mechanisms. *Acta Neuropathol,* 123**,** 13-30.
MUTHURAMAN, M., DEUSCHL, G., KOIRALA, N., RIEDEL, C., VOLKMANN, J. & GROPPA, S. 2017. Effects of DBS in parkinsonian patients depend on the structural integrity of frontal cortex. *Sci Rep,* 7**,** 43571.
MWANGI, B., HASAN, K. M. & SOARES, J. C. 2013. Prediction of individual subject's age across the human lifespan using diffusion tensor imaging: a machine learning approach. *Neuroimage,* 75**,** 58-67.
NENADIC, I., DIETZEK, M., LANGBEIN, K., SAUER, H. & GASER, C. 2017. BrainAGE score indicates accelerated brain aging in schizophrenia, but not bipolar disorder. *Psychiatry Res Neuroimaging,* 266**,** 86-89.
O'BRYANT, S. E., WARING, S. C., CULLUM, C. M., HALL, J., LACRITZ, L., MASSMAN, P. J., LUPO, P. J., REISCH, J. S., DOODY, R. & TEXAS ALZHEIMER'S RESEARCH, C. 2008. Staging dementia using Clinical Dementia Rating Scale Sum of Boxes scores: a Texas Alzheimer's research consortium study. *Arch Neurol,* 65**,** 1091-5.
ONG, M., FOO, H., CHANDER, R. J., WEN, M. C., AU, W. L., SITOH, Y. Y., TAN, L. & KANDIAH, N. 2017. Influence of diabetes mellitus on longitudinal atrophy and cognition in Parkinson's disease. *J Neurol Sci,* 377**,** 122-126.
ORBACH, L., MENASCU, S., HOFFMANN, C., MIRON, S. & ACHIRON, A. 2018. Focal cortical thinning in patients with stable relapsing-remitting multiple sclerosis: cross-sectional-based novel estimation of gray matter kinetics. *Neuroradiology,* 60**,** 179-187.
OSHER, J. E., WICKLUND, A. H., RADEMAKER, A., JOHNSON, N. & WEINTRAUB, S. 2007. The mini-mental state examination in behavioral variant frontotemporal dementia and primary progressive aphasia. *Am J Alzheimers Dis Other Demen,* 22**,** 468-73.
PAPMA, J. M., JISKOOT, L. C., PANMAN, J. L., DOPPER, E. G., DEN HEIJER, T., DONKER KAAT, L., PIJNENBURG, Y. A. L., MEETER, L. H., VAN MINKELEN, R., ROMBOUTS, S. & VAN SWIETEN, J. C. 2017. Cognition and gray and white matter characteristics of presymptomatic C9orf72 repeat expansion. *Neurology,* 89**,** 1256-1264.
PARETO, D., SASTRE-GARRIGA, J., AUGER, C., VIVES-GILABERT, Y., DELGADO, J., TINTORE, M., MONTALBAN, X. & ROVIRA, A. 2015. Juxtacortical Lesions and Cortical Thinning in Multiple Sclerosis. *AJNR Am J Neuroradiol,* 36**,** 2270-6.
PATERNICO, D., MANES, M., PREMI, E., COSSEDDU, M., GAZZINA, S., ALBERICI, A., ARCHETTI, S., BONOMI, E., COTELLI, M. S., COTELLI, M., TURLA, M., MICHELI, A., GASPAROTTI, R., PADOVANI, A. & BORRONI, B. 2016. Frontotemporal dementia and language networks: cortical thickness reduction is driven by dyslexia susceptibility genes. *Sci Rep,* 6**,** 30848.
PENG, B., WANG, S., ZHOU, Z., LIU, Y., TONG, B., ZHANG, T. & DAI, Y. 2017. A multilevel-ROI-features-based machine learning method for detection of morphometric biomarkers in Parkinson's disease. *Neurosci Lett,* 651**,** 88-94.
PERLMUTTER, J. S. 2009. Assessment of Parkinson disease manifestations. *Curr Protoc Neurosci,* Chapter 10**,** Unit10 1.
PETROU, M., DAVATZIKOS, C., HSIEH, M., FOERSTER, B. R., ALBIN, R. L., KOTAGAL, V., MULLER, M. L., KOEPPE, R. A., HERMAN, W. H., FREY, K. A. & BOHNEN, N. I. 2016. Diabetes, Gray Matter Loss, and Cognition in the Setting of Parkinson Disease. *Acad Radiol,* 23**,** 577-81.

PFEFFERBAUM, A. & SULLIVAN, E. V. 2015. Cross-sectional versus longitudinal estimates of age-related changes in the adult brain: overlaps and discrepancies. *Neurobiol Aging,* 36**,** 2563-7.

PITTERI, M., ROMUALDI, C., MAGLIOZZI, R., MONACO, S. & CALABRESE, M. 2017. Cognitive impairment predicts disability progression and cortical thinning in MS: An 8-year study. *Mult Scler,* 23**,** 848-854.

PRADIER, C., SAKAROVITCH, C., LE DUFF, F., LAYESE, R., METELKINA, A., ANTHONY, S., TIFRATENE, K. & ROBERT, P. 2014. The mini mental state examination at the time of Alzheimer's disease and related disorders diagnosis, according to age, education, gender and place of residence: a cross-sectional study among the French National Alzheimer database. *PLoS One,* 9**,** e103630.

PRAVATA, E., ROCCA, M. A., VALSASINA, P., RICCITELLI, G. C., GOBBI, C., COMI, G., FALINI, A. & FILIPPI, M. 2017. Gray matter trophism, cognitive impairment, and depression in patients with multiple sclerosis. *Mult Scler,* 23**,** 1864-1874.

R CORE TEAM 2018. R: A language and environment for statistical computing. Vienna, Austria: R Foundation for Statistical Computing.

RABINOVICI, G. D. 2019. Late-onset Alzheimer Disease. *Continuum (Minneap Minn),* 25**,** 14-33.

RABINOVICI, G. D. & MILLER, B. L. 2010. Frontotemporal lobar degeneration: epidemiology, pathophysiology, diagnosis and management. *CNS Drugs,* 24**,** 375-98.

RAVI SELKER, J. L. A. D. D. 2019. jmv: The 'jamovi' Analyses.

REUTER, M., ROSAS, H. D. & FISCHL, B. 2010. Highly Accurate Inverse Consistent Registration: A Robust Approach. *NeuroImage,* 53**,** 1181-1196.

REUTER, M., SCHMANSKY, N. J., ROSAS, H. D. & FISCHL, B. 2012. Within-Subject Template Estimation for Unbiased Longitudinal Image Analysis. *NeuroImage,* 61**,** 1402-1418.

RIGHART, R., SCHMIDT, P., DAHNKE, R., BIBERACHER, V., BEER, A., BUCK, D., HEMMER, B., KIRSCHKE, J. S., ZIMMER, C., GASER, C. & MUHLAU, M. 2017. Volume versus surface-based cortical thickness measurements: A comparative study with healthy controls and multiple sclerosis patients. *PLoS One,* 12**,** e0179590.

ROGENMOSER, L., KERNBACH, J., SCHLAUG, G. & GASER, C. 2018. Keeping brains young with making music. *Brain Struct Funct,* 223**,** 297-305.

ROHRER, J. D., NICHOLAS, J. M., CASH, D. M., VAN SWIETEN, J., DOPPER, E., JISKOOT, L., VAN MINKELEN, R., ROMBOUTS, S. A., CARDOSO, M. J., CLEGG, S., ESPAK, M., MEAD, S., THOMAS, D. L., DE VITA, E., MASELLIS, M., BLACK, S. E., FREEDMAN, M., KEREN, R., MACINTOSH, B. J., ROGAEVA, E., TANG-WAI, D., TARTAGLIA, M. C., LAFORCE, R., JR., TAGLIAVINI, F., TIRABOSCHI, P., REDAELLI, V., PRIONI, S., GRISOLI, M., BORRONI, B., PADOVANI, A., GALIMBERTI, D., SCARPINI, E., ARIGHI, A., FUMAGALLI, G., ROWE, J. B., COYLE-GILCHRIST, I., GRAFF, C., FALLSTROM, M., JELIC, V., STAHLBOM, A. K., ANDERSSON, C., THONBERG, H., LILIUS, L., FRISONI, G. B., PIEVANI, M., BOCCHETTA, M., BENUSSI, L., GHIDONI, R., FINGER, E., SORBI, S., NACMIAS, B., LOMBARDI, G., POLITO, C., WARREN, J. D., OURSELIN, S., FOX, N. C., ROSSOR, M. N. & BINETTI, G. 2015. Presymptomatic cognitive and neuroanatomical changes in genetic frontotemporal dementia in the Genetic Frontotemporal dementia Initiative (GENFI) study: a cross-sectional analysis. *Lancet Neurol,* 14**,** 253-62.

ROHRER, J. D. & ROSEN, H. J. 2013. Neuroimaging in frontotemporal dementia. *Int Rev Psychiatry,* 25**,** 221-9.

ROSAS, H. D., LIU, A. K., HERSCH, S., GLESSNER, M., FERRANTE, R. J., SALAT, D. H., VAN DER KOUWE, A., JENKINS, B. G., DALE, A. M. & FISCHL, B. 2002. Regional and progressive thinning of the cortical ribbon in Huntington's disease. *Neurology,* 58**,** 695-701.

SABUNCU, M. R. & VAN LEEMPUT, K. 2011. The Relevance Voxel Machine (RVoxM): a Bayesian method for image-based prediction. *Med Image Comput Comput Assist Interv,* 14**,** 99-106.

SALAT, D., BUCKNER, R. L., SNYDER, A. Z., GREVE, D. N., DESIKAN, R. S., BUSA, E., MORRIS, J. C., DALE, A. & FISCHL, B. 2004. Thinning of the cerebral cortex in aging. *Cerebral Cortex,* 14**,** 721-730.

SANAI, S. A., SAINI, V., BENEDICT, R. H., ZIVADINOV, R., TETER, B. E., RAMANATHAN, M. & WEINSTOCK-GUTTMAN, B. 2016. Aging and multiple sclerosis. *Mult Scler,* 22**,** 717-25.

SCHELTENS, P., BLENNOW, K., BRETELER, M. M., DE STROOPER, B., FRISONI, G. B., SALLOWAY, S. & VAN DER FLIER, W. M. 2016. Alzheimer's disease. *Lancet,* 388**,** 505-17.

SCHNACK, H. G., VAN HAREN, N. E., NIEUWENHUIS, M., HULSHOFF POL, H. E., CAHN, W. & KAHN, R. S. 2016. Accelerated Brain Aging in Schizophrenia: A Longitudinal Pattern Recognition Study. *Am J Psychiatry,* 173**,** 607-16.

SEGONNE, F., DALE, A. M., BUSA, E., GLESSNER, M., SALAT, D., HAHN, H. K. & FISCHL, B. 2004. A hybrid approach to the skull stripping problem in MRI. *NeuroImage,* 22**,** 1060-1075.

SEGONNE, F., PACHECO, J. & FISCHL, B. 2007. Geometrically accurate topology-correction of cortical surfaces using nonseparating loops. *IEEE Trans Med Imaging,* 26**,** 518-529.

SEGURA, B., BAGGIO, H. C., MARTI, M. J., VALLDEORIOLA, F., COMPTA, Y., GARCIA-DIAZ, A. I., VENDRELL, P., BARGALLO, N., TOLOSA, E. & JUNQUE, C. 2014. Cortical thinning associated with mild cognitive impairment in Parkinson's disease. *Mov Disord,* 29**,** 1495-503.

SEN, S. 2018. Neurostatus and EDSS Calculation with Cases. *Noro Psikiyatr Ars,* 55**,** S80-S83.

SEO, S. W., THIBODEAU, M. P., PERRY, D. C., HUA, A., SIDHU, M., SIBLE, I., VARGAS, J. N. S., GAUS, S. E., RABINOVICI, G. D., RANKIN, K. D., BOXER, A. L., KRAMER, J. H., ROSEN, H. J., GORNO-TEMPINI, M. L., GRINBERG, L. T., HUANG, E. J., DEARMOND, S. J., TROJANOWSKI, J. Q., MILLER, B. L. & SEELEY, W. W. 2018. Early vs late age at onset frontotemporal dementia and frontotemporal lobar degeneration. *Neurology,* 90**,** e1047-e1056.

SHAIKH, T. A. & ALI, R. 2019. Automated atrophy assessment for Alzheimer's disease diagnosis from brain MRI images. *Magn Reson Imaging,* 62**,** 167-173.

SLED, J. G., ZIJDENBOS, A. P. & EVANS, A. C. 1998. A nonparametric method for automatic correction of intensity nonuniformity in MRI data. *IEEE Trans Med Imaging,* 17**,** 87-97.

SMITH, S. M., VIDAURRE, D., ALFARO-ALMAGRO, F., NICHOLS, T. E. & MILLER, K. L. 2019. Estimation of brain age delta from brain imaging. *Neuroimage*.

SOBUE, G., ISHIGAKI, S. & WATANABE, H. 2018. Pathogenesis of Frontotemporal Lobar Degeneration: Insights From Loss of Function Theory and Early Involvement of the Caudate Nucleus. *Front Neurosci,* 12**,** 473.

STAFFARONI, A. M., COBIGO, Y., GOH, S. M., KORNAK, J., BAJOREK, L., CHIANG, K., APPLEBY, B., BOVE, J., BORDELON, Y., BRANNELLY, P., BRUSHABER, D., CASO, C., COPPOLA, G., DEVER, R., DHEEL, C., DICKERSON, B. C., DICKINSON, S., DOMINGUEZ, S., DOMOTO-REILLY, K., FABER, K., FERRALL, J., FIELDS, J. A., FISHMAN, A., FONG, J., FOROUD, T., FORSBERG, L. K., GAVRILOVA, R., GEARHART, D., GHAZANFARI, B., GHOSHAL, N., GOLDMAN, J., GRAFF-RADFORD, J., GRAFF-RADFORD, N., GRANT, I., GROSSMAN, M.,

HALEY, D., HEUER, H. W., HSIUNG, G. Y., HUEY, E. D., IRWIN, D. J., JONES, D. T., JONES, L., KANTARCI, K., KARYDAS, A., KAUFER, D. I., KERWIN, D. R., KNOPMAN, D. S., KRAFT, R., KRAMER, J. H., KREMERS, W. K., KUKULL, W. A., LITVAN, I., LJUBENKOV, P. A., LUCENTE, D., LUNGU, C., MACKENZIE, I. R., MALDONADO, M., MANOOCHEHRI, M., MCGINNIS, S. M., MCKINLEY, E., MENDEZ, M. F., MILLER, B. L., MULTANI, N., ONYIKE, C., PADMANABHAN, J., PANTELYAT, A., PEARLMAN, R., PETRUCELLI, L., POTTER, M., RADEMAKERS, R., RAMOS, E. M., RANKIN, K. P., RASCOVSKY, K., ROBERSON, E. D., ROGALSKI, E., SENGDY, P., SHAW, L. M., SYRJANEN, J., TARTAGLIA, M. C., TATTON, N., TAYLOR, J., TOGA, A., TROJANOWSKI, J. Q., WEINTRAUB, S., WANG, P., WONG, B., WSZOLEK, Z., BOXER, A. L., BOEVE, B. F., ROSEN, H. J. & CONSORTIUM, A. L. 2019. Individualized atrophy scores predict dementia onset in familial frontotemporal lobar degeneration. *Alzheimers Dement*.

STEENWIJK, M. D., DAAMS, M., POUWELS, P. J., BALK, L. J., TEWARIE, P. K., KILLESTEIN, J., UITDEHAAG, B. M., GEURTS, J. J., BARKHOF, F. & VRENKEN, H. 2014. What explains gray matter atrophy in long-standing multiple sclerosis? *Radiology,* 272**,** 832-42.

STEENWIJK, M. D., GEURTS, J. J., DAAMS, M., TIJMS, B. M., WINK, A. M., BALK, L. J., TEWARIE, P. K., UITDEHAAG, B. M., BARKHOF, F., VRENKEN, H. & POUWELS, P. J. 2016. Cortical atrophy patterns in multiple sclerosis are non-random and clinically relevant. *Brain,* 139**,** 115-26.

STEFFENER, J., HABECK, C., O'SHEA, D., RAZLIGHI, Q., BHERER, L. & STERN, Y. 2016. Differences between chronological and brain age are related to education and self-reported physical activity. *Neurobiol Aging,* 40**,** 138-144.

STEPAN-BUKSAKOWSKA, I., SZABO, N., HORINEK, D., TOTH, E., HORT, J., WARNER, J., CHARVAT, F., VECSEI, L., ROCEK, M. & KINCSES, Z. T. 2014. Cortical and subcortical atrophy in Alzheimer disease: parallel atrophy of thalamus and hippocampus. *Alzheimer Dis Assoc Disord,* 28**,** 65-72.

STORSVE, A. B., FJELL, A. M., TAMNES, C. K., WESTLYE, L. T., OVERBYE, K., AASLAND, H. W. & WALHOVD, K. B. 2014. Differential longitudinal changes in cortical thickness, surface area and volume across the adult life span: regions of accelerating and decelerating change. *J Neurosci,* 34**,** 8488-98.

TAN, K. S., LIBON, D. J., RASCOVSKY, K., GROSSMAN, M. & XIE, S. X. 2013. Differential longitudinal decline on the Mini-Mental State Examination in frontotemporal lobar degeneration and Alzheimer disease. *Alzheimer Dis Assoc Disord,* 27**,** 310-5.

TIBSHIRANI, R. 1996. Regression shrinkage and selection via the lasso. *Journal of the Royal Statistical Society: Series B (Methodological),* 58**,** 267-288.

TIKHONOV, A. N. & ARSENIN, V. I. 1977. *Solutions of ill-posed problems*, Winston, Washington, DC.

TILLEMA, J. M., HULST, H. E., ROCCA, M. A., VRENKEN, H., STEENWIJK, M. D., DAMJANOVIC, D., ENZINGER, C., ROPELE, S., TEDESCHI, G., GALLO, A., CICCARELLI, O., ROVIRA, A., MONTALBAN, X., DE STEFANO, N., STROMILLO, M. L., FILIPPI, M., BARKHOF, F. & GROUP, M. S. 2016. Regional cortical thinning in multiple sclerosis and its relation with cognitive impairment: A multicenter study. *Mult Scler,* 22**,** 901-9.

TREMLETT, H., PATY, D. & DEVONSHIRE, V. 2006. Disability progression in multiple sclerosis is slower than previously reported. *Neurology,* 66**,** 172-7.

TYSNES, O. B. & STORSTEIN, A. 2017. Epidemiology of Parkinson's disease. *J Neural Transm (Vienna),* 124**,** 901-905.

URIBE, C., SEGURA, B., BAGGIO, H. C., ABOS, A., MARTI, M. J., VALLDEORIOLA, F., COMPTA, Y., BARGALLO, N. & JUNQUE, C. 2016. Patterns of cortical thinning in nondemented Parkinson's disease patients. *Mov Disord,* 31**,** 699-708.

VALIZADEH, S. A., HANGGI, J., MERILLAT, S. & JANCKE, L. 2017. Age prediction on the basis of brain anatomical measures. *Hum Brain Mapp,* 38**,** 997-1008.

VASTIK, M., HOK, P., VALOSEK, J., HLUSTIK, P., MENSIKOVA, K. & KANOVSKY, P. 2017. Freezing of gait is associated with cortical thinning in mesial frontal cortex. *Biomed Pap Med Fac Univ Palacky Olomouc Czech Repub,* 161**,** 389-396.

VIDAL-JORDANA, A. & MONTALBAN, X. 2017. Multiple Sclerosis: Epidemiologic, Clinical, and Therapeutic Aspects. *Neuroimaging Clin N Am,* 27**,** 195-204.

WANG, B. & PHAM, T. D. 2011. MRI-based age prediction using hidden Markov models. *J Neurosci Methods,* 199**,** 140-5.

WANG, J., LI, W., MIAO, W., DAI, D., HUA, J. & HE, H. 2014. Age estimation using cortical surface pattern combining thickness with curvatures. *Med Biol Eng Comput,* 52**,** 331-41.

WARNE, R. 2014. A primer on multivariate analysis of variance (MANOVA) for behavioral scientists. *Practical Assessment, Research, and Evaluation,* 19**,** 17.

WEIL, R. S., COSTANTINI, A. A. & SCHRAG, A. E. 2018. Mild Cognitive Impairment in Parkinson's Disease-What Is It? *Curr Neurol Neurosci Rep,* 18**,** 17.

WELLER, J. & BUDSON, A. 2018. Current understanding of Alzheimer's disease diagnosis and treatment. *F1000Res,* 7.

WHITWELL, J. L., BOEVE, B. F., WEIGAND, S. D., SENJEM, M. L., GUNTER, J. L., BAKER, M. C., DEJESUS-HERNANDEZ, M., KNOPMAN, D. S., WSZOLEK, Z. K., PETERSEN, R. C., RADEMAKERS, R., JACK, C. R., JR. & JOSEPHS, K. A. 2015. Brain atrophy over time in genetic and sporadic frontotemporal dementia: a study of 198 serial magnetic resonance images. *Eur J Neurol,* 22**,** 745-52.

WILSON, H., NICCOLINI, F., PELLICANO, C. & POLITIS, M. 2019. Cortical thinning across Parkinson's disease stages and clinical correlates. *J Neurol Sci,* 398**,** 31-38.

WINKLER, A. M., GREVE, D. N., BJULAND, K. J., NICHOLS, T. E., SABUNCU, M. R., HABERG, A. K., SKRANES, J. & RIMOL, L. M. 2018. Joint Analysis of Cortical Area and Thickness as a Replacement for the Analysis of the Volume of the Cerebral Cortex. *Cereb Cortex,* 28**,** 738-749.

WINKLER, A. M., SABUNCU, M. R., YEO, B. T., FISCHL, B., GREVE, D. N., KOCHUNOV, P., NICHOLS, T. E., BLANGERO, J. & GLAHN, D. C. 2012. Measuring and comparing brain cortical surface area and other areal quantities. *Neuroimage,* 61**,** 1428-43.

YADAV, S. K., KATHIRESAN, N., MOHAN, S., VASILEIOU, G., SINGH, A., KAURA, D., MELHEM, E. R., GUPTA, R. K., WANG, E., MARINCOLA, F. M., BORTHAKUR, A. & HARIS, M. 2016. Gender-based analysis of cortical thickness and structural connectivity in Parkinson's disease. *J Neurol,* 263**,** 2308-2318.

YANG, H., XU, H., LI, Q., JIN, Y., JIANG, W., WANG, J., WU, Y., LI, W., YANG, C., LI, X., XIAO, S., SHI, F. & WANG, T. 2019. Study of brain morphology change in Alzheimer's disease and amnestic mild cognitive impairment compared with normal controls. *Gen Psychiatr,* 32**,** e100005.

YAU, Y., ZEIGHAMI, Y., BAKER, T. E., LARCHER, K., VAINIK, U., DADAR, M., FONOV, V. S., HAGMANN, P., GRIFFA, A., MISIC, B., COLLINS, D. L. & DAGHER, A. 2018. Network connectivity determines cortical thinning in early Parkinson's disease progression. *Nat Commun,* 9**,** 12.

YE, B. S., JEON, S., YOON, S., KANG, S. W., BAIK, K., LEE, Y., CHUNG, S. J., OH, J. S., MOON, H., KIM, J. S., LEE, P. H. & SOHN, Y. H. 2018. Effects of dopaminergic depletion and brain atrophy on neuropsychiatric symptoms in de novo Parkinson's disease. *J Neurol Neurosurg Psychiatry,* 89**,** 197-204.

YI, H. A., MOLLER, C., DIELEMAN, N., BOUWMAN, F. H., BARKHOF, F., SCHELTENS, P., VAN DER FLIER, W. M. & VRENKEN, H. 2016. Relation between subcortical grey matter atrophy and conversion from mild cognitive impairment to Alzheimer's disease. *J Neurol Neurosurg Psychiatry,* 87**,** 425-32.

ZHANG, Y. & LIU, S. 2018. Analysis of structural brain MRI and multi-parameter classification for Alzheimer's disease. *Biomed Tech (Berl),* 63**,** 427-437.

ZOU, H. & HASTIE, T. 2005. Regularization and variable selection via the elastic net. *Journal of the royal statistical society: series B (statistical methodology),* 67**,** 301-320.

Appendix

Table 1: Results (p-values) of MANOVAs comparing the DG to patient groups for CT regions

CT regions	MCI vs. DG	PD vs. DG	FTLD vs. DG	AD vs. DG	MS vs. DG
rh_bankssts_thickness	**0.0003947**	0.5458	**0.01896**	**4.94E-11**	**1.77E-08**
rh_caudalanteriorcingulate_thickness	0.5091	0.07764	**1.74E-13**	0.3577	**4.10E-11**
rh_caudalmiddlefrontal_thickness	**2.18E-10**	0.9812	**4.04E-12**	**2.20E-16**	**1.76E-13**
rh_cuneus_thickness	0.2105	**2.19E-07**	**2.20E-16**	0.7139	0.3385
rh_entorhinal_thickness	0.1431	0.4288	**2.20E-16**	**2.20E-16**	0.4571
rh_fusiform_thickness	0.1431	0.5082	0.3101	**2.20E-16**	0.1369
rh_inferiorparietal_thickness	**5.86E-15**	**0.02799**	0.5626	**2.20E-16**	**2.20E-16**
rh_inferiortemporal_thickness	0.3403	0.2159	**4.23E-15**	**2.20E-16**	**6.28E-06**
rh_isthmuscingulate_thickness	**0.02617**	**0.04287**	**3.80E-08**	**0.001298**	**9.34E-10**
rh_lateraloccipital_thickness	0.1227	**2.10E-05**	**1.81E-15**	**3.96E-08**	0.647
rh_lateralorbitofrontal_thickness	**6.03E-06**	0.861	**9.00E-12**	**2.47E-08**	**2.20E-16**
rh_lingual_thickness	0.1705	**1.75E-05**	**2.20E-16**	0.0562	**3.69E-05**
rh_medialorbitofrontal_thickness	**3.82E-07**	**0.02216**	**7.02E-11**	**4.42E-06**	**1.98E-15**
rh_middletemporal_thickness	**2.51E-07**	0.05611	**2.20E-16**	**2.20E-16**	**2.20E-16**
rh_parahippocampal_thickness	0.7756	**0.005367**	**1.25E-11**	**6.92E-09**	0.3875
rh_paracentral_thickness	**0.02595**	0.5087	**0.004081**	0.09455	**2.95E-07**
rh_parsopercularis_thickness	**1.41E-05**	0.4473	**6.58E-08**	**4.44E-09**	**1.60E-08**
rh_parsorbitalis_thickness	**4.35E-08**	**0.004691**	**2.29E-13**	**4.47E-06**	**2.20E-16**
rh_parstriangularis_thickness	**3.25E-15**	0.4373	**1.35E-06**	**3.15E-08**	**4.82E-06**
rh_pericalcarine_thickness	**0.0312**	**5.44E-11**	**2.20E-16**	0.2013	**2.20E-16**
rh_postcentral_thickness	**1.90E-15**	**2.95E-06**	**3.89E-08**	**2.20E-16**	0.1968
rh_posteriorcingulate_thickness	0.5977	**0.02655**	**6.86E-10**	**0.003301**	**6.32E-15**
rh_precentral_thickness	0.1159	0.9832	**0.009637**	**1.40E-05**	**0.01785**
rh_precuneus_thickness	**0.000216**	**0.01213**	**0.007835**	**2.20E-16**	**3.29E-12**
rh_rostralanteriorcingulate_thickness	**0.00129**	**0.002518**	**1.81E-07**	0.109	**2.20E-16**
rh_rostralmiddlefrontal_thickness	**2.20E-16**	0.1023	**1.67E-07**	**2.20E-16**	**9.12E-11**
rh_superiorfrontal_thickness	**5.30E-13**	0.05664	**2.20E-16**	**2.20E-16**	**2.20E-16**
rh_superiorparietal_thickness	**8.08E-15**	**3.05E-06**	**4.52E-06**	**2.20E-16**	0.1296
rh_superiortemporal_thickness	**6.07E-12**	0.5801	**1.84E-11**	**2.20E-16**	**4.50E-11**
rh_supramarginal_thickness	**9.15E-12**	0.2528	**0.009407**	**2.20E-16**	**2.20E-16**
rh_frontalpole_thickness	**9.56E-12**	0.4701	**0.0002763**	**0.0004919**	**2.56E-15**
rh_temporalpole_thickness	**3.60E-07**	0.5768	**2.20E-16**	**2.20E-16**	**3.83E-08**
rh_transversetemporal_thickness	**0.005055**	0.09283	**0.02389**	**2.25E-07**	**0.005947**
rh_insula_thickness	0.1449	0.2141	**2.20E-16**	**1.78E-08**	**2.20E-16**
lh_bankssts_thickness	**3.16E-07**	0.686	**3.39E-10**	**2.20E-16**	**0.006355**
lh_caudalanteriorcingulate_thickness	**0.02069**	0.1762	**1.96E-11**	**0.01635**	**2.20E-16**
lh_caudalmiddlefrontal_thickness	**3.00E-07**	0.1037	**2.20E-16**	**2.20E-16**	**7.12E-16**
lh_cuneus_thickness	0.2448	**2.00E-05**	**2.86E-12**	**0.04269**	**0.000206**
lh_entorhinal_thickness	0.1103	0.8505	**2.20E-16**	**2.20E-16**	0.5971
lh_fusiform_thickness	0.2318	0.3156	**6.36E-05**	**2.20E-16**	**4.96E-10**
lh_inferiorparietal_thickness	**2.20E-16**	0.2242	**0.01322**	**2.20E-16**	**2.20E-16**
lh_inferiortemporal_thickness	0.2191	0.924	**2.20E-16**	**2.20E-16**	**2.20E-16**
lh_isthmuscingulate_thickness	0.4677	0.5701	**3.17E-12**	**3.29E-06**	**6.63E-13**
lh_lateraloccipital_thickness	**0.004201**	**6.35E-06**	**3.24E-08**	**1.23E-08**	0.07449
lh_lateralorbitofrontal_thickness	**4.78E-06**	0.2802	**2.20E-16**	**7.09E-07**	**2.20E-16**
lh_lingual_thickness	0.9319	**1.18E-06**	**2.20E-16**	0.1276	**6.48E-13**
lh_medialorbitofrontal_thickness	**0.0002496**	0.2754	**2.20E-16**	**5.40E-08**	**5.56E-14**
lh_middletemporal_thickness	**4.97E-05**	**0.03608**	**2.20E-16**	**2.20E-16**	**2.20E-16**
lh_parahippocampal_thickness	0.3932	0.2254	**2.20E-16**	**6.09E-10**	**0.002548**
lh_paracentral_thickness	0.3633	0.6136	**0.008875**	**0.03198**	0.07407
lh_parsopercularis_thickness	**9.47E-05**	0.9333	**1.85E-15**	**5.22E-07**	**2.40E-07**
lh_parsorbitalis_thickness	**1.73E-05**	0.2328	**3.46E-13**	**8.51E-05**	**2.20E-16**
lh_parstriangularis_thickness	**1.57E-07**	0.9291	**1.01E-13**	**4.74E-09**	**2.32E-11**
lh_pericalcarine_thickness	**0.002839**	**1.46E-08**	**2.20E-16**	**0.02536**	**2.20E-16**
lh_postcentral_thickness	**1.18E-09**	**3.76E-05**	**5.56E-07**	**2.25E-13**	0.58
lh_posteriorcingulate_thickness	0.7307	0.4573	**2.58E-09**	**0.0005181**	**2.20E-16**
lh_precentral_thickness	0.8534	0.08991	0.085	**1.53E-05**	**3.53E-05**
lh_precuneus_thickness	**2.91E-08**	**0.001277**	0.5427	**2.20E-16**	**2.34E-14**
lh_rostralanteriorcingulate_thickness	0.4038	0.3062	**2.20E-16**	**0.03939**	**2.20E-16**
lh_rostralmiddlefrontal_thickness	**2.20E-16**	0.08915	**8.43E-12**	**2.20E-16**	**2.20E-16**
lh_superiorfrontal_thickness	**1.21E-11**	0.1139	**2.20E-16**	**2.20E-16**	**2.20E-16**
lh_superiorparietal_thickness	**1.60E-11**	**4.15E-07**	**8.04E-06**	**2.20E-16**	**0.00198**
lh_superiortemporal_thickness	**1.16E-06**	0.9052	**2.20E-16**	**2.20E-16**	**3.29E-15**
lh_supramarginal_thickness	**2.36E-07**	0.4221	**0.0004081**	**2.20E-16**	**2.20E-16**
lh_frontalpole_thickness	**1.24E-07**	0.6736	**4.21E-07**	**1.72E-07**	**2.20E-16**
lh_temporalpole_thickness	**1.89E-06**	0.6254	**2.20E-16**	**2.20E-16**	**1.74E-05**
lh_transversetemporal_thickness	0.1103	**0.03891**	**3.23E-08**	**0.0002367**	0.1921
lh_insula_thickness	0.5064	0.08104	**2.20E-16**	**0.001675**	**2.20E-16**

Table 2: Results (p-values) of MANOVAs comparing the DG to patient groups for CVol regions

CVol regions	MCI vs. DG	PD vs. DG	FTLD vs. DG	AD vs. DG	MS vs. DG
rh_bankssts_volume	**0.02204**	**5.31E-08**	**0.004016**	**1.95E-08**	**0.001799**
rh_caudalanteriorcingulate_volume	0.07381	**4.67E-05**	0.3186	**0.04167**	0.7515
rh_caudalmiddlefrontal_volume	0.1056	**8.29E-07**	**2.30E-05**	**7.45E-07**	**2.47E-06**
rh_cuneus_volume	**0.04694**	**2.04E-11**	**3.83E-11**	0.4315	0.9447
rh_entorhinal_volume	0.8937	**0.02659**	**5.53E-14**	**1.23E-13**	**0.002672**
rh_fusiform_volume	0.7774	**5.23E-08**	0.236	**1.17E-10**	0.07166
rh_inferiorparietal_volume	**1.29E-05**	**1.20E-10**	0.9062	**2.20E-16**	**8.05E-09**
rh_inferiortemporal_volume	0.7665	**2.65E-06**	**3.73E-09**	**1.07E-14**	**0.0001526**
rh_isthmuscingulate_volume	0.2498	**5.88E-13**	**0.02963**	**0.001606**	0.384
rh_lateraloccipital_volume	0.7196	**3.05E-08**	**5.07E-07**	**3.35E-05**	0.3487
rh_lateralorbitofrontal_volume	**0.005383**	**2.98E-05**	**3.41E-10**	**4.55E-05**	**1.16E-05**
rh_lingual_volume	**0.01219**	**3.33E-10**	**2.20E-16**	0.7046	0.3989
rh_medialorbitofrontal_volume	**0.002554**	**1.81E-05**	**1.06E-07**	**0.0001079**	**0.0112**
rh_middletemporal_volume	**0.002622**	**6.21E-06**	**7.79E-14**	**4.29E-16**	**1.08E-08**
rh_parahippocampal_volume	0.4812	**0.003381**	**0.001664**	**9.23E-09**	**0.04186**
rh_paracentral_volume	0.4316	**5.28E-09**	**7.28E-05**	0.1082	**0.002297**
rh_parsopercularis_volume	**0.008949**	**1.42E-05**	**0.03462**	**0.005789**	**0.01042**
rh_parsorbitalis_volume	**0.0001242**	**0.003763**	**1.42E-06**	**4.04E-07**	**6.71E-10**
rh_parstriangularis_volume	**1.93E-06**	**0.0003584**	0.2752	**0.001394**	**0.01118**
rh_pericalcarine_volume	0.5789	**2.14E-12**	**4.15E-14**	0.3214	**0.0003511**
rh_postcentral_volume	**0.01268**	**6.42E-13**	**0.002452**	**4.77E-06**	0.9607
rh_posteriorcingulate_volume	0.3174	**1.63E-08**	0.2164	**2.42E-05**	0.647
rh_precentral_volume	0.8466	**2.12E-10**	0.5939	0.05089	0.121
rh_precuneus_volume	0.05788	**9.37E-14**	**2.19E-05**	**2.74E-13**	0.05873
rh_rostralanteriorcingulate_volume	0.4665	**3.17E-06**	0.6186	0.8297	0.7433
rh_rostralmiddlefrontal_volume	**3.75E-05**	**3.29E-10**	**0.03435**	**2.97E-08**	**0.0005095**
rh_superiorfrontal_volume	**0.001839**	**2.76E-08**	**0.0001211**	**1.19E-06**	**2.14E-08**
rh_superiorparietal_volume	**0.000109**	**4.74E-10**	**0.0004123**	**9.46E-12**	0.06108
rh_superiortemporal_volume	**6.64E-06**	**5.91E-05**	**1.48E-05**	**2.87E-11**	**0.01691**
rh_supramarginal_volume	**0.006047**	**4.65E-05**	0.8381	**3.56E-10**	**0.008184**
rh_frontalpole_volume	**0.01345**	0.125	0.2169	**0.00222**	**2.37E-08**
rh_temporalpole_volume	**1.48E-05**	0.5189	**2.20E-16**	**2.00E-15**	**0.007333**
rh_transversetemporal_volume	**0.01512**	0.1282	0.05812	**1.90E-05**	**2.75E-06**
rh_insula_volume	0.4879	**7.57E-08**	**1.10E-05**	**0.01227**	0.3672
lh_bankssts_volume	**0.0003036**	**0.002578**	**1.81E-07**	**8.76E-11**	0.4059
lh_caudalanteriorcingulate_volume	0.5581	**5.26E-05**	**0.002715**	0.6902	**1.24E-05**
lh_caudalmiddlefrontal_volume	0.3993	**5.19E-07**	**7.75E-06**	**0.0001515**	**1.99E-07**
lh_cuneus_volume	0.5185	**7.26E-10**	**7.10E-09**	0.6121	0.5491
lh_entorhinal_volume	0.532	**2.72E-05**	**2.20E-16**	**2.20E-16**	**0.003067**
lh_fusiform_volume	0.6543	**1.21E-07**	**0.01131**	**3.79E-09**	**0.0001085**
lh_inferiorparietal_volume	**1.09E-07**	**2.13E-06**	0.06475	**2.20E-16**	**0.008126**
lh_inferiortemporal_volume	**0.03996**	**4.92E-07**	**2.20E-16**	**2.20E-16**	**9.59E-06**
lh_isthmuscingulate_volume	0.2283	**8.03E-14**	0.2688	**0.001071**	**0.006694**
lh_lateraloccipital_volume	0.2947	**1.86E-06**	**2.45E-05**	**1.42E-05**	0.9772
lh_lateralorbitofrontal_volume	**0.02662**	**7.62E-08**	**2.79E-15**	**6.08E-05**	**0.0005265**
lh_lingual_volume	0.1181	**5.61E-11**	**1.13E-13**	0.2497	0.01312
lh_medialorbitofrontal_volume	0.4352	**1.10E-06**	**8.41E-09**	0.121	0.0177
lh_middletemporal_volume	**0.02383**	**4.11E-05**	**2.20E-16**	**2.20E-16**	**6.87E-08**
lh_parahippocampal_volume	0.8037	**0.0002252**	**1.58E-10**	**1.59E-10**	**0.01961**
lh_paracentral_volume	0.8914	**8.65E-12**	**0.003968**	0.09487	**0.0293**
lh_parsopercularis_volume	**0.04019**	**5.47E-05**	**2.31E-05**	**0.02128**	**0.000529**
lh_parsorbitalis_volume	**0.000465**	**0.0002919**	**1.81E-11**	**9.09E-07**	**2.26E-12**
lh_parstriangularis_volume	**0.001208**	**0.01516**	**7.77E-06**	**0.0008086**	**0.02131**
lh_pericalcarine_volume	0.8533	**1.59E-12**	**1.80E-12**	0.3705	**0.001979**
lh_postcentral_volume	0.399	**6.93E-15**	**5.14E-06**	**0.0008564**	0.4575
lh_posteriorcingulate_volume	0.1906	**3.32E-11**	0.4834	**2.66E-06**	**0.01956**
lh_precentral_volume	0.2319	**7.57E-09**	0.2742	**0.04014**	**0.03849**
lh_precuneus_volume	**0.002355**	**2.75E-14**	**0.001486**	**1.05E-12**	**0.009715**
lh_rostralanteriorcingulate_volume	0.7662	**1.77E-08**	**2.41E-06**	0.1811	**0.0009323**
lh_rostralmiddlefrontal_volume	**0.0001723**	**1.02E-10**	**0.003078**	**1.28E-07**	**3.68E-05**
lh_superiorfrontal_volume	**0.001803**	**8.89E-10**	**7.79E-07**	**1.58E-09**	**3.63E-07**
lh_superiorparietal_volume	**0.002663**	**1.20E-11**	**0.0001446**	**1.80E-10**	**0.002323**
lh_superiortemporal_volume	**0.008886**	**6.90E-06**	**8.16E-09**	**7.67E-11**	**0.01193**
lh_supramarginal_volume	**0.005651**	**3.55E-05**	0.568	**9.78E-08**	**0.0007469**
lh_frontalpole_volume	**0.00516**	0.07733	0.05872	**0.0004478**	**2.91E-06**
lh_temporalpole_volume	**7.92E-07**	0.4797	**2.20E-16**	**2.58E-10**	**4.40E-05**
lh_transversetemporal_volume	0.07969	**0.003435**	**0.007801**	**0.008145**	**0.002544**
lh_insula_volume	0.5588	**1.61E-06**	**2.87E-08**	**0.0009124**	0.9391

Table 3: Results (p-values) of MANOVAs comparing the DG to patient groups for SubVol regions

SubVol regions	MCI vs. DG	PD vs. DG	FTLD vs. DG	AD vs. DG	MS vs. DG
Left-Cerebellum-Cortex	**0.009973**	**9.00E-13**	**0.0002145**	0.4085	**2.02E-15**
Left-Thalamus-Proper	**2.20E-16**	**5.23E-14**	**1.23E-12**	**5.05E-13**	**2.20E-16**
Left-Caudate	0.08866	**1.01E-07**	**3.47E-09**	0.9992	**6.31E-05**
Left-Putamen	**8.20E-07**	**9.38E-08**	**2.20E-16**	**1.57E-09**	**2.20E-16**
Left-Pallidum	0.7889	**1.00E-15**	**0.002802**	0.4499	**1.15E-09**
Brain-Stem	0.3038	**2.96E-16**	0.6646	0.4938	0.3553
Left-Hippocampus	**7.41E-16**	**1.37E-08**	**2.20E-16**	**2.20E-16**	0.958
Left-Amygdala	**2.20E-16**	**3.89E-12**	**2.20E-16**	**2.20E-16**	**0.007498**
Left-Accumbens-area	**0.001416**	0.3174	**1.83E-08**	**1.35E-10**	**2.20E-16**
Left-VentralDC	**1.75E-07**	**1.30E-08**	**3.64E-10**	**1.31E-10**	**9.02E-07**
Left-choroid-plexus	**2.97E-16**	**0.0192**	**1.60E-10**	**2.76E-16**	0 0.9986
Right-Cerebellum-Cortex	**0.006665**	**2.20E-16**	**0.001451**	0.5813	**2.20E-16**
Right-Thalamus-Proper	**2.72E-15**	**2.20E-16**	**0.0002892**	**2.59E-10**	**1.15E-05**
Right-Caudate	**0.001952**	**7.53E-06**	**7.25E-08**	0.9719	**4.68E-06**
Right-Putamen	**0.0007512**	**6.21E-06**	**2.20E-16**	**1.06E-08**	**1.66E-14**
Right-Pallidum	0.6583	**2.20E-16**	**0.03045**	0.3991	**2.20E-16**
Right-Hippocampus	**2.59E-15**	**1.06E-06**	**2.20E-16**	**2.20E-16**	**0.03277**
Right-Amygdala	**2.20E-16**	**6.22E-06**	**2.20E-16**	**2.20E-16**	**0.008306**
Right-Accumbens-area	**2.04E-05**	0.3559	**2.20E-16**	**2.20E-16**	**1.04E-11**
Right-VentralDC	**2.39E-07**	**2.13E-05**	**1.16E-09**	**3.50E-09**	**2.16E-07**
Right-choroid-plexus	**2.20E-16**	**0.001603**	**2.83E-14**	**2.20E-16**	0.2533
CC_Posterior	0.5025	**0.0005286**	0.06493	0.6782	**0.03369**
CC_Mid_Posterior	**5.00E-09**	0.1071	**3.03E-06**	**1.62E-05**	**8.64E-06**
CC_Central	**2.20E-16**	0.3048	**2.20E-16**	**2.66E-11**	0.0757
CC_Mid_Anterior	**2.20E-16**	**2.88E-05**	**2.20E-16**	**5.10E-14**	**0.0003888**
CC_Anterior	**0.004381**	**2.88E-07**	**6.81E-09**	**3.77E-05**	**7.75E-06**

Table 4: Results (p-values) of MANOVAs comparing the DG to patient groups for SA regions

SA regions	MCI vs. DG	PD vs. DG	FTLD vs. DG	AD vs. DG	MS vs. DG
rh_bankssts_area	0.414	**3.41E-14**	**0.0145**	**0.0001276**	0.0745
rh_caudalanteriorcingulate_area	0.08023	**1.44E-06**	**0.01262**	0.05422	**0.002954**
rh_caudalmiddlefrontal_area	0.4938	**2.20E-10**	**0.02085**	0.2019	**0.03748**
rh_cuneus_area	0.2399	**1.79E-05**	0.1338	0.1995	0.6556
rh_entorhinal_area	0.5911	**3.03E-05**	0.09314	0.552	**0.02472**
rh_fusiform_area	0.9749	**2.31E-10**	0.07325	**0.003095**	0.06578
rh_inferiorparietal_area	0.386	**1.08E-14**	0.761	**0.000264**	0.05225
rh_inferiortemporal_area	0.416	**8.47E-12**	**4.88E-05**	**2.13E-05**	**0.03782**
rh_isthmuscingulate_area	0.9376	**2.20E-16**	**8.85E-07**	0.05267	**6.61E-05**
rh_lateraloccipital_area	0.3372	**2.04E-07**	0.1539	0.01542	**0.01956**
rh_lateralorbitofrontal_area	0.5746	**0.002364**	**3.82E-10**	0.1002	0.2643
rh_lingual_area	0.08528	**7.94E-06**	**0.002454**	0.9706	0.1164
rh_medialorbitofrontal_area	0.304	**5.59E-08**	**5.67E-05**	**0.01982**	0.1136
rh_middletemporal_area	0.6598	**4.08E-14**	**0.0001618**	**4.24E-05**	0.4568
rh_parahippocampal_area	0.2778	**4.37E-09**	0.3389	**0.009679**	0.9535
rh_paracentral_area	**0.03461**	**9.33E-14**	**0.01582**	0.08479	0.3519
rh_parsopercularis_area	0.3115	**3.87E-07**	0.1829	0.4108	0.9383
rh_parsorbitalis_area	0.08342	**6.65E-06**	**0.0001962**	**0.001673**	0.723
rh_parstriangularis_area	**0.03144**	**0.0001887**	0.2902	0.08303	0.518
rh_pericalcarine_area	0.3748	**8.13E-07**	**0.0002724**	0.3839	0.08303
rh_postcentral_area	**0.01923**	**1.83E-11**	0.7878	0.7832	0.2718
rh_posteriorcingulate_area	0.07518	**2.76E-13**	**0.0002738**	**0.0004341**	**0.002006**
rh_precentral_area	0.388	**2.20E-16**	0.19	0.7952	0.7405
rh_precuneus_area	0.2641	**1.46E-13**	**0.004611**	**1.37E-05**	0.08145
rh_rostralanteriorcingulate_area	0.1051	**3.89E-08**	0.3349	0.07177	**3.63E-05**
rh_rostralmiddlefrontal_area	0.6538	**2.43E-08**	**0.0307**	**0.02031**	0.1531
rh_superiorfrontal_area	0.5036	**5.60E-13**	0.6634	0.1285	0.7801
rh_superiorparietal_area	0.9867	**3.84E-09**	**0.03042**	**0.003265**	0.1398
rh_superiortemporal_area	0.3181	**2.07E-10**	0.09382	0.1021	**0.01837**
rh_supramarginal_area	0.8317	**5.88E-08**	0.2064	**0.003638**	0.1468
rh_frontalpole_area	0.494	0.442	**0.001267**	**0.01069**	0.4272
rh_temporalpole_area	0.5204	**0.04382**	0.7287	0.6017	**0.0004692**
rh_transversetemporal_area	0.9766	**3.72E-06**	0.6941	0.4798	0.05267
rh_insula_area	0.3819	**1.09E-12**	**3.26E-05**	0.6905	**1.20E-08**
lh_bankssts_area	**0.02032**	**1.19E-05**	0.8812	**1.13E-06**	0.8612
lh_caudalanteriorcingulate_area	0.1907	**2.56E-07**	0.4038	0.5505	0.4981
lh_caudalmiddlefrontal_area	0.574	**5.47E-14**	**0.02668**	0.6892	**0.01928**
lh_cuneus_area	0.1799	**5.09E-06**	**1.44E-06**	0.9174	0.09604
lh_entorhinal_area	**0.01927**	**1.76E-05**	**0.01795**	0.07862	0.425
lh_fusiform_area	0.5191	**2.50E-09**	0.3254	**0.0009792**	0.1516
lh_inferiorparietal_area	**0.02129**	**6.17E-10**	0.3254	**4.80E-07**	0.18
lh_inferiortemporal_area	0.1347	**1.27E-08**	**1.27E-10**	**2.28E-08**	0.4273
lh_isthmuscingulate_area	0.5334	**1.68E-14**	1.80E-05	0.1388	**0.01617**
lh_lateraloccipital_area	0.7071	**0.0005697**	0.1428	**0.0177**	0.6509
lh_lateralorbitofrontal_area	0.9144	**6.27E-10**	**1.71E-07**	**0.005718**	0.8169
lh_lingual_area	0.1242	**1.15E-06**	**0.0328**	0.1865	0.06071
lh_medialorbitofrontal_area	**0.03106**	**5.34E-08**	**0.00383**	0.123	0.5512
lh_middletemporal_area	0.4243	**9.93E-11**	**7.91E-10**	**9.82E-07**	0.382
lh_parahippocampal_area	0.1766	**4.51E-08**	0.8795	**0.0008653**	0.6154
lh_paracentral_area	0.07169	**2.20E-16**	0.05762	0.1572	0.6814
lh_parsopercularis_area	0.4563	**2.17E-07**	**0.03207**	0.5457	0.1307
lh_parsorbitalis_area	**0.01855**	**2.28E-06**	**1.61E-06**	4.17E-05	0.7517
lh_parstriangularis_area	0.05872	**0.003652**	**0.01686**	0.0828	0.3867
lh_pericalcarine_area	0.1188	**2.05E-08**	**0.00122**	0.7339	**0.01134**
lh_postcentral_area	**0.01465**	**1.73E-14**	**0.0138**	0.5661	0.4644
lh_posteriorcingulate_area	0.1081	**7.80E-16**	0.06019	**0.0003933**	0.07551
lh_precentral_area	0.4567	**2.20E-16**	**0.003586**	0.5931	0.4217
lh_precuneus_area	0.08579	**7.25E-14**	**0.01331**	**1.37E-05**	0.3401
lh_rostralanteriorcingulate_area	0.2519	**2.48E-09**	0.3134	0.1725	**0.03052**
lh_rostralmiddlefrontal_area	0.56	**6.56E-11**	0.1347	0.07352	0.1388
lh_superiorfrontal_area	0.4699	**3.26E-16**	0.7396	**0.01282**	0.9902
lh_superiorparietal_area	0.803	**1.33E-09**	**0.02416**	**0.01196**	0.2083
lh_superiortemporal_area	0.7141	**9.39E-11**	**0.019**	0.1264	**0.003442**
lh_supramarginal_area	0.2306	**7.92E-08**	0.797	0.06924	0.3486
lh_frontalpole_area	0.8973	**0.00349**	0.1813	0.1193	0.7847
lh_temporalpole_area	0.6723	**0.01702**	**2.69E-15**	0.3293	**0.02839**
lh_transversetemporal_area	0.6418	**1.46E-09**	0.5081	0.5618	0.3189
lh_insula_area	**0.0242**	**4.47E-14**	0.5552	**0.006361**	**9.18E-11**

Table 5: Results (p-values) of MANOVAs comparing the DG to patient groups for CTSD regions

CTSD regions	MCI vs. DG	PD vs. DG	FTLD vs. DG	AD vs. DG	MS vs. DG
rh_bankssts_thicknessstd	0.5791	**8.83E-05**	**0.0001546**	**4.84E-06**	**7.41E-13**
rh_caudalanteriorcingulate_thicknessstd	**0.01292**	0.2619	**0.0003596**	**2.26E-07**	0.16
rh_caudalmiddlefrontal_thicknessstd	**1.47E-05**	**5.02E-05**	**0.000155**	**4.04E-05**	**4.23E-05**
rh_cuneus_thicknessstd	**0.001701**	**1.37E-07**	**0.02096**	0.863	**2.20E-16**
rh_entorhinal_thicknessstd	0.08233	**0.0002252**	0.9026	**0.02744**	**1.18E-15**
rh_fusiform_thicknessstd	**4.28E-16**	0.1579	**2.93E-09**	**1.26E-07**	**2.20E-16**
rh_inferiorparietal_thicknessstd	**0.0005056**	**1.15E-14**	**2.20E-16**	**0.02063**	**2.20E-16**
rh_inferiortemporal_thicknessstd	**1.58E-05**	0.9661	**1.18E-10**	**0.0003344**	**2.20E-16**
rh_isthmuscingulate_thicknessstd	0.9764	0.9691	0.6069	0.5111	**2.20E-16**
rh_lateraloccipital_thicknessstd	**7.96E-07**	**0.02283**	**1.71E-08**	**0.02915**	**2.20E-16**
rh_lateralorbitofrontal_thicknessstd	0.05127	0.7622	**0.0006923**	**6.55E-05**	**2.20E-16**
rh_lingual_thicknessstd	**5.65E-10**	**0.01924**	**0.001843**	**0.04455**	**2.20E-16**
rh_medialorbitofrontal_thicknessstd	**2.41E-14**	**0.004071**	**0.001902**	**4.68E-10**	**1.89E-09**
rh_middletemporal_thicknessstd	0.7455	**0.01671**	**2.20E-16**	**0.001206**	**2.20E-16**
rh_parahippocampal_thicknessstd	**1.25E-05**	0.2364	**2.37E-06**	**0.000215**	**2.20E-16**
rh_paracentral_thicknessstd	**2.20E-16**	**2.79E-07**	**1.85E-09**	**3.61E-08**	**2.20E-16**
rh_parsopercularis_thicknessstd	0.0647	**0.003891**	0.8431	**1.88E-05**	**0.006481**
rh_parsorbitalis_thicknessstd	**3.96E-06**	0.9566	**0.003347**	**3.53E-05**	**1.66E-14**
rh_parstriangularis_thicknessstd	0.218	0.06599	0.6658	**0.00134**	**5.35E-14**
rh_pericalcarine_thicknessstd	0.9905	**0.006412**	**2.76E-07**	0.7001	0.1419
rh_postcentral_thicknessstd	0.1497	**1.46E-12**	**2.20E-16**	0.4021	**2.20E-16**
rh_posteriorcingulate_thicknessstd	0.8869	0.7872	0.1317	0.5216	0.05942
rh_precentral_thicknessstd	**0.02213**	**1.75E-07**	**2.20E-16**	**0.0004218**	**5.29E-11**
rh_precuneus_thicknessstd	**2.20E-16**	**7.09E-10**	**5.26E-14**	**4.50E-07**	**2.20E-16**
rh_rostralanteriorcingulate_thicknessstd	**2.20E-16**	0.356	**3.89E-10**	**2.20E-16**	0.453
rh_rostralmiddlefrontal_thicknessstd	0.1521	**0.0186**	0.9684	**0.001154**	**3.13E-07**
rh_superiorfrontal_thicknessstd	**2.20E-16**	0.06789	0.2262	**6.10E-11**	**5.36E-14**
rh_superiorparietal_thicknessstd	**1.06E-06**	**1.61E-08**	**6.56E-15**	**0.01187**	**2.20E-16**
rh_superiortemporal_thicknessstd	**0.01273**	0.2927	**2.40E-15**	**0.00442**	**2.20E-16**
rh_supramarginal_thicknessstd	**2.83E-05**	**9.75E-13**	**4.42E-10**	**5.75E-05**	**2.20E-16**
rh_frontalpole_thicknessstd	0.8681	0.373	0.466	**0.0002244**	**1.84E-06**
rh_temporalpole_thicknessstd	0.331	**0.0002457**	0.8315	**5.24E-05**	**0.0003778**
rh_transversetemporal_thicknessstd	0.9176	**0.01367**	**8.48E-09**	0.0551	0.649
rh_insula_thicknessstd	**7.65E-11**	**0.00646**	0.8462	**2.76E-12**	**1.17E-06**
lh_bankssts_thicknessstd	0.1728	**0.03061**	**3.27E-05**	**2.15E-07**	**1.37E-14**
lh_caudalanteriorcingulate_thicknessstd	**9.39E-08**	0.7085	**0.0001539**	**1.96E-11**	0.06544
lh_caudalmiddlefrontal_thicknessstd	**3.88E-05**	**2.51E-06**	**6.01E-07**	**1.20E-05**	**1.35E-13**
lh_cuneus_thicknessstd	0.979	**4.83E-06**	0.4446	0.4227	**6.00E-15**
lh_entorhinal_thicknessstd	0.9878	**2.08E-05**	**0.02732**	0.2093	**2.20E-16**
lh_fusiform_thicknessstd	**1.41E-11**	0.06446	**7.28E-07**	**8.27E-11**	**2.20E-16**
lh_inferiorparietal_thicknessstd	**1.72E-05**	**5.14E-12**	**2.20E-16**	**0.001141**	**2.20E-16**
lh_inferiortemporal_thicknessstd	**0.002601**	0.9696	**4.85E-16**	**0.0002574**	**2.20E-16**
lh_isthmuscingulate_thicknessstd	0.1335	**0.008488**	0.2919	0.1235	**2.20E-16**
lh_lateraloccipital_thicknessstd	**0.0009229**	**7.51E-05**	**2.20E-16**	**0.01724**	**2.20E-16**
lh_lateralorbitofrontal_thicknessstd	**3.75E-07**	**0.009115**	**2.20E-16**	**3.72E-08**	**2.20E-16**
lh_lingual_thicknessstd	**1.21E-06**	**0.007923**	0.1481	**0.0002583**	**1.01E-14**
lh_medialorbitofrontal_thicknessstd	**5.13E-09**	**0.0004032**	**2.48E-05**	**7.37E-06**	**2.20E-16**
lh_middletemporal_thicknessstd	**0.001124**	0.3377	**8.58E-11**	**0.0001637**	**2.20E-16**
lh_parahippocampal_thicknessstd	**6.85E-08**	0.6491	**2.99E-06**	**0.01008**	**2.20E-16**
lh_paracentral_thicknessstd	**2.19E-12**	**1.27E-09**	**4.64E-13**	**7.14E-08**	**2.20E-16**
lh_parsopercularis_thicknessstd	0.1126	**0.01889**	**0.005635**	**3.05E-06**	**4.77E-07**
lh_parsorbitalis_thicknessstd	**1.78E-06**	0.9093	**0.0001095**	**1.33E-08**	**2.20E-16**
lh_parstriangularis_thicknessstd	**0.008981**	**0.008196**	**0.0009277**	**1.94E-06**	**2.20E-16**
lh_pericalcarine_thicknessstd	0.5584	0.2756	**0.007889**	0.9141	**0.04411**
lh_postcentral_thicknessstd	0.00108	**5.22E-09**	**2.20E-16**	0.1994	**2.20E-16**
lh_posteriorcingulate_thicknessstd	0.8938	0.8635	0.8875	**0.02574**	**0.0009484**
lh_precentral_thicknessstd	**0.01521**	**8.42E-06**	**2.20E-16**	**0.001353**	**2.20E-16**
lh_precuneus_thicknessstd	**2.20E-16**	**7.90E-12**	**2.20E-16**	**1.43E-06**	**2.20E-16**
lh_rostralanteriorcingulate_thicknessstd	**2.20E-16**	**0.02963**	**8.85E-08**	**2.20E-16**	0.2471
lh_rostralmiddlefrontal_thicknessstd	**0.01793**	**0.005394**	**0.01001**	**8.90E-06**	**6.71E-14**
lh_superiorfrontal_thicknessstd	**8.82E-12**	**0.009392**	**0.02029**	**1.98E-13**	**2.06E-10**
lh_superiorparietal_thicknessstd	**5.13E-09**	**1.96E-09**	**2.20E-16**	**0.0003269**	**2.20E-16**
lh_superiortemporal_thicknessstd	**0.003751**	0.8974	**2.20E-16**	**0.0164**	**2.20E-16**
lh_supramarginal_thicknessstd	**6.49E-05**	**2.29E-10**	**9.66E-10**	**2.99E-05**	**2.20E-16**
lh_frontalpole_thicknessstd	0.3156	**0.01108**	0.3265	0.06639	**1.11E-06**
lh_temporalpole_thicknessstd	0.07011	**0.006346**	0.2045	**0.04006**	**4.02E-07**
lh_transversetemporal_thicknessstd	0.7769	0.05203	**1.15E-12**	**0.01208**	0.1825
lh_insula_thicknessstd	**3.51E-06**	0.72	0.9607	**9.93E-08**	**0.0147**

Table 6: Results (p-values) of MANOVAs comparing the RG to patient groups for CT regions

CT regions	MCI vs. RG	PD vs. RG	FTLD vs. RG	AD vs. RG	MS vs. RG
rh_bankssts_thickness	0.2497	**0.009537**	0.6204	**1.69E-08**	**3.28E-14**
rh_caudalanteriorcingulate_thickness	**0.04311**	**8.43E-05**	**2.20E-16**	**0.02303**	**4.62E-05**
rh_caudalmiddlefrontal_thickness	**0.01234**	**0.000172**	**1.09E-05**	**2.20E-16**	**2.20E-16**
rh_cuneus_thickness	**2.20E-16**	**2.20E-16**	**2.20E-16**	**0.0006488**	**4.99E-06**
rh_entorhinal_thickness	**3.17E-07**	**1.06E-05**	**2.20E-16**	**2.20E-16**	**0.0001174**
rh_fusiform_thickness	**0.02497**	0.1915	0.6511	**2.20E-16**	**0.03659**
rh_inferiorparietal_thickness	**2.42E-10**	**0.0004401**	0.4879	**2.20E-16**	**2.20E-16**
rh_inferiortemporal_thickness	**0.001549**	**0.001192**	**2.20E-16**	**2.20E-16**	**0.001577**
rh_isthmuscingulate_thickness	0.8626	**0.0001478**	**9.75E-13**	**1.49E-05**	**4.88E-06**
rh_lateraloccipital_thickness	0.3293	**3.00E-09**	**2.20E-16**	**0.0001558**	**0.02058**
rh_lateralorbitofrontal_thickness	**2.20E-16**	**2.20E-16**	**0.005697**	0.3179	**2.20E-16**
rh_lingual_thickness	**2.17E-11**	**2.20E-16**	**2.20E-16**	0.4874	0.7049
rh_medialorbitofrontal_thickness	**2.20E-16**	**2.20E-16**	**1.78E-05**	**0.0009547**	**2.20E-16**
rh_middletemporal_thickness	0.059	0.3475	**2.20E-16**	**2.20E-16**	**2.20E-16**
rh_parahippocampal_thickness	**0.003756**	0.924	**6.21E-05**	**0.0001845**	**0.005676**
rh_paracentral_thickness	**3.45E-05**	0.0545	**2.85E-06**	0.2351	**1.59E-12**
rh_parsopercularis_thickness	**0.006319**	**2.29E-11**	0.6903	**0.006372**	**2.20E-16**
rh_parsorbitalis_thickness	**0.000173**	**6.99E-08**	0.5865	0.9087	**2.20E-16**
rh_parstriangularis_thickness	**0.001254**	**2.20E-16**	**0.0004385**	0.9842	**2.20E-16**
rh_pericalcarine_thickness	**2.20E-16**	**2.20E-16**	**2.20E-16**	**1.17E-05**	**0.009029**
rh_postcentral_thickness	**0.009169**	**2.20E-16**	**2.20E-16**	**8.40E-11**	**0.003151**
rh_posteriorcingulate_thickness	**0.0001456**	**3.00E-09**	**2.20E-16**	**9.03E-09**	**4.90E-08**
rh_precentral_thickness	**0.03425**	**0.003673**	0.8461	**0.008237**	**1.70E-07**
rh_precuneus_thickness	0.9287	**4.73E-08**	**5.55E-09**	**1.22E-13**	**2.20E-16**
rh_rostralanteriorcingulate_thickness	**5.93E-09**	0.7187	**0.005871**	**0.002141**	**2.20E-16**
rh_rostralmiddlefrontal_thickness	**0.04619**	**2.20E-16**	**0.000822**	**1.22E-07**	**2.20E-16**
rh_superiorfrontal_thickness	**0.0007975**	**0.03485**	**2.16E-14**	**3.00E-15**	**2.20E-16**
rh_superiorparietal_thickness	**1.41E-08**	**6.36E-12**	**6.26E-12**	**2.20E-16**	**0.0003706**
rh_superiortemporal_thickness	0.7244	**2.79E-07**	0.08429	**1.35E-14**	**2.20E-16**
rh_supramarginal_thickness	**3.48E-06**	**0.001967**	0.4047	**2.59E-14**	**2.20E-16**
rh_frontalpole_thickness	**4.09E-07**	**0.02202**	**0.02107**	**0.008255**	**2.20E-16**
rh_temporalpole_thickness	**0.0002042**	0.5275	**2.20E-16**	**2.20E-16**	**1.07E-10**
rh_transversetemporal_thickness	**0.00202**	0.05569	**0.02986**	**1.78E-08**	**0.002746**
rh_insula_thickness	**0.0001293**	**0.00152**	**2.20E-16**	**1.11E-13**	**2.20E-16**
lh_bankssts_thickness	**0.00148**	**4.58E-12**	0.7702	**5.21E-05**	**2.20E-16**
lh_caudalanteriorcingulate_thickness	**0.00485**	**3.81E-08**	**2.20E-16**	0.6873	**3.55E-09**
lh_caudalmiddlefrontal_thickness	**0.006958**	0.6644	**4.55E-15**	**2.20E-16**	**2.20E-16**
lh_cuneus_thickness	**2.20E-16**	**2.20E-16**	**2.20E-16**	**4.19E-06**	**1.11E-08**
lh_entorhinal_thickness	0.2649	0.8435	**2.20E-16**	**2.20E-16**	0.4032
lh_fusiform_thickness	**5.27E-10**	**1.40E-07**	0.8315	**1.48E-09**	**2.20E-16**
lh_inferiorparietal_thickness	**0.00152**	**5.12E-10**	**0.04577**	**2.20E-16**	**2.20E-16**
lh_inferiortemporal_thickness	**0.03401**	**0.001423**	**2.20E-16**	**2.62E-16**	**2.20E-16**
lh_isthmuscingulate_thickness	**0.02182**	**0.003019**	**9.24E-16**	**1.02E-07**	**0.0001098**
lh_lateraloccipital_thickness	**0.006189**	**2.20E-16**	**2.20E-16**	**0.01444**	**4.71E-09**
lh_lateralorbitofrontal_thickness	**0.0001157**	**1.06E-08**	**1.20E-10**	0.4157	**2.20E-16**
lh_lingual_thickness	**2.20E-16**	**2.20E-16**	**2.20E-16**	**3.80E-05**	0.6838
lh_medialorbitofrontal_thickness	**5.28E-05**	**5.54E-13**	**0.005226**	0.2831	**2.20E-16**
lh_middletemporal_thickness	0.9909	0.1674	**2.20E-16**	**2.20E-16**	**2.20E-16**
lh_parahippocampal_thickness	**3.84E-07**	**0.004235**	**9.63E-08**	**0.001915**	**1.47E-09**
lh_paracentral_thickness	**6.72E-05**	**0.005449**	**7.22E-08**	0.4193	**3.11E-05**
lh_parsopercularis_thickness	0.07848	**5.13E-06**	**1.80E-05**	**0.01468**	**2.20E-16**
lh_parsorbitalis_thickness	0.125	0.2046	**5.26E-08**	**0.007234**	**2.20E-16**
lh_parstriangularis_thickness	**0.008088**	**5.42E-12**	0.05506	**0.04618**	**2.20E-16**
lh_pericalcarine_thickness	**2.20E-16**	**2.20E-16**	**2.20E-16**	**2.82E-06**	0.8055
lh_postcentral_thickness	0.1347	**3.98E-16**	**2.20E-16**	**9.56E-08**	**1.61E-05**
lh_posteriorcingulate_thickness	**0.01392**	**0.002594**	**2.20E-16**	**2.51E-07**	**1.79E-15**
lh_precentral_thickness	0.06346	0.9148	0.8496	**0.0004541**	**9.36E-09**
lh_precuneus_thickness	0.9937	**2.05E-13**	**5.36E-07**	**1.45E-11**	**2.20E-16**
lh_rostralanteriorcingulate_thickness	**0.03454**	**0.0003696**	**2.20E-16**	**0.0003217**	**2.20E-16**
lh_rostralmiddlefrontal_thickness	**2.72E-13**	**8.43E-10**	**0.0001714**	**2.20E-16**	**2.20E-16**
lh_superiorfrontal_thickness	**2.74E-12**	0.1867	**2.20E-16**	**2.20E-16**	**2.20E-16**
lh_superiorparietal_thickness	**0.0001809**	**9.83E-15**	**9.44E-13**	**2.21E-15**	**1.79E-08**
lh_superiortemporal_thickness	0.2567	**0.001849**	**1.73E-08**	**2.20E-16**	**2.20E-16**
lh_supramarginal_thickness	0.478	**0.001968**	0.9731	**2.20E-16**	**2.20E-16**
lh_frontalpole_thickness	**7.76E-10**	0.7358	**1.23E-08**	**7.44E-09**	**3.98E-14**
lh_temporalpole_thickness	**0.000237**	0.6008	**2.20E-16**	**2.20E-16**	**1.40E-07**
lh_transversetemporal_thickness	**0.01156**	**0.003858**	**2.57E-07**	**8.27E-06**	**0.04159**
lh_insula_thickness	**0.005729**	**6.72E-06**	**2.20E-16**	**4.78E-08**	**2.20E-16**

Table 7: Results (p-values) of MANOVAs comparing the RG to patient groups for CVol regions

CVol regions	MCI vs. RG	PD vs. RG	FTLD vs. RG	AD vs. RG	MS vs. RG
rh_bankssts_volume	**2.20E-16**	0.4655	**5.96E-15**	**2.20E-16**	**0.01066**
rh_caudalanteriorcingulate_volume	**8.14E-10**	0.6615	**1.10E-05**	**7.57E-06**	**0.002022**
rh_caudalmiddlefrontal_volume	0.05226	**2.07E-14**	0.1155	**0.002113**	**7.21E-13**
rh_cuneus_volume	**2.20E-16**	**2.20E-16**	**2.20E-16**	**3.27E-05**	**8.62E-14**
rh_entorhinal_volume	**2.20E-16**	**2.20E-16**	0.5792	**0.006025**	**2.20E-16**
rh_fusiform_volume	0.08546	**0.0003287**	**0.009102**	**3.05E-13**	0.8117
rh_inferiorparietal_volume	**1.93E-07**	**4.96E-09**	0.4651	**2.20E-16**	**1.09E-07**
rh_inferiortemporal_volume	**2.31E-08**	**2.20E-16**	**0.01779**	**1.87E-08**	**2.61E-14**
rh_isthmuscingulate_volume	**0.0001837**	**2.20E-16**	**2.22E-05**	**0.04714**	**0.0056**
rh_lateraloccipital_volume	**2.20E-16**	**2.20E-16**	**2.20E-16**	**0.02588**	**2.20E-16**
rh_lateralorbitofrontal_volume	**2.20E-16**	**2.20E-16**	**0.0004934**	**0.0005055**	**2.20E-16**
rh_lingual_volume	**3.96E-15**	**2.20E-16**	**2.20E-16**	**0.01183**	**0.0008436**
rh_medialorbitofrontal_volume	**2.20E-16**	**2.20E-16**	**4.50E-15**	**3.36E-09**	**2.20E-16**
rh_middletemporal_volume	**0.004335**	**2.20E-16**	**0.0004223**	**2.24E-08**	**2.20E-16**
rh_parahippocampal_volume	**3.63E-06**	0.3515	**4.61E-09**	**3.30E-13**	0.2111
rh_paracentral_volume	**0.0179**	**5.18E-12**	**4.35E-07**	0.4654	**3.34E-05**
rh_parsopercularis_volume	0.5085	**1.56E-08**	0.4975	0.08556	**0.0001058**
rh_parsorbitalis_volume	**2.20E-16**	**2.20E-16**	**5.41E-05**	0.1982	**2.20E-16**
rh_parstriangularis_volume	0.1644	**2.20E-16**	**0.0003144**	0.93	**9.23E-14**
rh_pericalcarine_volume	**0.02432**	**2.20E-16**	**2.20E-16**	0.7104	**0.04931**
rh_postcentral_volume	0.4827	**2.20E-16**	**3.05E-08**	**0.002272**	**0.0104**
rh_posteriorcingulate_volume	0.8802	**5.56E-12**	**0.02459**	**6.58E-05**	0.1634
rh_precentral_volume	**0.004898**	**2.20E-16**	0.1547	0.5431	**0.0003929**
rh_precuneus_volume	0.7604	**2.20E-16**	**4.38E-08**	**1.92E-11**	**0.001612**
rh_rostralanteriorcingulate_volume	**0.02144**	**0.03678**	**0.004996**	0.06746	**0.04548**
rh_rostralmiddlefrontal_volume	0.3532	**2.20E-16**	0.7864	**8.86E-06**	**8.32E-11**
rh_superiorfrontal_volume	0.633	**2.20E-16**	0.1648	**0.0006092**	**2.20E-16**
rh_superiorparietal_volume	**5.56E-05**	**7.57E-11**	**0.0001814**	**1.30E-13**	**0.0436**
rh_superiortemporal_volume	**0.03182**	**2.20E-16**	0.6025	**0.0002158**	**3.73E-14**
rh_supramarginal_volume	0.06527	**1.52E-06**	0.3862	**2.14E-09**	**0.000729**
rh_frontalpole_volume	**2.63E-14**	**2.20E-16**	**5.54E-10**	**0.02429**	**2.20E-16**
rh_temporalpole_volume	**1.88E-09**	**2.20E-16**	**1.47E-06**	**0.0009865**	**2.20E-16**
rh_transversetemporal_volume	**0.02583**	0.1369	0.06531	**5.37E-05**	**1.13E-05**
rh_insula_volume	**2.20E-16**	**2.20E-16**	0.2432	0.0974	**4.56E-13**
lh_bankssts_volume	**5.43E-09**	0.2687	**5.27E-12**	**5.67E-15**	0.3855
lh_caudalanteriorcingulate_volume	**9.38E-14**	**0.02853**	**2.36E-16**	**4.78E-05**	0.2542
lh_caudalmiddlefrontal_volume	0.138	**1.49E-05**	**1.30E-06**	**4.28E-05**	**4.29E-06**
lh_cuneus_volume	**2.20E-16**	**2.20E-16**	**2.20E-16**	**1.10E-05**	**5.81E-10**
lh_entorhinal_volume	**2.20E-16**	**2.20E-16**	**3.21E-06**	**8.64E-07**	**2.20E-16**
lh_fusiform_volume	0.2895	**0.0001167**	**0.0004102**	**4.69E-11**	**0.008752**
lh_inferiorparietal_volume	**6.41E-12**	**0.0001866**	**0.002359**	**2.20E-16**	0.09005
lh_inferiortemporal_volume	**9.75E-11**	**2.20E-16**	**0.005125**	**8.90E-06**	**2.20E-16**
lh_isthmuscingulate_volume	0.9164	**1.48E-10**	0.7898	**0.0001477**	0.06216
lh_lateraloccipital_volume	**2.20E-16**	**2.20E-16**	**2.20E-16**	0.2592	**2.20E-16**
lh_lateralorbitofrontal_volume	**1.36E-11**	**2.20E-16**	**0.03518**	0.5788	**2.20E-16**
lh_lingual_volume	**4.61E-06**	**2.20E-16**	**2.20E-16**	0.6067	0.9628
lh_medialorbitofrontal_volume	**5.20E-14**	**2.20E-16**	0.6415	**0.003257**	**2.20E-16**
lh_middletemporal_volume	**5.60E-06**	**2.20E-16**	**6.81E-08**	**1.69E-08**	**2.20E-16**
lh_parahippocampal_volume	**6.77E-05**	0.5925	**2.20E-16**	**7.11E-15**	0.2387
lh_paracentral_volume	**0.0008166**	**2.20E-16**	**6.16E-08**	0.9932	**3.08E-06**
lh_parsopercularis_volume	**0.02538**	**0.0003476**	**2.47E-05**	**0.01847**	**0.002114**
lh_parsorbitalis_volume	**2.20E-16**	**2.20E-16**	**9.37E-05**	**0.003137**	**2.20E-16**
lh_parstriangularis_volume	**5.82E-06**	**2.20E-16**	0.2089	0.4965	**2.20E-16**
lh_pericalcarine_volume	**0.0002194**	**2.20E-16**	**2.20E-16**	**0.2715**	0.5737
lh_postcentral_volume	0.8065	**2.20E-16**	**2.50E-07**	**0.001391**	0.2101
lh_posteriorcingulate_volume	**0.0007976**	**2.52E-06**	**0.02054**	9.27E-09	0.4755
lh_precentral_volume	**0.0003338**	**3.03E-15**	**0.002911**	**0.3498**	**6.38E-05**
lh_precuneus_volume	0.1617	**2.20E-16**	**2.36E-06**	**8.95E-12**	**3.73E-05**
lh_rostralanteriorcingulate_volume	**0.00994**	**0.0006999**	**5.51E-12**	**0.003384**	0.2009
lh_rostralmiddlefrontal_volume	0.2451	**2.20E-16**	0.2517	**7.28E-06**	**2.33E-11**
lh_superiorfrontal_volume	0.3203	**2.20E-16**	**0.03064**	**9.85E-06**	**2.20E-16**
lh_superiorparietal_volume	0.05328	**2.08E-15**	**1.04E-06**	**4.94E-10**	**3.88E-05**
lh_superiortemporal_volume	**1.09E-10**	**2.20E-16**	0.6291	**0.01423**	**2.20E-16**
lh_supramarginal_volume	**2.10E-06**	**2.20E-16**	**1.74E-07**	**0.03278**	**2.20E-16**
lh_frontalpole_volume	**2.20E-16**	**2.20E-16**	**2.20E-16**	**3.95E-12**	**2.20E-16**
lh_temporalpole_volume	**0.002592**	**0.002989**	**2.20E-16**	1.07E-09	**1.30E-10**
lh_transversetemporal_volume	**0.0002175**	0.2268	0.2702	0.0002007	**5.88E-06**
lh_insula_volume	**2.20E-16**	**2.20E-16**	**0.0304**	0.02843	**2.80E-15**

Table 8: Results (p-values) of MANOVAs comparing the RG to patient groups for SubVol regions

SubVol regions	MCI vs. RG	PD vs. RG	FTLD vs. RG	AD vs. RG	MS vs. RG
Left-Cerebellum-Cortex	**2.20E-16**	**2.20E-16**	**2.20E-16**	**2.20E-16**	**2.20E-16**
Left-Thalamus-Proper	**2.20E-16**	**2.09E-14**	**1.09E-11**	**1.50E-12**	**2.20E-16**
Left-Caudate	**0.001017**	**0.5731**	**2.20E-16**	**0.007633**	**1.02E-14**
Left-Putamen	**2.20E-16**	**2.20E-16**	**2.20E-16**	**2.20E-16**	**2.20E-16**
Left-Pallidum	**2.20E-16**	**2.20E-16**	**2.20E-16**	**2.20E-16**	**2.20E-16**
Brain-Stem	0.116	**2.20E-16**	0.9935	0.6997	0.1833
Left-Hippocampus	**2.41E-10**	**5.46E-09**	**2.20E-16**	**2.20E-16**	0.4553
Left-Amygdala	**2.20E-16**	**3.83E-10**	**2.20E-16**	**2.20E-16**	**0.006209**
Left-Accumbens-area	**2.20E-16**	**3.77E-09**	**2.20E-16**	**2.20E-16**	**2.20E-16**
Left-VentralDC	**2.20E-16**	**2.20E-16**	**2.74E-07**	0.2012	**1.88E-11**
Left-choroid-plexus	**2.20E-16**	**2.20E-16**	**2.20E-16**	**2.20E-16**	**2.20E-16**
Right-Cerebellum-Cortex	**2.20E-16**	**2.20E-16**	**2.20E-16**	**3.26E-15**	**2.20E-16**
Right-Thalamus-Proper	0.3133	**2.20E-16**	0.07601	**0.0008195**	**2.20E-16**
Right-Caudate	**1.55E-05**	**0.01757**	**2.20E-16**	**5.33E-05**	**2.20E-16**
Right-Putamen	**2.20E-16**	**0.0003091**	**2.20E-16**	**2.20E-16**	**2.20E-16**
Right-Pallidum	**2.20E-16**	**2.20E-16**	**2.20E-16**	**2.20E-16**	**2.20E-16**
Right-Hippocampus	**2.93E-12**	**1.25E-05**	**2.20E-16**	**2.20E-16**	0.05362
Right-Amygdala	0.4134	**2.20E-16**	**0.0001409**	**2.20E-16**	**1.92E-07**
Right-Accumbens-area	**2.20E-16**	**1.36E-08**	**2.20E-16**	**2.20E-16**	**2.20E-16**
Right-VentralDC	**2.20E-16**	**2.20E-16**	**2.63E-05**	0.2867	**4.46E-08**
Right-choroid-plexus	**2.20E-16**	**2.20E-16**	**2.20E-16**	**2.20E-16**	**2.20E-16**
CC_Posterior	**2.20E-16**	**2.20E-16**	**1.20E-07**	**4.21E-06**	**2.20E-16**
CC_Mid_Posterior	**2.20E-16**	**2.20E-16**	**2.20E-16**	**2.20E-16**	**2.20E-16**
CC_Central	**2.20E-16**	**2.20E-16**	**2.01E-13**	**4.60E-05**	**2.20E-16**
CC_Mid_Anterior	**2.20E-16**	**2.20E-16**	**1.77E-06**	0.06934	**2.20E-16**
CC_Anterior	**2.20E-16**	**2.20E-16**	**2.41E-05**	**0.001631**	**2.20E-16**

Table 9: Results (p-values) of MANOVAs comparing the RG to patient groups for SA regions

SA regions	MCI vs. RG	PD vs. RG	FTLD vs. RG	AD vs. RG	MS vs. RG
rh_bankssts_area	**2.40E-13**	0.1357	**3.08E-13**	**2.84E-12**	**0.000261**
rh_caudalanteriorcingulate_area	**7.17E-14**	0.8607	**0.04967**	**6.07E-07**	**1.43E-13**
rh_caudalmiddlefrontal_area	**5.79E-05**	**2.20E-16**	0.7056	0.5647	**6.04E-06**
rh_cuneus_area	**2.20E-16**	**2.20E-16**	**2.20E-16**	**0.000255**	**3.17E-14**
rh_entorhinal_area	**2.20E-16**	**2.20E-16**	**1.98E-13**	**3.44E-12**	**2.20E-16**
rh_fusiform_area	**0.02098**	**4.51E-05**	**0.0005319**	**4.83E-05**	0.9962
rh_inferiorparietal_area	**0.002136**	**8.37E-09**	0.1566	**1.32E-06**	0.8292
rh_inferiortemporal_area	**2.20E-16**	**2.20E-16**	0.0991	0.7917	**1.91E-14**
rh_isthmuscingulate_area	0.9567	**2.20E-16**	**6.00E-07**	0.05887	**0.0001041**
rh_lateraloccipital_area	**2.20E-16**	**2.20E-16**	**2.20E-16**	**1.19E-05**	**2.20E-16**
rh_lateralorbitofrontal_area	**2.20E-16**	**2.20E-16**	**0.002287**	**1.88E-08**	**2.20E-16**
rh_lingual_area	**7.18E-10**	**2.20E-16**	**6.60E-11**	**0.01215**	**2.69E-07**
rh_medialorbitofrontal_area	**2.20E-16**	**2.20E-16**	**7.94E-14**	**1.01E-09**	**2.20E-16**
rh_middletemporal_area	**1.12E-10**	**2.20E-16**	0.194	0.5703	**7.94E-10**
rh_parahippocampal_area	**9.43E-10**	0.3171	**0.001865**	**5.56E-07**	**8.35E-05**
rh_paracentral_area	0.8955	**2.20E-16**	**5.43E-05**	0.57	0.4489
rh_parsopercularis_area	0.653	**6.94E-07**	0.3932	0.618	0.6685
rh_parsorbitalis_area	**2.20E-16**	**2.20E-16**	**4.38E-07**	**0.0009892**	**2.20E-16**
rh_parstriangularis_area	**0.0007659**	**2.20E-16**	**0.002145**	0.2439	**1.50E-06**
rh_pericalcarine_area	**0.02006**	**1.94E-10**	**5.69E-07**	0.8547	**0.003002**
rh_postcentral_area	**9.47E-06**	**2.20E-16**	0.0513	0.1463	**0.005621**
rh_posteriorcingulate_area	0.9401	**2.20E-16**	**8.61E-07**	**0.006992**	0.07079
rh_precentral_area	**0.005724**	**2.20E-16**	**0.005907**	0.1925	0.2172
rh_precuneus_area	0.51	**2.20E-16**	**3.95E-05**	**0.0005576**	0.7105
rh_rostralanteriorcingulate_area	**4.82E-07**	**0.02813**	0.07858	**0.0003704**	**3.80E-11**
rh_rostralmiddlefrontal_area	**0.0003252**	**2.20E-16**	0.9379	0.4298	**8.23E-05**
rh_superiorfrontal_area	**0.003629**	**2.20E-16**	**0.02759**	0.7852	**0.001858**
rh_superiorparietal_area	0.7677	**9.29E-09**	**0.04634**	**0.001248**	0.1924
rh_superiortemporal_area	**1.62E-07**	**2.20E-16**	**0.002405**	0.1162	**0.02853**
rh_supramarginal_area	0.8978	**1.19E-07**	0.2333	**0.002738**	0.1289
rh_frontalpole_area	**2.20E-16**	**2.20E-16**	**1.63E-10**	**3.57E-05**	**2.20E-16**
rh_temporalpole_area	**2.20E-16**	**2.20E-16**	0.9489	**3.79E-05**	**0.002135**
rh_transversetemporal_area	0.5087	**0.0002022**	0.8602	0.3214	**0.02312**
rh_insula_area	**2.20E-16**	**2.20E-16**	**3.53E-12**	**9.38E-07**	0.1192
lh_bankssts_area	**1.97E-07**	0.07294	**3.11E-10**	**1.45E-10**	**0.01393**
lh_caudalanteriorcingulate_area	**1.29E-11**	0.8782	**5.23E-05**	**0.0004488**	**1.57E-06**
lh_caudalmiddlefrontal_area	0.8228	**3.56E-11**	0.1635	0.4293	0.09197
lh_cuneus_area	**8.07E-09**	**2.20E-16**	**2.46E-09**	**0.007667**	**7.39E-08**
lh_entorhinal_area	**2.20E-16**	**2.20E-16**	**1.57E-06**	**7.31E-08**	**2.20E-16**
lh_fusiform_area	**0.01263**	**5.38E-05**	**0.0002742**	**3.55E-05**	0.9076
lh_inferiorparietal_area	**0.0001259**	**2.76E-06**	**0.02629**	**5.23E-09**	**0.009074**
lh_inferiortemporal_area	**2.40E-12**	**2.20E-16**	0.7813	0.2784	**6.21E-09**
lh_isthmuscingulate_area	0.09617	**4.24E-06**	0.06906	**0.02327**	**0.0003613**
lh_lateraloccipital_area	**2.20E-16**	**2.20E-16**	**2.20E-16**	**0.001639**	**2.20E-16**
lh_lateralorbitofrontal_area	**3.11E-10**	**2.20E-16**	0.3318	0.5956	**1.81E-07**
lh_lingual_area	0.06911	**6.82E-07**	**0.01966**	0.2723	**0.03704**
lh_medialorbitofrontal_area	**2.85E-14**	**2.20E-16**	**0.04924**	**1.34E-05**	**7.52E-05**
lh_middletemporal_area	**2.92E-09**	**2.20E-16**	0.1484	0.1109	**1.50E-05**
lh_parahippocampal_area	**1.00E-07**	0.1332	**0.001439**	**3.77E-07**	**0.0004128**
lh_paracentral_area	0.05647	**2.20E-16**	**1.81E-06**	0.5944	**0.001066**
lh_parsopercularis_area	**0.01016**	**0.00129**	**0.0006337**	0.1197	0.966
lh_parsorbitalis_area	**2.20E-16**	**2.20E-16**	**8.89E-10**	**4.23E-05**	**2.20E-16**
lh_parstriangularis_area	**3.50E-06**	**2.20E-16**	**0.01098**	0.07944	**2.37E-05**
lh_pericalcarine_area	**0.0321**	**1.87E-10**	**0.0001004**	0.9163	**0.001639**
lh_postcentral_area	**0.0009315**	**2.20E-16**	**0.001604**	0.2935	0.1567
lh_posteriorcingulate_area	**0.0004096**	**1.16E-07**	0.9976	**3.14E-05**	**0.001632**
lh_precentral_area	**0.0001569**	**2.20E-16**	**1.38E-07**	**0.02857**	**0.08904**
lh_precuneus_area	0.5792	**2.20E-16**	**0.0004496**	**6.28E-05**	0.9578
lh_rostralanteriorcingulate_area	**0.01233**	**1.63E-06**	**0.042**	**0.03492**	**0.001422**
lh_rostralmiddlefrontal_area	**0.0001634**	**2.20E-16**	0.461	0.8394	**6.86E-05**
lh_superiorfrontal_area	**5.62E-06**	**2.20E-16**	**0.0003691**	0.8885	**5.01E-05**
lh_superiorparietal_area	0.4272	**4.17E-11**	**0.006639**	**0.02004**	0.08553
lh_superiortemporal_area	**2.20E-16**	**2.20E-16**	**1.10E-05**	**0.001113**	**0.0001288**
lh_supramarginal_area	**7.45E-11**	**2.20E-16**	**5.13E-10**	**0.03265**	**3.51E-07**
lh_frontalpole_area	**2.20E-16**	**2.20E-16**	**2.20E-16**	**2.20E-16**	**2.20E-16**
lh_temporalpole_area	0.8934	**0.008122**	**2.24E-14**	0.3967	**0.04655**
lh_transversetemporal_area	0.74	**1.21E-09**	0.5759	0.6038	0.3703
lh_insula_area	**2.20E-16**	**2.20E-16**	**2.20E-16**	**6.23E-07**	**4.45E-06**

Table 9: Results of MANCOVAs comparing the DG to patient groups for CT regions

Dependent variable CT DG	Group				Gender				Ineteraction: Group & Gender			
	Sum of squares	Mean square	F	P	Sum of squares	Mean square	F	P	Sum of squares	Mean square	F	P
rh_bankssts_thickness	3.8	0.76	21.7	**<0.001**	0.1	0.10	2.8	0.092	0.4	0.09	2.5	**0.027**
rh_caudalanteriorcingulate_thickness	7.8	1.57	25.0	**<0.001**	1.9	1.90	30.4	**<0.001**	1.0	0.20	3.2	**0.007**
rh_caudalmiddlefrontal_thickness	8.2	1.64	55.1	**<0.001**	0.6	0.62	20.7	**<0.001**	0.1	0.02	0.8	0.564
rh_cuneus_thickness	3.2	0.64	28.3	**<0.001**	0.0	0.00	0.0	0.994	0.3	0.05	2.4	**0.038**
rh_entorhinal_thickness	43.7	8.74	43.0	**<0.001**	0.1	0.12	0.6	0.445	1.4	0.28	1.4	**0.223**
rh_fusiform_thickness	2.6	0.52	15.1	**<0.001**	0.0	0.00	0.1	0.722	0.4	0.08	2.2	0.055
rh_inferiorparietal_thickness	9.7	1.93	83.3	**<0.001**	0.4	0.41	17.5	**<0.001**	0.3	0.05	2.2	**0.049**
rh_inferiortemporal_thickness	6.8	1.36	41.1	**<0.001**	0.0	0.00	0.1	0.775	0.1	0.03	0.9	0.51
rh_isthmuscingulate_thickness	5.0	1.00	22.3	**<0.001**	0.3	0.31	6.9	**0.009**	0.5	0.10	2.2	0.057
rh_lateraloccipital_thickness	2.6	0.51	26.4	**<0.001**	0.0	0.00	0.0	0.918	0.2	0.04	2.1	0.06
rh_lateralorbitofrontal_thickness	8.4	1.68	65.8	**<0.001**	0.3	0.26	10.0	**0.002**	0.1	0.03	1.0	0.399
rh_lingual_thickness	3.6	0.72	34.9	**<0.001**	0.0	0.04	1.8	0.179	0.1	0.02	1.0	0.393
rh_medialorbitofrontal_thickness	4.7	0.93	34.5	**<0.001**	0.2	0.16	6.1	**0.014**	0.1	0.02	0.8	0.578
rh_middletemporal_thickness	13.8	2.75	85.6	**<0.001**	0.0	0.00	0.0	0.901	0.2	0.04	1.2	0.305
rh_parahippocampal_thickness	5.7	1.15	15.7	**<0.001**	1.5	1.51	20.7	**<0.001**	0.3	0.07	0.9	0.486
rh_paracentral_thickness	1.5	0.29	8.1	**<0.001**	0.2	0.24	6.6	**0.01**	0.1	0.03	0.7	0.626
rh_parsopercularis_thickness	3.7	0.74	27.1	**<0.001**	0.0	0.01	0.3	0.599	0.1	0.02	0.9	0.471
rh_parsorbitalis_thickness	12.5	2.51	61.2	**<0.001**	1.2	1.18	28.8	**<0.001**	0.5	0.09	2.2	**0.05**
rh_parstriangularis_thickness	3.9	0.78	31.8	**<0.001**	0.0	0.05	2.0	0.162	0.2	0.03	1.4	0.214
rh_pericalcarine_thickness	9.4	1.88	68.3	**<0.001**	0.0	0.04	1.5	0.223	0.1	0.01	0.4	0.825
rh_postcentral_thickness	5.0	1.00	51.5	**<0.001**	0.2	0.24	12.3	**<0.001**	0.2	0.03	1.8	0.114
rh_posteriorcingulate_thickness	4.9	0.98	30.2	**<0.001**	0.7	0.68	21.1	**<0.001**	0.2	0.05	1.5	0.182
rh_precentral_thickness	1.2	0.24	7.2	**<0.001**	0.3	0.33	9.7	**0.002**	0.2	0.04	1.3	0.274
rh_precuneus_thickness	4.3	0.86	37.3	**<0.001**	0.0	0.04	1.9	0.172	0.2	0.04	1.8	0.111
rh_rostralanteriorcingulate_thickness	9.4	1.87	28.1	**<0.001**	0.1	0.05	0.8	0.373	0.2	0.04	0.7	0.659
rh_rostralmiddlefrontal_thickness	7.8	1.56	80.5	**<0.001**	0.3	0.31	16.3	**<0.001**	0.3	0.06	2.9	**0.013**
rh_superiorfrontal_thickness	11.7	2.34	85.5	**<0.001**	1.1	1.07	39.3	**<0.001**	0.2	0.04	1.3	0.257
rh_superiorparietal_thickness	5.6	1.12	51.0	**<0.001**	0.2	0.20	9.3	**0.002**	0.1	0.02	1.1	0.337
rh_superiortemporal_thickness	9.1	1.83	58.8	**<0.001**	0.0	0.01	0.3	0.599	0.1	0.02	0.8	0.576
rh_supramarginal_thickness	6.3	1.27	49.6	**<0.001**	0.3	0.25	9.9	**0.002**	0.2	0.03	1.2	0.301
rh_frontalpole_thickness	11.9	2.37	35.6	**<0.001**	1.5	1.54	23.1	**<0.001**	0.4	0.07	1.1	0.346
rh_temporalpole_thickness	60.9	12.17	69.4	**<0.001**	0.1	0.12	0.7	0.415	0.8	0.17	0.9	0.453
rh_transversetemporal_thickness	2.9	0.59	9.4	**<0.001**	1.0	1.00	15.9	**<0.001**	0.3	0.07	1.0	0.388
rh_insula_thickness	12.5	2.50	58.7	**<0.001**	0.1	0.09	2.2	0.138	0.2	0.04	0.9	0.51
lh_bankssts_thickness	4.2	0.85	26.4	**<0.001**	0.1	0.11	3.5	0.06	0.4	0.07	2.3	**0.047**
lh_caudalanteriorcingulate_thickness	14.8	2.96	40.0	**<0.001**	1.8	1.79	24.3	**<0.001**	0.7	0.14	1.9	0.09
lh_caudalmiddlefrontal_thickness	9.2	1.85	56.9	**<0.001**	0.7	0.71	22.0	**<0.001**	0.1	0.02	0.7	0.618
lh_cuneus_thickness	2.6	0.52	23.9	**<0.001**	0.0	0.00	0.2	0.663	0.1	0.02	0.7	0.599
lh_entorhinal_thickness	66.1	13.21	71.3	**<0.001**	0.0	0.01	0.0	0.824	0.8	0.17	0.9	0.481
lh_fusiform_thickness	4.5	0.90	27.8	**<0.001**	0.1	0.12	3.8	**0.05**	0.3	0.06	2.0	0.077
lh_inferiorparietal_thickness	9.1	1.81	80.3	**<0.001**	0.6	0.55	24.5	**<0.001**	0.3	0.05	2.3	**0.046**
lh_inferiortemporal_thickness	12.5	2.50	73.8	**<0.001**	0.0	0.02	0.5	0.47	0.2	0.03	0.9	0.484
lh_isthmuscingulate_thickness	6.0	1.20	28.6	**<0.001**	0.1	0.06	1.3	0.25	0.3	0.06	1.4	0.213
lh_lateraloccipital_thickness	2.1	0.42	23.6	**<0.001**	0.0	0.05	2.6	0.105	0.1	0.02	1.2	0.319
lh_lateralorbitofrontal_thickness	9.1	1.83	75.2	**<0.001**	0.0	0.03	1.1	0.296	0.2	0.03	1.3	0.244
lh_lingual_thickness	4.3	0.85	44.9	**<0.001**	0.1	0.08	4.3	0.038	0.1	0.02	1.1	0.336
lh_medialorbitofrontal_thickness	5.3	1.05	42.0	**<0.001**	0.0	0.00	0.1	0.725	0.0	0.01	0.3	0.908
lh_middletemporal_thickness	18.9	3.79	109.0	**<0.001**	0.0	0.03	0.9	0.336	0.3	0.06	1.6	0.146
lh_parahippocampal_thickness	15.2	3.04	31.7	**<0.001**	1.8	1.83	19.0	**<0.001**	0.6	0.12	1.3	0.279
lh_paracentral_thickness	0.5	0.10	3.0	**0.010**	0.1	0.13	3.9	**0.05**	0.1	0.02	0.5	0.775
lh_parsopercularis_thickness	4.1	0.81	30.0	**<0.001**	0.0	0.03	1.2	0.273	0.2	0.03	1.3	0.268
lh_parsorbitalis_thickness	14.0	2.80	61.4	**<0.001**	1.5	1.51	33.1	**<0.001**	0.3	0.05	1.2	0.316
lh_parstriangularis_thickness	5.2	1.04	40.1	**<0.001**	0.2	0.25	9.5	**0.002**	0.1	0.03	1.1	0.354
lh_pericalcarine_thickness	8.1	1.61	65.2	**<0.001**	0.0	0.01	0.6	0.444	0.0	0.01	0.3	0.886
lh_postcentral_thickness	3.4	0.68	36.3	**<0.001**	0.3	0.26	14.1	**<0.001**	0.1	0.01	0.7	0.637
lh_posteriorcingulate_thickness	5.8	1.16	37.8	**<0.001**	0.4	0.36	11.9	**0.001**	0.4	0.08	2.6	**0.023**
lh_precentral_thickness	1.7	0.34	10.3	**<0.001**	0.1	0.13	4.1	**0.043**	0.3	0.06	1.8	0.102
lh_precuneus_thickness	5.5	1.09	44.4	**<0.001**	0.1	0.08	3.3	0.068	0.2	0.03	1.4	0.232
lh_rostralanteriorcingulate_thickness	17.8	3.56	58.6	**<0.001**	2.2	2.20	36.3	**<0.001**	0.2	0.05	0.8	0.536
lh_rostralmiddlefrontal_thickness	9.3	1.86	89.7	**<0.001**	0.3	0.32	15.7	**<0.001**	0.1	0.03	1.3	0.26
lh_superiorfrontal_thickness	13.0	2.60	90.5	**<0.001**	1.1	1.11	38.5	**<0.001**	0.1	0.03	1.0	0.408
lh_superiorparietal_thickness	5.3	1.05	47.9	**<0.001**	0.2	0.19	8.5	**0.004**	0.2	0.03	1.4	0.233
lh_superiortemporal_thickness	10.9	2.17	65.3	**<0.001**	0.1	0.07	2.2	0.139	0.4	0.07	2.1	0.059
lh_supramarginal_thickness	7.0	1.41	58.0	**<0.001**	0.5	0.55	22.6	**<0.001**	0.2	0.04	1.5	0.179
lh_frontalpole_thickness	12.4	2.48	37.2	**<0.001**	1.6	1.65	24.7	**<0.001**	0.2	0.03	0.5	0.782
lh_temporalpole_thickness	54.6	10.92	67.3	**<0.001**	0.5	0.55	3.4	0.067	0.6	0.12	0.8	0.573
lh_transversetemporal_thickness	3.6	0.72	12.7	**<0.001**	0.9	0.85	15.2	**<0.001**	0.3	0.06	1.2	0.329
lh_insula_thickness	10.5	2.10	47.3	**<0.001**	0.1	0.06	1.4	0.232	0.1	0.02	0.5	0.787

Table 10: Results of MANCOVAs comparing the DG to patient groups for CVol regions

Dependent variable CVol DG	Group				Gender				Ineteraction: Group & Gender			
	Sum of squares	Mean square	F	P	Sum of squares	Mean square	F	P	Sum of squares	Mean square	F	P
rh_bankssts_volume	1.3E+07	2.6E+06	23.3	**<0.001**	1.0E+07	1.0E+07	91.0	**<0.001**	3.3E+06	6.6E+05	5.9	**<0.001**
rh_caudalanteriorcingulate_volume	7.4E+06	1.5E+06	7.1	**<0.001**	9.5E+06	9.5E+06	46.0	**<0.001**	8.9E+05	1.8E+05	0.9	0.505
rh_caudalmiddlefrontal_volume	1.3E+08	2.5E+07	24.8	**<0.001**	7.6E+07	7.6E+07	74.9	**<0.001**	1.2E+07	2.5E+06	2.4	**0.032**
rh_cuneus_volume	3.3E+07	6.6E+06	19.4	**<0.001**	4.6E+07	4.6E+07	132.9	**<0.001**	1.0E+07	2.0E+06	5.9	**<0.001**
rh_entorhinal_volume	2.6E+07	5.3E+06	29.8	**<0.001**	1.4E+07	1.4E+07	80.7	**<0.001**	3.8E+06	7.6E+05	4.3	**<0.001**
rh_fusiform_volume	1.7E+08	3.5E+07	21.0	**<0.001**	4.6E+08	4.6E+08	281.8	**<0.001**	6.1E+07	1.2E+07	7.5	**<0.001**
rh_inferiorparietal_volume	9.3E+08	1.9E+08	46.3	**<0.001**	7.8E+08	7.8E+08	194.5	**<0.001**	1.0E+08	2.0E+07	5.0	**<0.001**
rh_inferiortemporal_volume	4.8E+08	9.5E+07	35.6	**<0.001**	6.3E+08	6.3E+08	237.7	**<0.001**	8.5E+07	1.7E+07	6.4	**<0.001**
rh_isthmuscingulate_volume	1.2E+07	2.5E+06	16.0	**<0.001**	2.4E+07	2.4E+07	155.9	**<0.001**	5.1E+06	1.0E+06	6.6	**<0.001**
rh_lateraloccipital_volume	2.7E+08	5.4E+07	18.9	**<0.001**	8.3E+08	8.3E+08	290.0	**<0.001**	1.7E+08	3.4E+07	11.7	**<0.001**
rh_lateralorbitofrontal_volume	1.1E+08	2.1E+07	29.6	**<0.001**	1.4E+08	1.4E+08	192.7	**<0.001**	1.9E+07	3.8E+06	5.2	**<0.001**
rh_lingual_volume	1.4E+08	2.9E+07	23.9	**<0.001**	1.9E+08	1.9E+08	153.5	**<0.001**	2.4E+07	4.8E+06	4.0	**0.001**
rh_medialorbitofrontal_volume	4.3E+07	8.7E+06	21.6	**<0.001**	8.7E+07	8.7E+07	216.8	**<0.001**	6.8E+06	1.4E+06	3.4	**0.005**
rh_middletemporal_volume	6.3E+08	1.3E+08	51.5	**<0.001**	5.3E+08	5.3E+08	218.4	**<0.001**	5.0E+07	9.9E+06	4.1	**0.001**
rh_parahippocampal_volume	5.3E+06	1.1E+06	12.7	**<0.001**	5.2E+06	5.2E+06	62.5	**<0.001**	6.2E+05	1.2E+05	1.5	0.186
rh_paracentral_volume	1.9E+07	3.7E+06	12.8	**<0.001**	2.9E+07	2.9E+07	99.0	**<0.001**	4.3E+06	8.5E+05	2.9	**0.012**
rh_parsopercularis_volume	2.2E+07	4.3E+06	12.4	**<0.001**	3.0E+07	3.0E+07	86.2	**<0.001**	7.0E+06	1.4E+06	4.1	**0.001**
rh_parsorbitalis_volume	2.2E+07	4.3E+06	29.5	**<0.001**	1.6E+07	1.6E+07	108.9	**<0.001**	1.1E+06	2.3E+05	1.6	0.168
rh_parstriangularis_volume	3.0E+07	6.0E+06	15.7	**<0.001**	5.9E+07	5.9E+07	152.1	**<0.001**	5.0E+06	9.9E+05	2.6	**0.025**
rh_pericalcarine_volume	4.2E+07	8.3E+06	32.0	**<0.001**	2.1E+07	2.1E+07	81.9	**<0.001**	4.8E+06	9.7E+05	3.7	**0.002**
rh_postcentral_volume	1.7E+08	3.4E+07	23.8	**<0.001**	2.0E+08	2.0E+08	138.2	**<0.001**	1.5E+07	2.9E+06	2.0	0.072
rh_posteriorcingulate_volume	1.8E+07	3.6E+06	14.5	**<0.001**	2.7E+07	2.7E+07	108.2	**<0.001**	4.6E+06	9.3E+05	3.8	**0.002**
rh_precentral_volume	1.7E+08	3.3E+07	12.6	**<0.001**	4.1E+08	4.1E+08	154.6	**<0.001**	4.3E+07	8.5E+06	3.2	**0.007**
rh_precuneus_volume	2.9E+08	5.8E+07	38.9	**<0.001**	3.1E+08	3.1E+08	209.3	**<0.001**	6.1E+07	1.2E+07	8.2	**<0.001**
rh_rostralanteriorcingulate_volume	4.6E+06	9.3E+05	5.5	**<0.001**	1.9E+07	1.9E+07	110.6	**<0.001**	2.4E+06	4.7E+05	2.8	**0.016**
rh_rostralmiddlefrontal_volume	6.5E+08	1.3E+08	31.1	**<0.001**	1.1E+09	1.1E+09	268.5	**<0.001**	6.3E+07	1.3E+07	3.0	**0.01**
rh_superiorfrontal_volume	1.1E+09	2.1E+08	32.6	**<0.001**	1.3E+09	1.3E+09	192.4	**<0.001**	2.3E+08	4.7E+07	7.1	**<0.001**
rh_superiorparietal_volume	4.8E+08	9.7E+07	34.3	**<0.001**	3.5E+08	3.5E+08	124.4	**<0.001**	7.0E+07	1.4E+07	5.0	**<0.001**
rh_superiortemporal_volume	2.7E+08	5.3E+07	27.6	**<0.001**	3.1E+08	3.1E+08	157.4	**<0.001**	4.1E+07	8.3E+06	4.3	**<0.001**
rh_supramarginal_volume	1.8E+08	3.5E+07	18.8	**<0.001**	2.9E+08	2.9E+08	152.5	**<0.001**	5.1E+07	1.0E+07	5.5	**<0.001**
rh_frontalpole_volume	2.1E+06	4.2E+05	13.1	**<0.001**	1.5E+06	1.5E+06	46.2	**<0.001**	3.3E+05	6.5E+04	2.0	**0.07**
rh_temporalpole_volume	4.6E+07	9.1E+06	48.1	**<0.001**	8.0E+06	8.0E+06	41.9	**<0.001**	1.7E+06	3.4E+05	1.8	0.11
rh_transversetemporal_volume	1.5E+06	3.0E+05	12.3	**<0.001**	1.0E+06	1.0E+06	42.0	**<0.001**	3.6E+05	7.2E+04	2.9	**0.012**
rh_insula_volume	6.3E+07	1.3E+07	17.0	**<0.001**	2.4E+08	2.4E+08	320.5	**<0.001**	1.7E+07	3.4E+06	4.5	**<0.001**
lh_bankssts_volume	2.0E+07	3.9E+06	22.5	**<0.001**	1.8E+07	1.8E+07	103.4	**<0.001**	4.3E+06	8.7E+05	4.9	**<0.001**
lh_caudalanteriorcingulate_volume	9.9E+06	2.0E+06	11.2	**<0.001**	5.9E+06	5.9E+06	33.4	**<0.001**	1.2E+06	2.5E+05	1.4	0.226
lh_caudalmiddlefrontal_volume	1.2E+08	2.4E+07	24.4	**<0.001**	8.8E+07	8.8E+07	87.8	**<0.001**	1.9E+07	3.7E+06	3.7	**0.002**
lh_cuneus_volume	2.5E+07	5.0E+06	16.7	**<0.001**	3.4E+07	3.4E+07	112.5	**<0.001**	6.4E+06	1.3E+06	4.3	**<0.001**
lh_entorhinal_volume	6.1E+07	1.2E+07	64.3	**<0.001**	1.6E+07	1.6E+07	83.5	**<0.001**	4.7E+06	9.4E+05	5.0	**<0.001**
lh_fusiform_volume	1.9E+08	3.7E+07	21.8	**<0.001**	3.9E+08	3.9E+08	226.1	**<0.001**	5.4E+07	1.1E+07	6.3	**<0.001**
lh_inferiorparietal_volume	5.3E+08	1.1E+08	37.1	**<0.001**	3.3E+08	3.3E+08	115.3	**<0.001**	4.5E+07	8.9E+06	3.1	**0.008**
lh_inferiortemporal_volume	7.5E+08	1.5E+08	53.3	**<0.001**	5.8E+08	5.8E+08	206.7	**<0.001**	5.1E+07	1.0E+07	3.6	**0.003**
lh_isthmuscingulate_volume	1.6E+07	3.3E+06	19.6	**<0.001**	4.2E+07	4.2E+07	254.5	**<0.001**	7.7E+06	1.5E+06	9.2	**<0.001**
lh_lateraloccipital_volume	2.2E+08	4.3E+07	17.0	**<0.001**	5.5E+08	5.5E+08	213.8	**<0.001**	1.3E+08	2.6E+07	10.4	**<0.001**
lh_lateralorbitofrontal_volume	1.4E+08	2.9E+07	37.8	**<0.001**	1.7E+08	1.7E+08	220.8	**<0.001**	1.7E+07	3.4E+06	4.5	**<0.001**
lh_lingual_volume	1.3E+08	2.6E+07	25.5	**<0.001**	1.4E+08	1.4E+08	135.8	**<0.001**	2.7E+07	5.3E+06	5.2	**<0.001**
lh_medialorbitofrontal_volume	4.2E+07	8.5E+06	20.0	**<0.001**	1.1E+08	1.1E+08	251.7	**<0.001**	8.3E+06	1.7E+06	3.9	**0.002**
lh_middletemporal_volume	7.6E+08	1.5E+08	62.8	**<0.001**	4.7E+08	4.7E+08	194.8	**<0.001**	5.7E+07	1.1E+07	4.7	**<0.001**
lh_parahippocampal_volume	1.3E+07	2.5E+06	24.0	**<0.001**	4.3E+06	4.3E+06	41.2	**<0.001**	3.1E+06	6.3E+05	6.0	**<0.001**
lh_paracentral_volume	1.6E+07	3.1E+06	14.7	**<0.001**	2.2E+07	2.2E+07	104.0	**<0.001**	1.3E+06	2.6E+05	1.2	0.308
lh_parsopercularis_volume	4.0E+07	8.0E+06	15.4	**<0.001**	3.5E+07	3.5E+07	67.7	**<0.001**	7.2E+06	1.4E+06	2.8	**0.016**
lh_parsorbitalis_volume	2.1E+07	4.2E+06	39.1	**<0.001**	1.0E+07	1.0E+07	94.2	**<0.001**	1.3E+06	2.6E+05	2.4	**0.034**
lh_parstriangularis_volume	2.1E+07	4.2E+06	14.2	**<0.001**	3.4E+07	3.4E+07	112.3	**<0.001**	6.0E+06	1.2E+06	4.0	**0.001**
lh_pericalcarine_volume	2.9E+07	5.8E+06	27.9	**<0.001**	1.2E+07	1.2E+07	55.3	**<0.001**	3.2E+06	6.3E+05	3.0	**0.01**
lh_postcentral_volume	1.9E+08	3.8E+07	24.6	**<0.001**	2.3E+08	2.3E+08	149.9	**<0.001**	2.9E+07	5.8E+06	3.7	**0.002**
lh_posteriorcingulate_volume	2.2E+07	4.3E+06	19.6	**<0.001**	3.2E+07	3.2E+07	145.9	**<0.001**	4.3E+06	8.6E+05	3.9	**0.002**
lh_precentral_volume	1.4E+08	2.7E+07	10.7	**<0.001**	4.9E+08	4.9E+08	192.1	**<0.001**	7.5E+07	1.5E+07	6.0	**<0.001**
lh_precuneus_volume	3.0E+08	5.9E+07	39.5	**<0.001**	2.6E+08	2.6E+08	174.0	**<0.001**	4.3E+07	8.6E+06	5.7	**<0.001**
lh_rostralanteriorcingulate_volume	2.4E+07	4.7E+06	18.4	**<0.001**	3.4E+07	3.4E+07	134.6	**<0.001**	4.3E+06	8.7E+05	3.4	**0.005**
lh_rostralmiddlefrontal_volume	6.9E+08	1.4E+08	32.1	**<0.001**	9.4E+08	9.4E+08	220.6	**<0.001**	1.0E+08	2.0E+07	4.7	**<0.001**
lh_superiorfrontal_volume	1.4E+09	2.7E+08	39.7	**<0.001**	1.2E+09	1.2E+09	178.8	**<0.001**	2.0E+08	4.1E+07	6.0	**<0.001**
lh_superiorparietal_volume	4.9E+08	9.8E+07	33.0	**<0.001**	3.1E+08	3.1E+08	106.1	**<0.001**	4.6E+07	9.1E+06	3.1	**0.009**
lh_superiortemporal_volume	3.9E+08	7.7E+07	31.3	**<0.001**	4.5E+08	4.5E+08	182.8	**<0.001**	8.1E+07	1.6E+07	6.6	**<0.001**
lh_supramarginal_volume	2.5E+08	5.1E+07	19.1	**<0.001**	5.4E+08	5.4E+08	202.1	**<0.001**	9.0E+07	1.8E+07	6.8	**<0.001**
lh_frontalpole_volume	1.4E+06	2.8E+05	12.0	**<0.001**	8.5E+05	8.5E+05	36.4	**<0.001**	1.7E+05	3.3E+04	1.4	0.217
lh_temporalpole_volume	5.5E+07	1.1E+07	54.1	**<0.001**	9.3E+06	9.3E+06	45.5	**<0.001**	2.3E+06	4.5E+05	2.2	**0.049**
lh_transversetemporal_volume	2.1E+06	4.2E+05	9.7	**<0.001**	3.1E+06	3.1E+06	72.0	**<0.001**	8.3E+05	1.7E+05	3.9	**0.002**
lh_insula_volume	6.7E+07	1.3E+07	19.6	**<0.001**	1.7E+08	1.7E+08	248.7	**<0.001**	1.2E+07	2.4E+06	3.5	**0.004**

Table 11: Results of MANCOVAs comparing the DG to patient groups for SubVol regions

Dependent variable SubVol DG	Group				Gender				Ineteraction: Group & Gender			
	Sum of squares	Mean square	F	P	Sum of squares	Mean square	F	P	Sum of squares	Mean square	F	P
Left_Cerebellum_Cortex	3.9E+09	7.8E+08	26.0	**<0.001**	9.0E+09	9.0E+09	300.3	**<0.001**	7.7E+08	1.5E+08	5.1	**<0.001**
Left_Thalamus_Proper	3.9E+08	7.8E+07	134.5	**<0.001**	8.5E+07	8.5E+07	146.4	**<0.001**	2.5E+07	5.0E+06	8.6	**<0.001**
Left_Caudate	2.7E+07	5.3E+06	21.7	**<0.001**	2.7E+07	2.7E+07	108.2	**<0.001**	3.8E+06	7.5E+05	3.1	**0.009**
Left_Putamen	1.3E+08	2.6E+07	65.1	**<0.001**	5.7E+07	5.7E+07	142.4	**<0.001**	1.3E+07	2.6E+06	6.5	**<0.001**
Left_Pallidum	1.0E+07	2.0E+06	28.0	**<0.001**	1.3E+07	1.3E+07	180.0	**<0.001**	1.3E+06	2.6E+05	3.6	**0.003**
Brain_Stem	5.2E+08	1.0E+08	19.5	**<0.001**	1.6E+09	1.6E+09	302.8	**<0.001**	2.5E+08	5.0E+07	9.4	**<0.001**
Left_Hippocampus	1.1E+08	2.1E+07	105.5	**<0.001**	1.8E+07	1.8E+07	90.9	**<0.001**	4.9E+06	9.9E+05	4.9	**<0.001**
Left_Amygdala	3.1E+07	6.3E+06	109.9	**<0.001**	8.8E+06	8.8E+06	154.0	**<0.001**	1.0E+06	2.0E+05	3.6	**0.003**
Left_Accumbens_area	6.1E+06	1.2E+06	101.3	**<0.001**	4.9E+05	4.9E+05	40.5	**<0.001**	2.1E+05	4.3E+04	3.6	**0.003**
Left_VentralDC	3.8E+07	7.5E+06	46.9	**<0.001**	5.0E+07	5.0E+07	313.5	**<0.001**	8.9E+06	1.8E+06	11.1	**<0.001**
Left_choroid_plexus	9.0E+06	1.8E+06	32.6	**<0.001**	1.3E+07	1.3E+07	233.8	**<0.001**	3.2E+05	6.3E+04	1.1	0.332
Right_Cerebellum_Cortex	6.1E+09	1.2E+09	37.5	**<0.001**	1.0E+10	1.0E+10	313.7	**<0.001**	1.1E+09	2.2E+08	6.8	**<0.001**
Right_Thalamus_Proper	2.1E+08	4.2E+07	79.2	**<0.001**	8.3E+07	8.3E+07	157.4	**<0.001**	3.3E+07	6.7E+06	12.6	**<0.001**
Right_Caudate	2.7E+07	5.5E+06	21.0	**<0.001**	3.0E+07	3.0E+07	113.5	**<0.001**	5.2E+06	1.0E+06	4.0	**0.001**
Right_Putamen	8.9E+07	1.8E+07	43.3	**<0.001**	5.2E+07	5.2E+07	126.7	**<0.001**	1.4E+07	2.8E+06	6.8	**<0.001**
Right_Pallidum	1.8E+07	3.6E+06	47.3	**<0.001**	1.3E+07	1.3E+07	168.5	**<0.001**	3.4E+05	6.9E+04	0.9	0.48
Right_Hippocampus	9.5E+07	1.9E+07	88.1	**<0.001**	2.0E+07	2.0E+07	93.9	**<0.001**	3.8E+06	7.6E+05	3.5	**0.004**
Right_Amygdala	3.0E+07	6.1E+06	101.8	**<0.001**	1.5E+07	1.5E+07	245.5	**<0.001**	1.5E+06	2.9E+05	4.9	**<0.001**
Right_Accumbens_area	2.0E+06	4.0E+05	47.2	**<0.001**	5.1E+05	5.1E+05	60.2	**<0.001**	1.8E+05	3.6E+04	4.2	**<0.001**
Right_VentralDC	2.9E+07	5.8E+06	39.3	**<0.001**	5.4E+07	5.4E+07	366.8	**<0.001**	8.7E+06	1.7E+06	11.9	**<0.001**
Right_choroid_plexus	1.1E+07	2.2E+06	37.7	**<0.001**	1.5E+07	1.5E+07	259.9	**<0.001**	6.6E+05	1.3E+05	2.3	**0.047**
CC_Posterior	8.0E+05	1.6E+05	4.9	**<0.001**	1.1E+06	1.1E+06	34.3	**<0.001**	7.3E+04	1.5E+04	0.4	0.814
CC_Mid_Posterior	1.7E+06	3.4E+05	23.4	**<0.001**	4.5E+04	4.5E+04	3.1	0.079	1.9E+04	3.8E+03	0.3	0.937
CC_Central	4.0E+06	8.0E+05	52.9	**<0.001**	1.2E+03	1.2E+03	0.1	0.774	6.3E+04	1.3E+04	0.8	0.525
CC_Mid_Anterior	5.8E+06	1.2E+06	71.9	**<0.001**	5.3E+04	5.3E+04	3.3	0.07	9.1E+04	1.8E+04	1.1	0.342
CC_Anterior	3.6E+06	7.2E+05	28.0	**<0.001**	1.1E+06	1.1E+06	44.1	**<0.001**	1.8E+05	3.5E+04	1.4	0.231

Table 12: Results of MANCOVAs comparing the DG to patient groups for SA regions

Dependent variable Surface Area DG	Group				Gender				Ineteraction: Group & Gender			
	Sum of squares	Mean square	F	P	Sum of squares	Mean square	F	P	Sum of squares	Mean square	F	P
rh_bankssts_area	1.7E+06	3.4E+05	24.1	**<0.001**	2.2E+06	2.2E+06	154.8	**<0.001**	3.3E+05	6.6E+04	4.6	**<0.001**
rh_caudalanteriorcingulate_area	1.6E+06	3.1E+05	13.0	**<0.001**	2.4E+06	2.4E+06	98.5	**<0.001**	3.1E+05	6.1E+04	2.5	**0.026**
rh_caudalmiddlefrontal_area	8.2E+06	1.6E+06	14.2	**<0.001**	1.8E+07	1.8E+07	153.7	**<0.001**	2.3E+06	4.7E+05	4.0	**0.001**
rh_cuneus_area	1.3E+06	2.6E+05	5.4	**<0.001**	9.8E+06	9.8E+06	201.9	**<0.001**	1.1E+06	2.3E+05	4.7	**<0.001**
rh_entorhinal_area	2.2E+05	4.5E+04	6.2	**<0.001**	7.5E+05	7.5E+05	103.7	**<0.001**	9.3E+04	1.9E+04	2.6	**0.025**
rh_fusiform_area	1.1E+07	2.1E+06	17.4	**<0.001**	4.8E+07	4.8E+07	395.2	**<0.001**	3.6E+06	7.2E+05	5.9	**<0.001**
rh_inferiorparietal_area	5.4E+07	1.1E+07	22.6	**<0.001**	1.6E+08	1.6E+08	342.5	**<0.001**	1.2E+07	2.4E+06	5.0	**<0.001**
rh_inferiortemporal_area	2.6E+07	5.2E+06	24.5	**<0.001**	6.1E+07	6.1E+07	282.8	**<0.001**	5.9E+06	1.2E+06	5.5	**<0.001**
rh_isthmuscingulate_area	3.2E+06	6.3E+05	32.4	**<0.001**	4.4E+06	4.4E+06	222.7	**<0.001**	9.6E+05	1.9E+05	9.8	**<0.001**
rh_lateraloccipital_area	1.7E+07	3.4E+06	9.9	**<0.001**	1.2E+08	1.2E+08	348.7	**<0.001**	2.0E+07	3.9E+06	11.3	**<0.001**
rh_lateralorbitofrontal_area	8.0E+06	1.6E+06	15.5	**<0.001**	2.0E+07	2.0E+07	192.8	**<0.001**	2.2E+06	4.4E+05	4.3	**<0.001**
rh_lingual_area	4.9E+06	9.9E+05	5.5	**<0.001**	2.8E+07	2.8E+07	156.0	**<0.001**	3.7E+06	7.4E+05	4.1	**0.001**
rh_medialorbitofrontal_area	4.3E+06	8.5E+05	17.8	**<0.001**	1.4E+07	1.4E+07	285.2	**<0.001**	1.4E+06	2.8E+05	5.8	**<0.001**
rh_middletemporal_area	2.4E+07	4.8E+06	28.8	**<0.001**	5.1E+07	5.1E+07	305.2	**<0.001**	3.9E+06	7.8E+05	4.7	**<0.001**
rh_parahippocampal_area	4.0E+05	8.0E+04	12.9	**<0.001**	1.2E+06	1.2E+06	199.6	**<0.001**	9.4E+04	1.9E+04	3.0	**0.01**
rh_paracentral_area	3.9E+06	7.9E+05	21.7	**<0.001**	6.5E+06	6.5E+06	178.9	**<0.001**	5.6E+05	1.1E+05	3.1	**0.009**
rh_parsopercularis_area	1.5E+06	3.1E+05	8.6	**<0.001**	4.9E+06	4.9E+06	136.5	**<0.001**	8.0E+05	1.6E+05	4.4	**<0.001**
rh_parsorbitalis_area	7.6E+05	1.5E+05	13.8	**<0.001**	2.7E+06	2.7E+06	240.5	**<0.001**	2.5E+05	5.0E+04	4.5	**<0.001**
rh_parstriangularis_area	1.6E+06	3.3E+05	7.1	**<0.001**	1.0E+07	1.0E+07	215.8	**<0.001**	8.3E+05	1.7E+05	3.6	**0.003**
rh_pericalcarine_area	3.0E+06	6.0E+05	7.8	**<0.001**	6.3E+06	6.3E+06	81.1	**<0.001**	1.9E+06	3.8E+05	5.0	**<0.001**
rh_postcentral_area	1.0E+07	2.1E+06	11.0	**<0.001**	6.0E+07	6.0E+07	320.4	**<0.001**	5.2E+06	1.0E+06	5.5	**<0.001**
rh_posteriorcingulate_area	4.3E+06	8.6E+05	27.3	**<0.001**	5.3E+06	5.3E+06	166.8	**<0.001**	9.3E+05	1.9E+05	5.9	**<0.001**
rh_precentral_area	2.9E+07	5.9E+06	21.5	**<0.001**	9.1E+07	9.1E+07	335.0	**<0.001**	6.6E+06	1.3E+06	4.8	**<0.001**
rh_precuneus_area	2.8E+07	5.6E+06	27.2	**<0.001**	6.3E+07	6.3E+07	304.4	**<0.001**	8.6E+06	1.7E+06	8.3	**<0.001**
rh_rostralanteriorcingulate_area	1.2E+06	2.5E+05	15.5	**<0.001**	2.2E+06	2.2E+06	136.6	**<0.001**	3.4E+05	6.7E+04	4.2	**<0.001**
rh_rostralmiddlefrontal_area	4.0E+07	8.1E+06	13.3	**<0.001**	2.2E+08	2.2E+08	353.0	**<0.001**	1.5E+07	3.0E+06	5.0	**<0.001**
rh_superiorfrontal_area	6.1E+07	1.2E+07	17.4	**<0.001**	2.3E+08	2.3E+08	330.7	**<0.001**	3.0E+07	6.0E+06	8.6	**<0.001**
rh_superiorparietal_area	2.4E+07	4.8E+06	13.3	**<0.001**	9.0E+07	9.0E+07	247.1	**<0.001**	1.3E+07	2.6E+06	7.1	**<0.001**
rh_superiortemporal_area	1.2E+07	2.5E+06	17.5	**<0.001**	4.0E+07	4.0E+07	282.3	**<0.001**	3.7E+06	7.5E+05	5.3	**<0.001**
rh_supramarginal_area	1.4E+07	2.7E+06	12.1	**<0.001**	5.6E+07	5.6E+07	248.7	**<0.001**	7.1E+06	1.4E+06	6.3	**<0.001**
rh_frontalpole_area	3.5E+04	7.0E+03	4.9	**<0.001**	2.7E+05	2.7E+05	187.7	**<0.001**	1.9E+04	3.8E+03	2.7	**0.019**
rh_temporalpole_area	2.9E+05	5.8E+04	14.6	**<0.001**	6.6E+05	6.6E+05	168.9	**<0.001**	6.9E+04	1.4E+04	3.5	**0.004**
rh_transversetemporal_area	8.0E+04	1.6E+04	7.4	**<0.001**	3.1E+05	3.1E+05	142.6	**<0.001**	3.9E+04	7.8E+03	3.6	**0.003**
rh_insula_area	1.1E+07	2.3E+06	25.9	**<0.001**	3.1E+07	3.1E+07	350.2	**<0.001**	1.8E+06	3.7E+05	4.2	**<0.001**
lh_bankssts_area	2.1E+06	4.3E+05	17.8	**<0.001**	3.6E+06	3.6E+06	147.4	**<0.001**	4.6E+05	9.3E+04	3.9	**0.002**
lh_caudalanteriorcingulate_area	7.4E+05	1.5E+05	7.9	**<0.001**	1.4E+06	1.4E+06	75.4	**<0.001**	1.6E+05	3.1E+04	1.7	0.14
lh_caudalmiddlefrontal_area	9.5E+06	1.9E+06	16.4	**<0.001**	2.1E+07	2.1E+07	185.6	**<0.001**	2.7E+06	5.4E+05	4.7	**<0.001**
lh_cuneus_area	1.2E+06	2.5E+05	5.1	**<0.001**	7.0E+06	7.0E+06	144.8	**<0.001**	9.9E+05	2.0E+05	4.1	**0.001**
lh_entorhinal_area	6.5E+05	1.3E+05	13.1	**<0.001**	8.3E+05	8.3E+05	82.6	**<0.001**	2.2E+05	4.4E+04	4.4	**<0.001**
lh_fusiform_area	1.1E+07	2.1E+06	17.0	**<0.001**	4.5E+07	4.5E+07	354.8	**<0.001**	2.6E+06	5.2E+05	4.1	**0.001**
lh_inferiorparietal_area	3.7E+07	7.5E+06	21.8	**<0.001**	7.8E+07	7.8E+07	227.5	**<0.001**	5.8E+06	1.2E+06	3.4	**0.005**
lh_inferiortemporal_area	3.4E+07	6.9E+06	31.9	**<0.001**	5.6E+07	5.6E+07	258.7	**<0.001**	3.9E+06	7.8E+05	3.6	**0.003**
lh_isthmuscingulate_area	2.9E+06	5.8E+05	24.6	**<0.001**	7.1E+06	7.1E+06	304.7	**<0.001**	1.2E+06	2.3E+05	9.9	**<0.001**
lh_lateraloccipital_area	8.8E+06	1.8E+06	5.2	**<0.001**	9.3E+07	9.3E+07	273.5	**<0.001**	2.0E+07	3.9E+06	11.6	**<0.001**
lh_lateralorbitofrontal_area	9.8E+06	2.0E+06	22.9	**<0.001**	2.0E+07	2.0E+07	238.8	**<0.001**	1.8E+06	3.7E+05	4.3	**<0.001**
lh_lingual_area	5.3E+06	1.1E+06	6.9	**<0.001**	2.1E+07	2.1E+07	137.1	**<0.001**	3.8E+06	7.5E+05	4.9	**<0.001**
lh_medialorbitofrontal_area	3.3E+06	6.5E+05	12.5	**<0.001**	1.7E+07	1.7E+07	321.8	**<0.001**	1.6E+06	3.1E+05	6.0	**<0.001**
lh_middletemporal_area	2.8E+07	5.6E+06	33.3	**<0.001**	4.6E+07	4.6E+07	272.6	**<0.001**	4.8E+06	9.5E+05	5.7	**<0.001**
lh_parahippocampal_area	4.2E+05	8.4E+04	12.9	**<0.001**	1.0E+06	1.0E+06	154.1	**<0.001**	1.6E+05	3.2E+04	4.9	**<0.001**
lh_paracentral_area	3.2E+06	6.4E+05	25.1	**<0.001**	4.8E+06	4.8E+06	188.0	**<0.001**	2.2E+05	4.4E+04	1.7	0.127
lh_parsopercularis_area	2.7E+06	5.5E+05	9.6	**<0.001**	6.0E+06	6.0E+06	105.6	**<0.001**	8.6E+05	1.7E+05	3.0	**0.011**
lh_parsorbitalis_area	7.3E+05	1.5E+05	19.2	**<0.001**	1.8E+06	1.8E+06	240.1	**<0.001**	2.3E+05	4.6E+04	6.1	**<0.001**
lh_parstriangularis_area	1.1E+06	2.1E+05	6.1	**<0.001**	6.8E+06	6.8E+06	193.5	**<0.001**	9.4E+05	1.9E+05	5.4	**<0.001**
lh_pericalcarine_area	2.7E+06	5.4E+05	8.2	**<0.001**	3.7E+06	3.7E+06	56.6	**<0.001**	1.2E+06	2.5E+05	3.8	**0.002**
lh_postcentral_area	1.5E+07	2.9E+06	15.5	**<0.001**	6.7E+07	6.7E+07	357.6	**<0.001**	6.1E+06	1.2E+06	6.5	**<0.001**
lh_posteriorcingulate_area	3.5E+06	6.9E+05	25.2	**<0.001**	5.7E+06	5.7E+06	208.2	**<0.001**	8.1E+05	1.6E+05	5.9	**<0.001**
lh_precentral_area	3.6E+07	7.1E+06	28.9	**<0.001**	9.4E+07	9.4E+07	381.1	**<0.001**	7.9E+06	1.6E+06	6.4	**<0.001**
lh_precuneus_area	2.6E+07	5.3E+06	27.6	**<0.001**	5.3E+07	5.3E+07	279.8	**<0.001**	6.5E+06	1.3E+06	6.9	**<0.001**
lh_rostralanteriorcingulate_area	2.0E+06	4.0E+05	13.7	**<0.001**	5.8E+06	5.8E+06	200.1	**<0.001**	6.9E+05	1.4E+05	4.8	**<0.001**
lh_rostralmiddlefrontal_area	4.3E+07	8.6E+06	14.5	**<0.001**	2.0E+08	2.0E+08	330.5	**<0.001**	1.8E+07	3.6E+06	6.1	**<0.001**
lh_superiorfrontal_area	8.4E+07	1.7E+07	23.2	**<0.001**	2.4E+08	2.4E+08	329.6	**<0.001**	2.4E+07	4.8E+06	6.5	**<0.001**
lh_superiorparietal_area	2.5E+07	4.9E+06	12.2	**<0.001**	7.8E+07	7.8E+07	194.3	**<0.001**	7.2E+06	1.4E+06	3.6	**0.003**
lh_superiortemporal_area	1.9E+07	3.7E+06	20.3	**<0.001**	6.4E+07	6.4E+07	351.5	**<0.001**	8.1E+06	1.6E+06	8.8	**<0.001**
lh_supramarginal_area	2.0E+07	3.9E+06	11.3	**<0.001**	1.1E+08	1.1E+08	304.2	**<0.001**	1.5E+07	2.9E+06	8.4	**<0.001**
lh_frontalpole_area	1.8E+04	3.6E+03	3.7	**0.002**	1.8E+05	1.8E+05	192.2	**<0.001**	1.5E+04	3.0E+03	3.1	**0.008**
lh_temporalpole_area	4.2E+05	8.3E+04	20.9	**<0.001**	8.1E+05	8.1E+05	202.2	**<0.001**	1.1E+05	2.3E+04	5.7	**<0.001**
lh_transversetemporal_area	2.8E+05	5.5E+04	11.6	**<0.001**	7.4E+05	7.4E+05	156.7	**<0.001**	8.4E+04	1.7E+04	3.6	**0.003**
lh_insula_area	1.3E+07	2.7E+06	37.0	**<0.001**	2.3E+07	2.3E+07	317.7	**<0.001**	1.7E+06	3.4E+05	4.7	**<0.001**

Table 13: Results of MANCOVAs comparing the DG to patient groups for CTSD regions

	Group				Gender				Ineteraction: Group & Gender			
Depedent variable CTSD DG	Sum of squares	Mean square	F	P	Sum of squares	Mean square	F	P	Sum of squares	Mean square	F	P
rh_bankssts_thicknessstd	0.59	0.12	25.3	**<0.001**	0.05	0.05	10.2	**0.001**	0.01	0.00	0.5	0.773
rh_caudalanteriorcingulate_thicknessstd	0.86	0.17	9.7	**<0.001**	0.23	0.23	13.2	**<0.001**	0.10	0.02	1.1	0.351
rh_caudalmiddlefrontal_thicknessstd	0.57	0.11	21.5	**<0.001**	0.00	0.00	0.2	0.665	0.10	0.02	3.8	**0.002**
rh_cuneus_thicknessstd	0.93	0.19	39.1	**<0.001**	0.00	0.00	0.4	0.505	0.05	0.01	2.1	0.068
rh_entorhinal_thicknessstd	1.58	0.32	15.6	**<0.001**	0.61	0.61	30.1	**<0.001**	0.01	0.00	0.1	0.983
rh_fusiform_thicknessstd	1.33	0.27	61.0	**<0.001**	0.08	0.08	18.0	**<0.001**	0.02	0.00	0.8	0.528
rh_inferiorparietal_thicknessstd	1.75	0.35	77.1	**<0.001**	0.00	0.00	0.0	0.866	0.04	0.01	1.7	0.14
rh_inferiortemporal_thicknessstd	2.16	0.43	86.0	**<0.001**	0.04	0.04	7.1	**0.008**	0.02	0.00	0.8	0.548
rh_isthmuscingulate_thicknessstd	0.98	0.20	20.1	**<0.001**	0.53	0.53	54.4	**<0.001**	0.04	0.01	0.9	0.469
rh_lateraloccipital_thicknessstd	1.47	0.29	71.0	**<0.001**	0.13	0.13	31.0	**<0.001**	0.05	0.01	2.4	**0.037**
rh_lateralorbitofrontal_thicknessstd	0.92	0.18	22.9	**<0.001**	0.00	0.00	0.3	0.562	0.02	0.00	0.5	0.81
rh_lingual_thicknessstd	0.62	0.12	36.1	**<0.001**	0.04	0.04	12.0	**<0.001**	0.04	0.01	2.1	0.065
rh_medialorbitofrontal_thicknessstd	1.34	0.27	31.7	**<0.001**	0.00	0.00	0.0	0.980	0.02	0.00	0.4	0.851
rh_middletemporal_thicknessstd	2.05	0.41	75.4	**<0.001**	0.02	0.02	3.1	0.079	0.07	0.01	2.4	**0.034**
rh_parahippocampal_thicknessstd	2.47	0.49	37.2	**<0.001**	0.04	0.04	3.4	0.066	0.07	0.01	1.0	0.402
rh_paracentral_thicknessstd	1.66	0.33	80.9	**<0.001**	0.02	0.02	4.0	**0.046**	0.01	0.00	0.5	0.752
rh_parsopercularis_thicknessstd	0.23	0.05	8.4	**<0.001**	0.01	0.01	1.7	0.192	0.02	0.00	0.6	0.681
rh_parsorbitalis_thicknessstd	0.90	0.18	21.5	**<0.001**	0.02	0.02	2.2	0.135	0.08	0.02	1.8	0.111
rh_parstriangularis_thicknessstd	0.44	0.09	14.8	**<0.001**	0.00	0.00	0.4	0.554	0.02	0.00	0.8	0.525
rh_pericalcarine_thicknessstd	0.20	0.04	8.2	**<0.001**	0.01	0.01	3.0	0.083	0.02	0.00	0.8	0.557
rh_postcentral_thicknessstd	1.38	0.28	66.8	**<0.001**	0.00	0.00	0.9	0.347	0.07	0.01	3.6	**0.003**
rh_posteriorcingulate_thicknessstd	0.13	0.03	1.5	0.19	0.66	0.66	38.8	**<0.001**	0.02	0.00	0.2	0.954
rh_precentral_thicknessstd	1.16	0.23	51.1	**<0.001**	0.00	0.00	0.0	0.853	0.08	0.02	3.5	**0.004**
rh_precuneus_thicknessstd	1.47	0.29	100.0	**<0.001**	0.00	0.00	0.3	0.596	0.02	0.00	1.4	0.204
rh_rostralanteriorcingulate_thicknessstd	3.92	0.78	42.4	**<0.001**	0.44	0.44	23.6	**<0.001**	0.11	0.02	1.2	0.33
rh_rostralmiddlefrontal_thicknessstd	0.22	0.04	10.1	**<0.001**	0.01	0.01	1.7	0.192	0.09	0.02	4.3	**<0.001**
rh_superiorfrontal_thicknessstd	0.64	0.13	31.7	**<0.001**	0.01	0.01	3.6	0.059	0.02	0.00	1.2	0.325
rh_superiorparietal_thicknessstd	1.59	0.32	69.1	**<0.001**	0.00	0.00	0.6	**0.430**	0.03	0.01	1.3	0.246
rh_superiortemporal_thicknessstd	1.51	0.30	64.5	**<0.001**	0.03	0.03	5.6	**0.018**	0.01	0.00	0.6	0.682
rh_supramarginal_thicknessstd	1.35	0.27	60.9	**<0.001**	0.00	0.00	0.1	0.726	0.04	0.01	1.6	0.159
rh_frontalpole_thicknessstd	0.47	0.09	8.1	**<0.001**	0.04	0.04	3.2	0.072	0.04	0.01	0.7	0.597
rh_temporalpole_thicknessstd	0.71	0.14	6.9	**<0.001**	0.18	0.18	8.6	**0.003**	0.04	0.01	0.4	0.866
rh_transversetemporal_thicknessstd	0.30	0.06	10.6	**<0.001**	0.09	0.09	15.9	**<0.001**	0.06	0.01	1.9	0.084
rh_insula_thicknessstd	1.10	0.22	25.7	**<0.001**	0.11	0.11	12.8	**<0.001**	0.04	0.01	0.9	0.494
lh_bankssts_thicknessstd	0.65	0.13	25.6	**<0.001**	0.00	0.00	0.7	0.388	0.01	0.00	0.6	0.726
lh_caudalanteriorcingulate_thicknessstd	1.60	0.32	15.6	**<0.001**	0.36	0.36	17.6	**<0.001**	0.09	0.02	0.9	0.498
lh_caudalmiddlefrontal_thicknessstd	0.90	0.18	35.4	**<0.001**	0.00	0.00	0.2	0.662	0.08	0.02	3.2	**0.007**
lh_cuneus_thicknessstd	0.34	0.07	16.3	**<0.001**	0.01	0.01	1.7	0.192	0.04	0.01	1.9	0.095
lh_entorhinal_thicknessstd	1.69	0.34	22.6	**<0.001**	0.49	0.49	32.5	**<0.001**	0.13	0.03	1.8	0.118
lh_fusiform_thicknessstd	1.14	0.23	53.0	**<0.001**	0.09	0.09	20.3	**<0.001**	0.02	0.00	0.9	0.506
lh_inferiorparietal_thicknessstd	1.69	0.34	79.0	**<0.001**	0.00	0.00	0.3	0.611	0.03	0.01	1.4	0.207
lh_inferiortemporal_thicknessstd	1.77	0.35	66.5	**<0.001**	0.05	0.05	9.1	**0.003**	0.02	0.00	0.7	0.631
lh_isthmuscingulate_thicknessstd	0.86	0.17	22.0	**<0.001**	0.32	0.32	41.4	**<0.001**	0.04	0.01	1.1	0.363
lh_lateraloccipital_thicknessstd	1.38	0.28	67.7	**<0.001**	0.05	0.05	12.0	**<0.001**	0.02	0.00	0.8	0.54
lh_lateralorbitofrontal_thicknessstd	2.41	0.48	81.1	**<0.001**	0.00	0.00	0.7	0.395	0.04	0.01	1.3	0.265
lh_lingual_thicknessstd	0.24	0.05	14.6	**<0.001**	0.06	0.06	16.9	**<0.001**	0.04	0.01	2.7	**0.02**
lh_medialorbitofrontal_thicknessstd	1.47	0.29	47.4	**<0.001**	0.02	0.02	3.1	0.077	0.01	0.00	0.4	0.844
lh_middletemporal_thicknessstd	1.92	0.38	78.1	**<0.001**	0.03	0.03	6.2	**0.013**	0.05	0.01	1.9	0.099
lh_parahippocampal_thicknessstd	2.02	0.40	31.7	**<0.001**	0.00	0.00	0.2	0.682	0.01	0.00	0.1	0.995
lh_paracentral_thicknessstd	1.47	0.29	59.6	**<0.001**	0.00	0.00	0.6	0.452	0.03	0.01	1.4	0.233
lh_parsopercularis_thicknessstd	0.35	0.07	14.4	**<0.001**	0.00	0.00	0.7	0.403	0.03	0.01	1.2	0.286
lh_parsorbitalis_thicknessstd	1.34	0.27	29.2	**<0.001**	0.01	0.01	1.6	0.209	0.03	0.01	0.7	0.626
lh_parstriangularis_thicknessstd	1.07	0.21	39.4	**<0.001**	0.00	0.00	0.2	0.620	0.02	0.00	0.6	0.697
lh_pericalcarine_thicknessstd	0.09	0.02	3.6	**0.003**	0.02	0.02	3.9	**0.049**	0.01	0.00	0.3	0.914
lh_postcentral_thicknessstd	1.78	0.36	84.3	**<0.001**	0.00	0.00	1.0	0.309	0.06	0.01	3.0	**0.01**
lh_posteriorcingulate_thicknessstd	0.20	0.04	3.1	**0.008**	0.25	0.25	19.8	**<0.001**	0.04	0.01	0.6	0.709
lh_precentral_thicknessstd	1.15	0.23	51.2	**<0.001**	0.00	0.00	1.0	0.315	0.07	0.01	3.0	**0.01**
lh_precuneus_thicknessstd	1.37	0.27	91.1	**<0.001**	0.00	0.00	0.4	0.516	0.03	0.01	1.7	0.136
lh_rostralanteriorcingulate_thicknessstd	4.52	0.90	40.2	**<0.001**	0.85	0.85	37.7	**<0.001**	0.07	0.01	0.6	0.674
lh_rostralmiddlefrontal_thicknessstd	0.45	0.09	20.6	**<0.001**	0.02	0.02	4.8	**0.028**	0.06	0.01	2.8	**0.015**
lh_superiorfrontal_thicknessstd	0.64	0.13	30.1	**<0.001**	0.01	0.01	1.7	0.195	0.03	0.01	1.6	0.155
lh_superiorparietal_thicknessstd	1.57	0.31	74.3	**<0.001**	0.00	0.00	0.7	0.393	0.03	0.01	1.4	0.235
lh_superiortemporal_thicknessstd	1.95	0.39	86.0	**<0.001**	0.03	0.03	6.6	**0.010**	0.01	0.00	0.3	0.927
lh_supramarginal_thicknessstd	1.48	0.30	72.0	**<0.001**	0.00	0.00	0.2	0.643	0.02	0.00	0.8	0.53
lh_frontalpole_thicknessstd	0.61	0.12	9.5	**<0.001**	0.01	0.01	0.5	0.496	0.07	0.01	1.2	0.33
lh_temporalpole_thicknessstd	0.94	0.19	9.5	**<0.001**	0.07	0.07	3.4	0.065	0.13	0.03	1.3	0.252
lh_transversetemporal_thicknessstd	0.38	0.08	15.4	**<0.001**	0.04	0.04	8.8	**0.003**	0.03	0.01	1.2	0.3
lh_insula_thicknessstd	0.69	0.14	11.5	**<0.001**	0.02	0.02	1.8	0.185	0.10	0.02	1.6	0.154

Table 14: Results of MANCOVAs comparing the RG to patient groups for CT regions

Dependent variable CT RG	Group				Gender				Ineteraction: Group & Gender			
	Sum of squares	Mean square	F	P	Sum of squares	Mean square	F	P	Sum of squares	Mean square	F	P
rh_bankssts_thickness	3.8	0.76	23.7	**<0.001**	0.2	0.21	6.4	**0.011**	0.4	0.08	2.5	**0.028**
rh_caudalanteriorcingulate_thickness	8.9	1.79	26.9	**<0.001**	1.2	1.15	17.3	**<0.001**	0.9	0.17	2.6	**0.025**
rh_caudalmiddlefrontal_thickness	7.6	1.52	57.2	**<0.001**	0.8	0.82	30.6	**<0.001**	0.1	0.02	0.7	0.614
rh_cuneus_thickness	6.6	1.33	68.2	**<0.001**	0.0	0.02	1.1	0.288	0.3	0.05	2.6	**0.025**
rh_entorhinal_thickness	58.5	11.70	58.6	**<0.001**	0.7	0.71	3.6	0.059	1.0	0.19	1.0	0.435
rh_fusiform_thickness	2.6	0.52	16.8	**<0.001**	0.1	0.09	2.8	0.096	0.3	0.05	1.8	0.119
rh_inferiorparietal_thickness	9.6	1.92	89.4	**<0.001**	0.6	0.61	28.6	**<0.001**	0.3	0.06	2.9	**0.013**
rh_inferiortemporal_thickness	7.6	1.52	52.2	**<0.001**	0.0	0.02	0.5	0.46	0.1	0.02	0.6	0.713
rh_isthmuscingulate_thickness	5.3	1.05	24.2	**<0.001**	0.4	0.42	9.6	**0.002**	0.5	0.10	2.4	**0.036**
rh_lateraloccipital_thickness	3.1	0.61	31.9	**<0.001**	0.1	0.11	5.8	**0.016**	0.2	0.05	2.5	**0.026**
rh_lateralorbitofrontal_thickness	13.4	2.68	110.5	**<0.001**	0.3	0.25	10.4	**0.001**	0.1	0.03	1.0	0.39
rh_lingual_thickness	5.3	1.07	61.3	**<0.001**	0.0	0.00	0.0	0.97	0.1	0.02	1.2	0.294
rh_medialorbitofrontal_thickness	10.2	2.03	72.7	**<0.001**	0.0	0.01	0.4	0.55	0.2	0.03	1.2	0.322
rh_middletemporal_thickness	12.8	2.56	87.1	**<0.001**	0.0	0.04	1.3	0.254	0.2	0.03	1.1	0.333
rh_parahippocampal_thickness	4.8	0.97	12.6	**<0.001**	2.3	2.32	30.3	**<0.001**	0.2	0.05	0.6	0.671
rh_paracentral_thickness	1.9	0.39	12.8	**<0.001**	0.4	0.40	13.2	**<0.001**	0.1	0.03	0.8	0.515
rh_parsopercularis_thickness	4.4	0.88	36.0	**<0.001**	0.0	0.02	0.7	0.419	0.1	0.02	1.0	0.444
rh_parsorbitalis_thickness	15.0	2.99	79.6	**<0.001**	1.5	1.53	40.7	**<0.001**	0.5	0.11	2.8	**0.015**
rh_parstriangularis_thickness	5.5	1.11	51.7	**<0.001**	0.2	0.22	10.4	**0.001**	0.1	0.03	1.4	0.224
rh_pericalcarine_thickness	14.2	2.83	138.1	**<0.001**	0.1	0.07	3.6	0.059	0.1	0.01	0.6	0.718
rh_postcentral_thickness	5.4	1.08	60.4	**<0.001**	0.3	0.28	15.7	**<0.001**	0.2	0.04	2.2	0.053
rh_posteriorcingulate_thickness	5.9	1.18	40.9	**<0.001**	0.5	0.54	18.6	**<0.001**	0.3	0.06	2.0	0.079
rh_precentral_thickness	1.4	0.29	9.4	**<0.001**	0.9	0.90	29.8	**<0.001**	0.1	0.03	0.9	0.453
rh_precuneus_thickness	4.9	0.98	47.4	**<0.001**	0.1	0.08	4.1	**0.043**	0.2	0.04	2.0	0.069
rh_rostralanteriorcingulate_thickness	10.9	2.18	31.7	**<0.001**	0.0	0.01	0.1	0.78	0.2	0.03	0.5	0.793
rh_rostralmiddlefrontal_thickness	8.1	1.62	98.1	**<0.001**	0.2	0.22	13.0	**<0.001**	0.2	0.05	2.9	**0.012**
rh_superiorfrontal_thickness	10.8	2.17	92.4	**<0.001**	0.8	0.83	35.5	**<0.001**	0.2	0.03	1.3	0.252
rh_superiorparietal_thickness	5.6	1.12	56.7	**<0.001**	0.3	0.26	13.4	**<0.001**	0.2	0.03	1.5	0.172
rh_superiortemporal_thickness	8.5	1.70	60.5	**<0.001**	0.1	0.10	3.4	0.064	0.1	0.02	0.6	0.688
rh_supramarginal_thickness	6.2	1.25	54.0	**<0.001**	0.4	0.41	17.6	**<0.001**	0.1	0.03	1.2	0.302
rh_frontalpole_thickness	11.6	2.32	35.8	**<0.001**	1.0	0.97	15.0	**<0.001**	0.5	0.09	1.4	0.222
rh_temporalpole_thickness	57.0	11.40	66.4	**<0.001**	0.3	0.34	2.0	0.16	0.5	0.10	0.6	0.699
rh_transversetemporal_thickness	3.0	0.60	10.4	**<0.001**	0.9	0.89	15.5	**<0.001**	0.4	0.07	1.3	0.278
rh_insula_thickness	13.1	2.62	67.1	**<0.001**	0.2	0.17	4.5	**0.035**	0.1	0.03	0.6	0.665
lh_bankssts_thickness	4.5	0.90	29.9	**<0.001**	0.1	0.11	3.8	0.053	0.4	0.07	2.5	**0.03**
lh_caudalanteriorcingulate_thickness	16.2	3.23	41.3	**<0.001**	1.9	1.94	24.8	**<0.001**	0.7	0.14	1.8	0.11
lh_caudalmiddlefrontal_thickness	8.6	1.71	55.7	**<0.001**	0.8	0.78	25.5	**<0.001**	0.1	0.02	0.7	0.608
lh_cuneus_thickness	8.6	1.72	94.4	**<0.001**	0.0	0.00	0.0	0.986	0.1	0.02	0.8	0.526
lh_entorhinal_thickness	64.0	12.79	68.5	**<0.001**	0.1	0.08	0.4	0.508	0.6	0.12	0.7	0.648
lh_fusiform_thickness	5.7	1.13	37.9	**<0.001**	0.3	0.26	8.9	**0.003**	0.2	0.05	1.7	0.14
lh_inferiorparietal_thickness	9.2	1.84	92.4	**<0.001**	0.8	0.75	37.8	**<0.001**	0.3	0.05	2.6	**0.026**
lh_inferiortemporal_thickness	12.3	2.46	81.1	**<0.001**	0.2	0.20	6.6	**0.01**	0.1	0.03	0.9	0.504
lh_isthmuscingulate_thickness	7.0	1.39	29.3	**<0.001**	0.5	0.50	10.4	**0.001**	0.4	0.08	1.6	0.149
lh_lateraloccipital_thickness	3.5	0.69	39.5	**<0.001**	0.2	0.23	12.9	**<0.001**	0.2	0.04	2.3	**0.044**
lh_lateralorbitofrontal_thickness	9.7	1.93	83.2	**<0.001**	0.1	0.11	4.9	**0.027**	0.2	0.03	1.5	0.203
lh_lingual_thickness	8.3	1.66	104.6	**<0.001**	0.0	0.04	2.6	0.107	0.1	0.03	1.6	0.151
lh_medialorbitofrontal_thickness	6.3	1.26	46.7	**<0.001**	0.0	0.00	0.0	0.988	0.0	0.01	0.2	0.942
lh_middletemporal_thickness	17.9	3.57	110.2	**<0.001**	0.1	0.05	1.6	0.201	0.3	0.06	1.8	0.106
lh_parahippocampal_thickness	15.1	3.02	29.3	**<0.001**	3.0	2.99	29.1	**<0.001**	0.4	0.07	0.7	0.604
lh_paracentral_thickness	1.2	0.24	8.2	**<0.001**	0.2	0.20	6.7	**0.01**	0.1	0.02	0.7	0.627
lh_parsopercularis_thickness	4.0	0.80	32.3	**<0.001**	0.1	0.12	4.8	**0.028**	0.1	0.02	1.0	0.414
lh_parsorbitalis_thickness	14.0	2.80	66.0	**<0.001**	1.6	1.57	37.0	**<0.001**	0.3	0.06	1.4	0.223
lh_parstriangularis_thickness	5.8	1.17	49.1	**<0.001**	0.5	0.53	22.3	**<0.001**	0.2	0.03	1.4	0.235
lh_pericalcarine_thickness	14.0	2.81	153.9	**<0.001**	0.0	0.01	0.8	0.375	0.1	0.01	0.6	0.665
lh_postcentral_thickness	3.9	0.78	47.0	**<0.001**	0.4	0.43	26.2	**<0.001**	0.1	0.03	1.6	0.171
lh_posteriorcingulate_thickness	6.1	1.22	42.4	**<0.001**	0.7	0.69	24.1	**<0.001**	0.4	0.08	2.7	**0.019**
lh_precentral_thickness	1.8	0.35	12.1	**<0.001**	0.7	0.67	23.2	**<0.001**	0.2	0.04	1.3	0.28
lh_precuneus_thickness	6.5	1.29	56.0	**<0.001**	0.2	0.18	7.9	**0.005**	0.2	0.04	1.7	0.136
lh_rostralanteriorcingulate_thickness	18.5	3.70	60.1	**<0.001**	2.1	2.08	33.7	**<0.001**	0.3	0.05	0.8	0.537
lh_rostralmiddlefrontal_thickness	8.6	1.72	91.2	**<0.001**	0.4	0.40	21.4	**<0.001**	0.2	0.03	1.6	0.151
lh_superiorfrontal_thickness	12.7	2.55	98.4	**<0.001**	1.3	1.28	49.3	**<0.001**	0.2	0.03	1.2	0.286
lh_superiorparietal_thickness	5.5	1.10	54.3	**<0.001**	0.3	0.29	14.2	**<0.001**	0.2	0.04	2.0	0.074
lh_superiortemporal_thickness	10.1	2.03	66.1	**<0.001**	0.3	0.28	9.3	**0.002**	0.2	0.04	1.4	0.209
lh_supramarginal_thickness	7.1	1.42	66.7	**<0.001**	0.6	0.61	28.5	**<0.001**	0.2	0.04	1.7	0.121
lh_frontalpole_thickness	12.8	2.55	38.8	**<0.001**	1.8	1.78	27.1	**<0.001**	0.2	0.03	0.5	0.78
lh_temporalpole_thickness	51.3	10.25	65.9	**<0.001**	1.3	1.29	8.3	**0.004**	0.5	0.10	0.6	0.683
lh_transversetemporal_thickness	3.7	0.75	15.0	**<0.001**	1.2	1.17	23.5	**<0.001**	0.2	0.04	0.8	0.559
lh_insula_thickness	11.3	2.27	56.4	**<0.001**	0.0	0.05	1.1	0.289	0.2	0.03	0.8	0.531

Table 15: Results of MANCOVAs comparing the RG to patient groups for CVol regions

Dependent variable CVol RG	Group				Gender				Ineteraction: Group & Gender			
	Sum of squares	Mean square	F	P	Sum of squares	Mean square	F	P	Sum of squares	Mean square	F	P
rh_bankssts_volume	2.3E+07	4.7E+06	40.0	**<0.001**	8.1E+06	8.1E+06	69.3	**<0.001**	3.0E+06	5.9E+05	5.1	**<0.001**
rh_caudalanteriorcingulate_volume	1.3E+07	2.6E+06	13.4	**<0.001**	8.7E+06	8.7E+06	43.9	**<0.001**	9.7E+05	1.9E+05	1.0	0.426
rh_caudalmiddlefrontal_volume	1.5E+08	3.0E+07	29.4	**<0.001**	8.6E+07	8.6E+07	85.7	**<0.001**	1.9E+07	3.8E+06	3.8	**0.002**
rh_cuneus_volume	1.1E+08	2.2E+07	75.5	**<0.001**	3.7E+07	3.7E+07	128.1	**<0.001**	1.0E+07	2.0E+06	6.9	**<0.001**
rh_entorhinal_volume	4.2E+07	8.4E+06	51.3	**<0.001**	1.6E+07	1.6E+07	97.2	**<0.001**	4.8E+06	9.5E+05	5.8	**<0.001**
rh_fusiform_volume	1.7E+08	3.5E+07	21.5	**<0.001**	4.2E+08	4.2E+08	259.1	**<0.001**	6.2E+07	1.2E+07	7.7	**<0.001**
rh_inferiorparietal_volume	9.3E+08	1.9E+08	49.5	**<0.001**	8.0E+08	8.0E+08	214.1	**<0.001**	1.1E+08	2.2E+07	5.8	**<0.001**
rh_inferiortemporal_volume	5.7E+08	1.2E+08	45.8	**<0.001**	5.0E+08	5.0E+08	197.5	**<0.001**	7.8E+07	1.6E+07	6.3	**<0.001**
rh_isthmuscingulate_volume	1.7E+07	3.4E+06	23.6	**<0.001**	2.4E+07	2.4E+07	162.9	**<0.001**	5.4E+06	1.1E+06	7.4	**<0.001**
rh_lateraloccipital_volume	1.3E+09	2.6E+08	100.7	**<0.001**	7.1E+08	7.1E+08	274.3	**<0.001**	1.7E+08	3.3E+07	12.7	**<0.001**
rh_lateralorbitofrontal_volume	2.9E+08	5.9E+07	90.2	**<0.001**	1.2E+08	1.2E+08	176.7	**<0.001**	1.7E+07	3.4E+06	5.3	**<0.001**
rh_lingual_volume	2.8E+08	5.5E+07	53.5	**<0.001**	1.8E+08	1.8E+08	168.8	**<0.001**	2.5E+07	5.0E+06	4.8	**<0.001**
rh_medialorbitofrontal_volume	2.2E+08	4.3E+07	117.7	**<0.001**	8.1E+07	8.1E+07	219.2	**<0.001**	7.1E+06	1.4E+06	3.8	**0.002**
rh_middletemporal_volume	6.9E+08	1.4E+08	60.5	**<0.001**	4.5E+08	4.5E+08	198.0	**<0.001**	4.6E+07	9.3E+06	4.1	**0.001**
rh_parahippocampal_volume	8.3E+06	1.7E+06	19.9	**<0.001**	7.4E+06	7.4E+06	88.0	**<0.001**	1.2E+06	2.3E+05	2.8	**0.017**
rh_paracentral_volume	2.5E+07	4.9E+06	16.9	**<0.001**	2.5E+07	2.5E+07	84.4	**<0.001**	4.1E+06	8.3E+05	2.8	**0.015**
rh_parsopercularis_volume	2.4E+07	4.7E+06	13.2	**<0.001**	2.4E+07	2.4E+07	66.1	**<0.001**	6.4E+06	1.3E+06	3.6	**0.003**
rh_parsorbitalis_volume	5.0E+07	9.9E+06	73.9	**<0.001**	1.3E+07	1.3E+07	92.9	**<0.001**	9.1E+05	1.8E+05	1.4	0.236
rh_parstriangularis_volume	4.9E+07	9.8E+06	27.5	**<0.001**	4.4E+07	4.4E+07	123.3	**<0.001**	3.5E+06	7.0E+05	2.0	0.081
rh_pericalcarine_volume	5.0E+07	9.9E+06	46.0	**<0.001**	1.9E+07	1.9E+07	89.9	**<0.001**	5.0E+06	9.9E+05	4.6	**<0.001**
rh_postcentral_volume	2.2E+08	4.3E+07	31.3	**<0.001**	1.8E+08	1.8E+08	133.1	**<0.001**	1.5E+07	2.9E+06	2.1	0.06
rh_posteriorcingulate_volume	1.9E+07	3.9E+06	16.8	**<0.001**	2.4E+07	2.4E+07	104.5	**<0.001**	4.9E+06	9.7E+05	4.2	**<0.001**
rh_precentral_volume	2.4E+08	4.7E+07	19.0	**<0.001**	4.2E+08	4.2E+08	167.0	**<0.001**	5.4E+07	1.1E+07	4.3	**<0.001**
rh_precuneus_volume	3.1E+08	6.3E+07	44.8	**<0.001**	3.1E+08	3.1E+08	220.6	**<0.001**	6.7E+07	1.3E+07	9.5	**<0.001**
rh_rostralanteriorcingulate_volume	4.6E+06	9.2E+05	5.5	**<0.001**	1.7E+07	1.7E+07	100.1	**<0.001**	2.4E+06	4.7E+05	2.8	**0.015**
rh_rostralmiddlefrontal_volume	7.2E+08	1.5E+08	38.5	**<0.001**	1.0E+09	1.0E+09	273.9	**<0.001**	6.5E+07	1.3E+07	3.5	**0.004**
rh_superiorfrontal_volume	1.2E+09	2.5E+08	40.2	**<0.001**	1.1E+09	1.1E+09	187.6	**<0.001**	2.4E+08	4.8E+07	7.8	**<0.001**
rh_superiorparietal_volume	4.8E+08	9.7E+07	38.0	**<0.001**	3.2E+08	3.2E+08	125.3	**<0.001**	6.9E+07	1.4E+07	5.5	**<0.001**
rh_superiortemporal_volume	3.3E+08	6.6E+07	36.8	**<0.001**	2.3E+08	2.3E+08	128.6	**<0.001**	3.3E+07	6.6E+06	3.7	**0.003**
rh_supramarginal_volume	1.8E+08	3.6E+07	19.9	**<0.001**	2.5E+08	2.5E+08	137.8	**<0.001**	4.9E+07	9.8E+06	5.5	**<0.001**
rh_frontalpole_volume	7.7E+06	1.5E+06	47.9	**<0.001**	1.8E+06	1.8E+06	57.7	**<0.001**	4.7E+05	9.4E+04	2.9	**0.012**
rh_temporalpole_volume	4.6E+07	9.3E+06	53.9	**<0.001**	4.9E+06	4.9E+06	28.5	**<0.001**	1.2E+06	2.4E+05	1.4	0.231
rh_transversetemporal_volume	1.5E+06	3.0E+05	12.0	**<0.001**	1.0E+06	1.0E+06	40.7	**<0.001**	4.6E+05	9.2E+04	3.7	**0.003**
rh_insula_volume	1.5E+08	2.9E+07	42.2	**<0.001**	2.1E+08	2.1E+08	305.4	**<0.001**	1.6E+07	3.2E+06	4.7	**<0.001**
lh_bankssts_volume	2.4E+07	4.8E+06	28.2	**<0.001**	1.3E+07	1.3E+07	76.5	**<0.001**	3.4E+06	6.8E+05	4.0	**0.001**
lh_caudalanteriorcingulate_volume	2.0E+07	4.1E+06	21.4	**<0.001**	5.8E+06	5.8E+06	30.4	**<0.001**	1.4E+06	2.8E+05	1.5	0.197
lh_caudalmiddlefrontal_volume	1.2E+08	2.4E+07	23.8	**<0.001**	7.7E+07	7.7E+07	76.1	**<0.001**	1.9E+07	3.7E+06	3.7	**0.003**
lh_cuneus_volume	7.7E+07	1.5E+07	63.9	**<0.001**	3.1E+07	3.1E+07	130.0	**<0.001**	6.3E+06	1.3E+06	5.3	**<0.001**
lh_entorhinal_volume	7.8E+07	1.6E+07	87.8	**<0.001**	1.8E+07	1.8E+07	99.4	**<0.001**	6.0E+06	1.2E+06	6.8	**<0.001**
lh_fusiform_volume	1.8E+08	3.7E+07	22.3	**<0.001**	3.6E+08	3.6E+08	215.4	**<0.001**	5.7E+07	1.1E+07	6.9	**<0.001**
lh_inferiorparietal_volume	5.6E+08	1.1E+08	43.0	**<0.001**	3.6E+08	3.6E+08	137.9	**<0.001**	5.1E+07	1.0E+07	4.0	**0.001**
lh_inferiortemporal_volume	9.4E+08	1.9E+08	71.0	**<0.001**	4.4E+08	4.4E+08	167.4	**<0.001**	4.2E+07	8.4E+06	3.2	**0.007**
lh_isthmuscingulate_volume	1.5E+07	2.9E+06	17.7	**<0.001**	4.4E+07	4.4E+07	270.6	**<0.001**	8.7E+06	1.7E+06	10.7	**<0.001**
lh_lateraloccipital_volume	8.4E+08	1.7E+08	75.8	**<0.001**	4.8E+08	4.8E+08	216.3	**<0.001**	1.3E+08	2.6E+07	11.9	**<0.001**
lh_lateralorbitofrontal_volume	2.1E+08	4.2E+07	59.8	**<0.001**	1.2E+08	1.2E+08	175.3	**<0.001**	1.5E+07	2.9E+06	4.1	**0.001**
lh_lingual_volume	1.8E+08	3.7E+07	38.8	**<0.001**	1.6E+08	1.6E+08	171.4	**<0.001**	3.2E+07	6.4E+06	6.8	**<0.001**
lh_medialorbitofrontal_volume	9.5E+07	1.9E+07	44.7	**<0.001**	1.2E+08	1.2E+08	276.0	**<0.001**	1.2E+07	2.3E+06	5.5	**<0.001**
lh_middletemporal_volume	8.2E+08	1.6E+08	71.1	**<0.001**	4.4E+08	4.4E+08	190.9	**<0.001**	6.2E+07	1.2E+07	5.4	**<0.001**
lh_parahippocampal_volume	1.7E+07	3.5E+06	31.8	**<0.001**	5.2E+06	5.2E+06	47.4	**<0.001**	3.9E+06	7.8E+05	7.1	**<0.001**
lh_paracentral_volume	2.6E+07	5.2E+06	25.3	**<0.001**	2.2E+07	2.2E+07	105.5	**<0.001**	1.6E+06	3.1E+05	1.5	0.179
lh_parsopercularis_volume	4.0E+07	8.0E+06	15.1	**<0.001**	3.7E+07	3.7E+07	70.3	**<0.001**	9.0E+06	1.8E+06	3.4	**0.005**
lh_parsorbitalis_volume	5.2E+07	1.0E+07	105.3	**<0.001**	8.5E+06	8.5E+06	86.7	**<0.001**	1.3E+06	2.6E+05	2.6	**0.024**
lh_parstriangularis_volume	3.9E+07	7.8E+06	28.4	**<0.001**	2.4E+07	2.4E+07	87.6	**<0.001**	5.3E+06	1.1E+06	3.8	**0.002**
lh_pericalcarine_volume	3.9E+07	7.8E+06	44.9	**<0.001**	1.2E+07	1.2E+07	66.9	**<0.001**	3.5E+06	7.0E+05	4.0	**0.001**
lh_postcentral_volume	2.0E+08	4.0E+07	27.5	**<0.001**	1.9E+08	1.9E+08	131.8	**<0.001**	2.8E+07	5.6E+06	3.8	**0.002**
lh_posteriorcingulate_volume	2.1E+07	4.3E+06	19.3	**<0.001**	3.2E+07	3.2E+07	142.2	**<0.001**	4.7E+06	9.4E+05	4.2	**<0.001**
lh_precentral_volume	2.1E+08	4.1E+07	18.2	**<0.001**	4.5E+08	4.5E+08	197.3	**<0.001**	7.8E+07	1.6E+07	6.8	**<0.001**
lh_precuneus_volume	3.2E+08	6.4E+07	46.8	**<0.001**	2.4E+08	2.4E+08	177.3	**<0.001**	4.5E+07	9.0E+06	6.6	**<0.001**
lh_rostralanteriorcingulate_volume	2.4E+07	4.8E+06	19.5	**<0.001**	3.2E+07	3.2E+07	130.8	**<0.001**	4.7E+06	9.4E+05	3.8	**0.002**
lh_rostralmiddlefrontal_volume	7.4E+08	1.5E+08	38.0	**<0.001**	7.9E+08	7.9E+08	202.2	**<0.001**	9.1E+07	1.8E+07	4.7	**<0.001**
lh_superiorfrontal_volume	1.5E+09	3.0E+08	48.4	**<0.001**	1.1E+09	1.1E+09	180.6	**<0.001**	2.2E+08	4.4E+07	7.0	**<0.001**
lh_superiorparietal_volume	5.1E+08	1.0E+08	37.8	**<0.001**	3.0E+08	3.0E+08	108.9	**<0.001**	4.5E+07	9.1E+06	3.3	**0.005**
lh_superiortemporal_volume	6.0E+08	1.2E+08	54.2	**<0.001**	3.2E+08	3.2E+08	143.2	**<0.001**	5.9E+07	1.2E+07	5.4	**<0.001**
lh_supramarginal_volume	4.9E+08	9.8E+07	42.6	**<0.001**	4.2E+08	4.2E+08	179.9	**<0.001**	7.4E+07	1.5E+07	6.4	**<0.001**
lh_frontalpole_volume	1.5E+07	3.0E+06	131.1	**<0.001**	9.7E+05	9.7E+05	42.4	**<0.001**	1.9E+05	3.8E+04	1.7	0.139
lh_temporalpole_volume	5.0E+07	1.0E+07	54.9	**<0.001**	6.5E+06	6.5E+06	35.5	**<0.001**	1.7E+06	3.3E+05	1.8	0.103
lh_transversetemporal_volume	2.4E+06	4.9E+05	11.5	**<0.001**	2.2E+06	2.2E+06	53.1	**<0.001**	6.5E+05	1.3E+05	3.1	**0.009**
lh_insula_volume	1.8E+08	3.5E+07	54.4	**<0.001**	1.5E+08	1.5E+08	238.9	**<0.001**	1.2E+07	2.5E+06	3.8	**0.002**

Table 16: Results of MANCOVAs comparing the RG to patient groups for SubVol regions

Dependent variable SubVol RG	Group				Gender				Ineteraction: Group & Gender			
	Sum of squares	Mean square	F	P	Sum of squares	Mean square	F	P	Sum of squares	Mean square	F	P
Left_Cerebellum_Cortex	3.0E+10	6.0E+09	244.0	**<0.001**	7.6E+09	7.6E+09	306.2	**<0.001**	7.3E+08	1.5E+08	6.0	**<0.001**
Left_Thalamus_Proper	3.9E+08	7.7E+07	123.3	**<0.001**	7.3E+07	7.3E+07	115.8	**<0.001**	2.5E+07	5.0E+06	8.0	**<0.001**
Left_Caudate	3.9E+07	7.7E+06	29.7	**<0.001**	2.5E+07	2.5E+07	94.4	**<0.001**	3.8E+06	7.6E+05	2.9	**0.012**
Left_Putamen	4.5E+08	9.0E+07	201.6	**<0.001**	5.2E+07	5.2E+07	116.8	**<0.001**	1.4E+07	2.7E+06	6.0	**<0.001**
Left_Pallidum	1.8E+08	3.6E+07	517.9	**<0.001**	1.1E+07	1.1E+07	155.2	**<0.001**	1.2E+06	2.4E+05	3.5	**0.004**
Brain_Stem	5.4E+08	1.1E+08	21.2	**<0.001**	1.7E+09	1.7E+09	342.3	**<0.001**	3.0E+08	6.0E+07	11.8	**<0.001**
Left_Hippocampus	1.0E+08	2.0E+07	93.2	**<0.001**	1.2E+07	1.2E+07	53.8	**<0.001**	4.4E+06	8.9E+05	4.1	**0.001**
Left_Amygdala	3.1E+07	6.3E+06	108.0	**<0.001**	6.7E+06	6.7E+06	115.1	**<0.001**	9.6E+05	1.9E+05	3.3	**0.006**
Left_Accumbens_area	1.0E+07	2.0E+06	184.3	**<0.001**	2.9E+05	2.9E+05	26.6	**<0.001**	2.3E+05	4.5E+04	4.1	**0.001**
Left_VentralDC	7.3E+07	1.5E+07	94.7	**<0.001**	5.0E+07	5.0E+07	324.3	**<0.001**	1.0E+07	2.0E+06	13.1	**<0.001**
Left_choroid_plexus	2.4E+08	4.9E+07	696.4	**<0.001**	1.8E+07	1.8E+07	255.3	**<0.001**	1.5E+06	3.0E+05	4.4	**<0.001**
Right_Cerebellum_Cortex	2.4E+10	4.8E+09	184.5	**<0.001**	8.6E+09	8.6E+09	328.4	**<0.001**	1.1E+09	2.2E+08	8.3	**<0.001**
Right_Thalamus_Proper	2.5E+08	5.0E+07	104.0	**<0.001**	6.8E+07	6.8E+07	141.6	**<0.001**	3.2E+07	6.5E+06	13.4	**<0.001**
Right_Caudate	5.2E+07	1.0E+07	39.3	**<0.001**	2.7E+07	2.7E+07	100.9	**<0.001**	5.2E+06	1.0E+06	3.9	**0.002**
Right_Putamen	2.1E+08	4.1E+07	91.4	**<0.001**	4.6E+07	4.6E+07	102.4	**<0.001**	1.4E+07	2.8E+06	6.3	**<0.001**
Right_Pallidum	1.4E+08	2.8E+07	429.2	**<0.001**	8.4E+06	8.4E+06	130.9	**<0.001**	5.0E+05	1.0E+05	1.6	0.171
Right_Hippocampus	9.4E+07	1.9E+07	81.2	**<0.001**	1.6E+07	1.6E+07	70.8	**<0.001**	3.7E+06	7.4E+05	3.2	**0.007**
Right_Amygdala	2.5E+07	5.0E+06	82.4	**<0.001**	1.2E+07	1.2E+07	194.6	**<0.001**	1.4E+06	2.7E+05	4.5	**<0.001**
Right_Accumbens_area	4.9E+06	9.9E+05	97.5	**<0.001**	4.8E+05	4.8E+05	47.5	**<0.001**	1.9E+05	3.9E+04	3.8	**0.002**
Right_VentralDC	5.0E+07	1.0E+07	73.1	**<0.001**	4.4E+07	4.4E+07	323.7	**<0.001**	8.2E+06	1.6E+06	12.0	**<0.001**
Right_choroid_plexus	6.9E+08	1.4E+08	1183.3	**<0.001**	3.1E+07	3.1E+07	268.8	**<0.001**	7.6E+06	1.5E+06	13.2	**<0.001**
CC_Posterior	5.3E+06	1.1E+06	34.1	**<0.001**	6.9E+05	6.9E+05	22.3	**<0.001**	1.5E+05	3.0E+04	1.0	0.433
CC_Mid_Posterior	1.3E+07	2.5E+06	202.0	**<0.001**	2.0E+04	2.0E+04	1.6	0.205	2.3E+04	4.5E+03	0.4	0.874
CC_Central	7.3E+06	1.5E+06	135.3	**<0.001**	3.0E+03	3.0E+03	0.3	0.597	5.2E+04	1.0E+04	1.0	0.441
CC_Mid_Anterior	9.5E+06	1.9E+06	149.8	**<0.001**	5.1E+04	5.1E+04	4.0	**0.045**	8.6E+04	1.7E+04	1.4	0.239
CC_Anterior	1.0E+07	2.1E+06	83.0	**<0.001**	3.3E+05	3.3E+05	13.2	**<0.001**	1.9E+05	3.8E+04	1.5	0.181

Table 17: Results of MANCOVAs comparing the RG to patient groups for SA regions

	Group				Gender				Ineteraction: Group & Gender			
Depedent variable SA RG	Sum of squares	Mean square	F	P	Sum of squares	Mean square	F	P	Sum of squares	Mean square	F	P
rh_bankssts_area	2.6E+06	5.1E+05	34.0	**<0.001**	2.0E+06	2.0E+06	130.0	**<0.001**	3.3E+05	6.6E+04	4.40	**<0.001**
rh_caudalanteriorcingulate_area	2.7E+06	5.5E+05	23.0	**<0.001**	2.0E+06	2.0E+06	83.0	**<0.001**	2.8E+05	5.6E+04	2.34	**0.039**
rh_caudalmiddlefrontal_area	1.3E+07	2.6E+06	22.0	**<0.001**	2.0E+07	2.0E+07	170.0	**<0.001**	3.3E+06	6.5E+05	5.49	**<0.001**
rh_cuneus_area	1.1E+07	2.1E+06	48.0	**<0.001**	8.9E+06	8.9E+06	200.0	**<0.001**	1.2E+06	2.3E+05	5.21	**<0.001**
rh_entorhinal_area	2.3E+06	4.5E+05	66.0	**<0.001**	9.5E+05	9.5E+05	140.0	**<0.001**	1.2E+05	2.5E+04	3.64	**0.003**
rh_fusiform_area	1.0E+07	2.1E+06	17.0	**<0.001**	4.7E+07	4.7E+07	380.0	**<0.001**	4.0E+06	8.0E+05	6.46	**<0.001**
rh_inferiorparietal_area	5.1E+07	1.0E+07	22.0	**<0.001**	1.8E+08	1.8E+08	390.0	**<0.001**	1.5E+07	3.0E+06	6.57	**<0.001**
rh_inferiortemporal_area	5.3E+07	1.1E+07	52.0	**<0.001**	4.8E+07	4.8E+07	240.0	**<0.001**	5.5E+06	1.1E+06	5.43	**<0.001**
rh_isthmuscingulate_area	3.2E+06	6.3E+05	33.0	**<0.001**	4.4E+06	4.4E+06	230.0	**<0.001**	1.0E+06	2.1E+05	11.02	**<0.001**
rh_lateraloccipital_area	1.5E+08	3.1E+07	94.0	**<0.001**	1.2E+08	1.2E+08	360.0	**<0.001**	2.0E+07	4.1E+06	12.58	**<0.001**
rh_lateralorbitofrontal_area	3.0E+07	6.1E+06	62.0	**<0.001**	1.7E+07	1.7E+07	180.0	**<0.001**	2.1E+06	4.3E+05	4.36	**<0.001**
rh_lingual_area	1.8E+07	3.6E+06	22.0	**<0.001**	3.1E+07	3.1E+07	180.0	**<0.001**	4.2E+06	8.3E+05	5.02	**<0.001**
rh_medialorbitofrontal_area	2.3E+07	4.5E+06	100.0	**<0.001**	1.1E+07	1.1E+07	240.0	**<0.001**	1.2E+06	2.4E+05	5.23	**<0.001**
rh_middletemporal_area	4.1E+07	8.3E+06	52.0	**<0.001**	4.7E+07	4.7E+07	290.0	**<0.001**	4.0E+06	8.1E+05	5.05	**<0.001**
rh_parahippocampal_area	6.1E+05	1.2E+05	19.0	**<0.001**	1.9E+06	1.9E+06	290.0	**<0.001**	1.5E+05	3.1E+04	4.75	**<0.001**
rh_paracentral_area	4.7E+06	9.4E+05	26.0	**<0.001**	6.5E+06	6.5E+06	180.0	**<0.001**	7.0E+05	1.4E+05	3.88	**0.002**
rh_parsopercularis_area	1.6E+06	3.2E+05	8.0	**<0.001**	4.2E+06	4.2E+06	100.0	**<0.001**	7.7E+05	1.5E+05	3.82	**0.002**
rh_parsorbitalis_area	3.2E+06	6.4E+05	62.0	**<0.001**	2.4E+06	2.4E+06	240.0	**<0.001**	2.6E+05	5.2E+04	5.03	**<0.001**
rh_parstriangularis_area	4.1E+06	8.2E+05	18.0	**<0.001**	8.7E+06	8.7E+06	190.0	**<0.001**	7.9E+05	1.6E+05	3.50	**0.004**
rh_pericalcarine_area	4.0E+06	8.1E+05	12.0	**<0.001**	5.7E+06	5.7E+06	81.0	**<0.001**	2.0E+06	3.9E+05	5.61	**<0.001**
rh_postcentral_area	1.6E+07	3.2E+06	17.0	**<0.001**	5.9E+07	5.9E+07	310.0	**<0.001**	5.6E+06	1.1E+06	5.99	**<0.001**
rh_posteriorcingulate_area	4.7E+06	9.3E+05	30.0	**<0.001**	4.5E+06	4.5E+06	140.0	**<0.001**	8.9E+05	1.8E+05	5.74	**<0.001**
rh_precentral_area	3.7E+07	7.5E+06	28.0	**<0.001**	1.1E+08	1.1E+08	410.0	**<0.001**	1.1E+07	2.1E+06	7.84	**<0.001**
rh_precuneus_area	3.1E+07	6.3E+06	31.0	**<0.001**	6.7E+07	6.7E+07	330.0	**<0.001**	1.0E+07	2.0E+06	10.22	**<0.001**
rh_rostralanteriorcingulate_area	1.6E+06	3.2E+05	19.0	**<0.001**	1.7E+06	1.7E+06	110.0	**<0.001**	2.9E+05	5.8E+04	3.53	**0.004**
rh_rostralmiddlefrontal_area	5.9E+07	1.2E+07	21.0	**<0.001**	1.9E+08	1.9E+08	340.0	**<0.001**	1.5E+07	3.0E+06	5.30	**<0.001**
rh_superiorfrontal_area	9.0E+07	1.8E+07	28.0	**<0.001**	2.1E+08	2.1E+08	330.0	**<0.001**	3.1E+07	6.1E+06	9.47	**<0.001**
rh_superiorparietal_area	2.3E+07	4.6E+06	13.0	**<0.001**	8.7E+07	8.7E+07	260.0	**<0.001**	1.4E+07	2.7E+06	8.04	**<0.001**
rh_superiortemporal_area	2.3E+07	4.5E+06	34.0	**<0.001**	3.4E+07	3.4E+07	260.0	**<0.001**	3.3E+06	6.7E+05	5.03	**<0.001**
rh_supramarginal_area	1.3E+07	2.7E+06	12.0	**<0.001**	5.2E+07	5.2E+07	240.0	**<0.001**	7.4E+06	1.5E+06	6.68	**<0.001**
rh_frontalpole_area	4.5E+05	9.1E+04	58.0	**<0.001**	2.8E+05	2.8E+05	180.0	**<0.001**	2.2E+04	4.4E+03	2.85	**0.014**
rh_temporalpole_area	5.6E+05	1.1E+05	30.0	**<0.001**	5.4E+05	5.4E+05	140.0	**<0.001**	6.7E+04	1.3E+04	3.56	**0.003**
rh_transversetemporal_area	7.8E+04	1.6E+04	6.7	**<0.001**	3.0E+05	3.0E+05	130.0	**<0.001**	4.9E+04	9.7E+03	4.20	**<0.001**
rh_insula_area	2.8E+07	5.5E+06	69.0	**<0.001**	2.8E+07	2.8E+07	360.0	**<0.001**	1.8E+06	3.7E+05	4.61	**<0.001**
lh_bankssts_area	2.8E+06	5.6E+05	23.0	**<0.001**	2.6E+06	2.6E+06	110.0	**<0.001**	3.4E+05	6.8E+04	2.78	**0.017**
lh_caudalanteriorcingulate_area	1.5E+06	2.9E+05	15.0	**<0.001**	1.6E+06	1.6E+06	82.0	**<0.001**	2.2E+05	4.5E+04	2.28	**0.044**
lh_caudalmiddlefrontal_area	8.6E+06	1.7E+06	15.0	**<0.001**	1.9E+07	1.9E+07	160.0	**<0.001**	2.7E+06	5.5E+05	4.65	**<0.001**
lh_cuneus_area	4.4E+06	8.9E+05	20.0	**<0.001**	7.0E+06	7.0E+06	160.0	**<0.001**	1.0E+06	2.0E+05	4.61	**<0.001**
lh_entorhinal_area	2.9E+06	5.9E+05	67.0	**<0.001**	1.1E+06	1.1E+06	120.0	**<0.001**	2.8E+05	5.6E+04	6.40	**<0.001**
lh_fusiform_area	1.1E+07	2.2E+06	17.0	**<0.001**	4.4E+07	4.4E+07	340.0	**<0.001**	2.9E+06	5.8E+05	4.53	**<0.001**
lh_inferiorparietal_area	4.0E+07	7.9E+06	24.0	**<0.001**	9.0E+07	9.0E+07	270.0	**<0.001**	7.9E+06	1.6E+06	4.78	**<0.001**
lh_inferiortemporal_area	5.3E+07	1.1E+07	50.0	**<0.001**	5.0E+07	5.0E+07	230.0	**<0.001**	3.9E+06	7.9E+05	3.70	**0.002**
lh_isthmuscingulate_area	2.5E+06	5.1E+05	18.0	**<0.001**	8.6E+06	8.6E+06	300.0	**<0.001**	1.5E+06	3.0E+05	10.33	**<0.001**
lh_lateraloccipital_area	8.5E+07	1.7E+07	56.0	**<0.001**	9.3E+07	9.3E+07	300.0	**<0.001**	2.1E+07	4.1E+06	13.50	**<0.001**
lh_lateralorbitofrontal_area	1.5E+07	3.1E+06	37.0	**<0.001**	1.7E+07	1.7E+07	210.0	**<0.001**	1.7E+06	3.4E+05	4.06	**0.001**
lh_lingual_area	5.6E+06	1.1E+06	7.6	**<0.001**	2.6E+07	2.6E+07	180.0	**<0.001**	5.5E+06	1.1E+06	7.48	**<0.001**
lh_medialorbitofrontal_area	9.6E+06	1.9E+06	32.0	**<0.001**	1.9E+07	1.9E+07	320.0	**<0.001**	2.1E+06	4.2E+05	6.89	**<0.001**
lh_middletemporal_area	3.7E+07	7.5E+06	47.0	**<0.001**	4.4E+07	4.4E+07	280.0	**<0.001**	5.3E+06	1.1E+06	6.60	**<0.001**
lh_parahippocampal_area	6.0E+05	1.2E+05	18.0	**<0.001**	1.4E+06	1.4E+06	200.0	**<0.001**	2.4E+05	4.8E+04	7.03	**<0.001**
lh_paracentral_area	4.6E+06	9.1E+05	37.0	**<0.001**	4.9E+06	4.9E+06	200.0	**<0.001**	3.2E+05	6.5E+04	2.60	**0.024**
lh_parsopercularis_area	2.7E+06	5.5E+05	9.1	**<0.001**	7.0E+06	7.0E+06	120.0	**<0.001**	1.1E+06	2.3E+05	3.76	**0.002**
lh_parsorbitalis_area	3.1E+06	6.2E+05	87.0	**<0.001**	1.6E+06	1.6E+06	230.0	**<0.001**	2.3E+05	4.6E+04	6.50	**<0.001**
lh_parstriangularis_area	2.9E+06	5.8E+05	18.0	**<0.001**	6.0E+06	6.0E+06	190.0	**<0.001**	9.3E+05	1.9E+05	5.75	**<0.001**
lh_pericalcarine_area	2.9E+06	5.9E+05	9.9	**<0.001**	3.8E+06	3.8E+06	65.0	**<0.001**	1.4E+06	2.8E+05	4.66	**<0.001**
lh_postcentral_area	1.7E+07	3.3E+06	19.0	**<0.001**	6.4E+07	6.4E+07	360.0	**<0.001**	6.3E+06	1.3E+06	7.06	**<0.001**
lh_posteriorcingulate_area	3.4E+06	6.8E+05	22.0	**<0.001**	6.4E+06	6.4E+06	210.0	**<0.001**	1.0E+06	2.1E+05	6.75	**<0.001**
lh_precentral_area	5.1E+07	1.0E+07	43.0	**<0.001**	1.1E+08	1.1E+08	450.0	**<0.001**	1.0E+07	2.1E+06	8.60	**<0.001**
lh_precuneus_area	2.8E+07	5.6E+06	32.0	**<0.001**	5.2E+07	5.2E+07	300.0	**<0.001**	7.4E+06	1.5E+06	8.38	**<0.001**
lh_rostralanteriorcingulate_area	2.0E+06	4.0E+05	14.0	**<0.001**	5.5E+06	5.5E+06	190.0	**<0.001**	7.4E+05	1.5E+05	5.23	**<0.001**
lh_rostralmiddlefrontal_area	6.4E+07	1.3E+07	23.0	**<0.001**	1.7E+08	1.7E+08	300.0	**<0.001**	1.7E+07	3.4E+06	6.06	**<0.001**
lh_superiorfrontal_area	1.4E+08	2.8E+07	42.0	**<0.001**	2.3E+08	2.3E+08	340.0	**<0.001**	2.6E+07	5.3E+06	7.86	**<0.001**
lh_superiorparietal_area	2.6E+07	5.2E+06	14.0	**<0.001**	8.2E+07	8.2E+07	220.0	**<0.001**	8.5E+06	1.7E+06	4.50	**<0.001**
lh_superiortemporal_area	4.5E+07	9.1E+06	54.0	**<0.001**	5.3E+07	5.3E+07	320.0	**<0.001**	7.2E+06	1.4E+06	8.54	**<0.001**
lh_supramarginal_area	5.9E+07	1.2E+07	39.0	**<0.001**	8.7E+07	8.7E+07	290.0	**<0.001**	1.3E+07	2.6E+06	8.65	**<0.001**
lh_frontalpole_area	1.1E+06	2.2E+05	230.0	**<0.001**	1.8E+05	1.8E+05	190.0	**<0.001**	1.6E+04	3.2E+03	3.26	**0.006**
lh_temporalpole_area	4.1E+05	8.1E+04	21.0	**<0.001**	7.6E+05	7.6E+05	190.0	**<0.001**	1.2E+05	2.4E+04	6.12	**<0.001**
lh_transversetemporal_area	2.8E+05	5.5E+04	12.0	**<0.001**	6.6E+05	6.6E+05	140.0	**<0.001**	8.2E+04	1.6E+04	3.52	**0.004**
lh_insula_area	3.9E+07	7.7E+06	110.0	**<0.001**	1.9E+07	1.9E+07	280.0	**<0.001**	1.4E+06	2.8E+05	4.15	**<0.001**

Acknowledgments

I would like to express my greatest gratitude to my primary supervisor,…, who guided me throughout the whole project and offered deep insight into this study. I would also like to thank my family and friends for their encouragement and guidance through the journey. Further, I wish to extend my special thanks to…for providing me with this great opportunity and letting me be part of his team.

PHILOPATIR FARAG

Persönliche Daten

Vorname:
Philopatir

Nachname:
Farag

Geburtsdaten:
21.05.1996 in Alexandria

Sprachen

Deutsch – Verhandlungssicher
Französisch – Muttersprache
Englisch – Verhandlungssicher
Arabisch – Muttersprache

Praktische Erfahrungen

06/21-09/21 **Allgemeine Innere Medizin – PJ**
Schweizer Paraplegiker Zentrum, Nottwil, Schweiz

03/21-06/21 **Allgemein- und Viszeralchirurgie – PJ**
LKH Graz II Standort West, Graz, Österreich

11/20-03/21 **Urologie – PJ**
Kantonsspital Baden, Baden, Schweiz

03/2019 **Urologie – Famulatur**
Universitätsmedizin Mainz, DE

02/2019 **Allgemeinmedizin – Famulatur**
Hausarztspraxis, Hattersheim am Main, DE

09/2018 **Notaufnahme– Famulatur**
CMC Vellore, Indien

02/2018 **Orthopädie – Famulatur**
Diakoniekrankenhaus Kirn, DE

2017 - 2018 **Wissenschaftliche Hilfskraft in der Anatomie**
Präparierkurs, Universitätsmedizin Mainz, DE

Akademischer Werdegang

2015 - 2021 Studium der Humanmedizin an der Johannes-Gutenberg-Universität, Mainz

Seit 02/2018 Stipendiat der Konrad-Adenauer Stiftung

Seit 02/2018 Doktorand Klinik und Poliklinik für Neurologie

Schulbildung

2015 Abschluss: International Baccalaureate (IB)

2013 - 2015 Frankfurt International School, Oberursel am Taunus, DE

2011 - 2013 International School of Boston, USA

2002 - 2011 Lycée Francais Victor Hugo, Frankfurt, DE